UNIVERSIDADE NOVA DE LISBOA

Faculdade de Ciências e Tecnologia

Departamento de Engenharia Electrotécnica e de Computadores

Design and Performance Evaluation of Turbo FDE Receivers

Por

Fábio J. Silva

Dissertação apresentada na Faculdade de Ciências e Tecnologia
da Universidade Nova de Lisboa para obtenção do Grau
de Mestre em Engenharia Electrotécnica e de Computadores.

Orientador: Prof. Doutor Rui Dinis

Co-Orientador: Prof. Doutor Paulo Montezuma

Lisboa

2010

Dedication

To my family and fiancee

Acknowledgements

It is a pleasure to thank the many people who made this thesis possible.

First and foremost I offer my sincerest gratitude to my supervisors, Prof. Dr. Rui Dinis and Prof. Dr. Paulo Montezuma, who have supported me throughout my thesis with their patience and knowledge, as well as their academic experience, whilst allowing me the room to work in my own way. I attribute the level of my Masters degree to their encouragement, effort, and belief in my competencies. Without them this thesis would not have been completed or written. I simply could not wish for better or friendlier supervisors.

In my office in the Department of Electrical Engineering and Computers, I was surrounded by knowledgeable and friendly people who helped me daily. I would like to show my gratitude to my office mates, André Garrido, Edgar da Silva and João Garcia for being so nice and helpful.

It is an honor for me to thank to my many student colleagues for providing a stimulating and fun environment in which to learn and grow. I am especially grateful to Bruno Alves, David Gonçalves, Filipe Correia, Pedro Arruda and Tiago Gaspar.

I am very lucky to have the support of many good friends. Life would not have been the same without my friends at the Focolores, Grupo de Jovens das Mercês and Temas. Thank you for your never-ending support.

I will always remain grateful to Chiara Lubich for her contribution to peace and unity

among peoples, religions and cultures. “That all may be one.”

I am indebted to my family, especially my parents, Rosa and Paulo, as well as my brother Roberto, who have been a constant source of support – emotional, moral and of course financial – during my graduation years, who taught me to follow my dreams without disappointment and fatigue. This thesis would certainly not have existed without them.

Last but not least, my deep gratitude goes to my beloved fiancee Rita for her support, patience and understanding, who shared time with me on this journey and who always trusted in my abilities. I would not have completed this thesis and earned my Masters degree without her strength during the whole period that went into pursuing my graduate studies.

Resumo

Foram desenvolvidas nos últimos anos, diversas técnicas de transmissão por blocos para sistemas de comunicação sem fios em banda larga, adequadas para lidar com canais fortemente selectivos na frequência. Nomeadamente, técnicas como OFDM (Orthogonal Frequency Division Multiplexing) e SC-FDE (Single Carrier Frequency Domain Equalization) são capazes de fornecer ritmos de transmissão elevados apesar das adversidades do canal. Nesta tese concentramo-nos no estudo da modulação monoportadora, com especial ênfase no desenho de estruturas de recepção adequadas a cenários caracterizados por canais fortemente dispersivos no tempo. São usadas técnicas de transmissão por blocos assistidas por prefixos cíclicos (CP), permitindo implementações de baixo custo através do processamento de sinal baseado na FFT (Fast Fourier Transform).

É investigado o impacto do número de componentes multipercurso, bem como da ordem de diversidade no desempenho assimptótico de esquemas SC-FDE.

É também proposta uma estrutura de recepção capaz de realizar um método de detecção e estimação conjunta, na qual é possível combinar as estimativas do canal, baseadas em sequências de treino, com as estimativas de canal baseadas no método *decision-directed*.

Finalmente é apresentado um estudo sobre o impacto da estimação do factor de correlação no desempenho dos receptores IB-DFE (Iterative Block-Decision Feedback Equalizer).

Palavras Chave: Matched filter bound, OFDM, SC-FDE, Igualização no Domínio da Frequência (FDE), Turbo–Igualização, Diversidade, Estimação de Canal, Sequências de Treino, Receptores Iterativos, Estimação do Coeficiente de Correlação.

Abstract

In recent years, block transmission techniques were proposed and developed for broadband wireless communication systems, which have to deal with strongly frequency-selective fading channels. Techniques like Orthogonal Frequency-Division Multiplexing (OFDM) and Single Carrier with Frequency Domain Equalization (SC-FDE) are able to provide high bit rates despite the channel adversities.

In this thesis we concentrate on the study of single carrier block transmission techniques considering receiver structures suitable to scenarios with strongly time-dispersive channels. CP-assisted (Cycle Prefix) block transmission techniques are employed to cope with frequency selective channels, allowing cost-effective implementations through FFT-based (Fast Fourier Transform) signal processing.

It is investigated the impact of the number of multipath components as well as the diversity order on the asymptotic performance of SC-FDE schemes.

We also propose a receiver structure able to perform a joint detection and channel estimation method, in which it is possible to combine the channel estimates, based on training sequences, with decision-directed channel estimates.

A study about the impact of the correlation factor estimation in the performance of Iterative Block-Decision Feedback Equalizer (IB-DFE) receivers is also presented.

Keywords: Matched filter bound, OFDM, SC-FDE, Frequency-Domain Equalization (FDE), Turbo Equalization, Diversity, Channel Estimation, Training Sequences, Iterative Receivers, Correlation Coefficient Estimation.

Contents

List Of Acronyms

ADC Analog-to-Digital Converter

AWGN Additive White Gaussian Noise

BER Bit Error Rate

CP Cyclic Prefix

CIR Channel Impulsive Response

DAC Digital-to-Analog Converter

DFT Discrete Fourier Transform

DFE Decision Feedback Equalizer

FDE Frequency-Domain Equalization

FDM Frequency Division Multiplexing

FFT Fast Fourier Transform

IB-DFE Iterative Block-Decision Feedback Equalizer

IDFT Inverse Discrete Fourier Transform

IFFT Inverse Fast Fourier Transform

IBI Inter-Block Interference

ICI Inter-Carrier Interference

ISI Inter-Symbol Interference

MC Multi-Carrier

MFB Matched Filter Bound

MMSE Minimum Mean Square Error

MRC Maximal-Ratio Combining

MSE Mean Square Error

OFDM Orthogonal Frequency-Division Multiplexing

PMEPR Peak-to-Mean Envelope Power Ratio

PDP Power Delay Profile

PSD Power Spectrum Density

PSK Phase Shift Keying

QAM Quadrature Amplitude Modulation

QPSK quadrature Phase-Shift Keying

SC Single Carrier

SC-FDE Single Carrier with Frequency Domain Equalization

SINR Signal to Interference-plus-Noise Ratio

SNR Signal to Noise Ratio

SISO Soft-In, Soft-Out

ZF Zero-Forcing

List Of Symbols

General Symbols

B_k feedback equalizer coefficient for the k^{th} frequency

E_b average bit energy

E_s average symbol energy

F subcarrier separation

F_k feedforward equalizer coefficient for the k^{th} frequency

$F_k^{(l)}$ feedforward equalizer coefficient for the k^{th} frequency and l^{th} diversity branch

f frequency variable

f_k k^{th} frequency

$g(t)$ impulse response of the transmit filter

H_k overall channel frequency response for the k^{th} frequency

$\tilde{H}_{kL}$ overall channel frequency response estimation for the k^{th} frequency

$H_k^{(l)}$ overall channel frequency response for the k^{th} frequency and l^{th} diversity branch

$H_k^{(m)}$ overall channel frequency response for the k^{th} frequency of the m^{th} time block

$\tilde{H}_k^D$ data overall channel basic frequency response estimation for the k^{th} frequency

$\hat{H}_k^D$ data overall channel enhanced frequency response estimation for the k^{th} frequency

$\tilde{H}_k^{TS}$ training sequence overall channel basic frequency response estimation for the k^{th} frequency

$\hat{H}_k^{TS}$ training sequence overall channel enhanced frequency response estimation for the k^{th} frequency

$\tilde{H}_k^{TS,D}$ overall channel basic frequency response combined estimation for the k^{th} frequency

$\hat{H}_k^{TS,D}$ overall channel enhanced frequency response combined estimation for the k^{th} frequency

$h(\tau, t)$ channel impulse response

$h_T(t)$ pulse shaping filter

$\tilde{h}_n^D$ data overall channel basic impulsive response estimation for the n^{th} time-domain sample

$\hat{h}_n^D$ data overall channel enhanced impulsive response estimation for the n^{th} time-domain sample

$\tilde{h}_n^{TS}$ training sequence overall channel basic impulsive response estimation for the n^{th} time-domain sample

$\hat{h}_n^{TS}$ training sequence overall channel enhanced impulsive response estimation for the n^{th} time-domain sample

$\tilde{h}_n^{TS,D}$ overall channel basic impulsive response combined estimation for the n^{th} time-domain sample

$\hat{h}_n^{TS,D}$ overall channel enhanced impulsive response combined estimation for the n^{th} time-domain sample

i tap index of the diversity branch

k frequency index

L power of 2

$L_n^{I(i)}$ in-phase log-likelihood ratio for the n^{th} symbol at the i^{th} iteration

$L_n^{Q(i)}$ quadrature log-likelihood ratio for the n^{th} symbol at the i^{th} iteration

l antenna index/diversity branch

m data symbol index

N number of symbols/subcarriers

N_0 noise power spectral density (unilateral)

N_D number of data blocks

N_{Rx} space diversity order

N_{TS} number of symbols of the training sequence

N_k channel noise for the k^{th} frequency

N_k^{TS} training sequence channel noise for the k^{th} frequency

$N_k^{(l)}$ channel noise for the k^{th} frequency and l^{th} diversity branch

$N_k^{(m)}$ channel noise for the k^{th} frequency of the m^{th} time block

N_G number of guard samples

n time index

$n(t)$ noise signal

P_b AWGN channel performance

$P_{b,\mathrm{MFB}}$ matched filter bound performance

P_e bit error rate

$\hat{P}_e$ estimated bit error rate

$R(f)$ Fourier transform of $r(t)$

$R(\tau)$ autocorrelation function

$r(t)$ rectangular pulse/shaping pulse

$S(f)$ frequency-domain signal

S_k k^{th} frequency-domain data symbol

S_k^{TS} training sequence k^{th} frequency-domain data symbol

$S_k^{(m)}$ k^{th} frequency-domain data symbol of the m^{th} data block

$\tilde{S}_k$ estimate for the k^{th} frequency-domain data symbol

$\tilde{S}_k^{(m)}$ estimate for the k^{th} frequency-domain data symbol of the m^{th} data block

$\hat{S}_k$ "hard decision" for the k^{th} frequency-domain data symbol

$\hat{S}_k^{(m)}$ "hard decision" for the k^{th} frequency-domain data symbol of the m^{th} data block

$\overline{S}_k$ "soft decision" for the k^{th} frequency-domain data symbol

s symbol of an QPSK constellation

$s(t)$ time-domain signal

$s(t)^{(m)}$ signal associated to the m^{th} data block

$s^I(t)$ continuous in-phase component

$s^Q(t)$ continuous quadrature component

s_n	n^{th} time-domain data symbol
s_n^I	discrete in-phase component
s_n^Q	discrete quadrature component
s_n^{TS}	training sequence n^{th} symbol
$\tilde{s}_n$	sample estimate of the n^{th} time-domain data symbol
$\tilde{s}_n^{(m)}$	estimate of the n^{th} time-domain data symbol of the m^{th} data block
$\hat{s}_n$	"hard decision" of the n^{th} time-domain data symbol
$\hat{s}_n^{(m)}$	"hard decision" of the n^{th} time-domain data symbol of the m^{th} data block
$\overline{s}_n$	"soft decision" of the n^{th} time-domain data symbol
T	duration of the useful part of the block
T_B	block duration
T_{CP}	duration of the cyclic prefix
T_D	duration of the data blocks
T_F	frame duration
T_G	guard period
T_{TS}	duration of the training block
T_a	sampling interval
T_s	symbol duration
t	time variable
U_l	discrete taps order for the l^{th} diversity branch
U_{total}	total of discrete taps order for N_{Rx} space diversity order
Y_k	received sample for the k^{th} frequency
Y_k^{TS}	training sequence k^{th} frequency-domain received sample
$Y_k^{(m)}$	k^{th} frequency-domain received sample of the m^{th} data block
$Y_k^{(l)}$	received sample for the k^{th} frequency and l^{th} diversity branch
y_n	n^{th} time-domain received sample
y_n^{TS}	training sequence n^{th} time-domain received sample

$y_n^{(l)}$ n^{th} time-domain received sample for the l^{th} diversity branch

$y(t)$ received signal

w_n n^{th} channel noise sample

α inverse of the SNR

β relation between the average power of the training sequences and the data power

$\Delta_k^{(i)}$ error term for the k^{th} frequency-domain "hard decision" estimate

$\Delta_k^{(m)}$ zero-mean error term for the k^{th} frequency-domain "hard decision" estimate of the m^{th} data block

$\gamma^{(i)}$ average overall channel frequency response at the i^{th} iteration

$\kappa^{(i)}$ normalization constant for the FDE

$\rho^{(i)}$ correlation coefficient at the i^{th} iteration

$\hat{\rho}$ estimated value of ρ

$\rho_{Est+Comp}$ compensated correlation coefficient

$\chi(\hat{\rho})$ compensation factor of the correlation coefficient

ρ_m correlation coefficient of the m^{th} data block

ρ_n^I correlation coefficient of the "in-phase bit of the n^{th} data symbol

ρ_n^Q correlation coefficient of the "quadrature bit of the n^{th} data symbol

σ_{Eq}^2 total variance of the overall noise plus residual ISI

$\hat{\sigma}_{Eq}^2$ approximated value of σ_{Eq}^2

σ_{MSE}^2 mean-squared error (MSE) variance

σ_N^2 variance of channel noise

σ_S^2 variance of the transmitted frequency-domain data symbols

$\sigma_{H,TS}^2$ variance of the noise in the channel estimates related with the training sequence

σ_D^2 variance of the noise in the channel estimates related with the data blocks

$\sigma_{TS,D}^2$ variance of the noise in the combined channel estimates

Θ_k overall error for the k^{th} frequency-domain sample

$\Theta(k)$ mean-squared error (MSE) in the time-domain

$\varepsilon_k^{(i)}$ global error consisting of the residual ISI plus the channel noise at the i^{th} iteration

$\varepsilon_k^{Eq(i)}$ denotes the overall error for the k^{th} frequency-domain symbol

ϑ_n^I error in $\hat{s}_n^I$

ϑ_n^Q error in $\hat{s}_n^Q$

$\Omega_{i,l}^2$ mean square value of the magnitude of each tap i for the l^{th} diversity branch

$\varphi_{i,l}(t)$ zero-mean complex Gaussian random process

$\tau_{i,l}$ delay associated to the i^{th} tap and l^{th} diversity branch

$\delta(t)$ Dirac function

ν_l represents AWGN samples

ϵ_{kL}^H channel estimation error

ϵ_k^D data channel estimation error

ϵ_k^{TS} training sequence channel estimation error

$\epsilon_k^{TS,D}$ combined training and data channel estimation error

Matrix Symbols

$\mathbf{z}$ $U_{total} \times 1$ vector

$\mathbf{z}^H$ conjugate transpose of $\mathbf{z}$

$\mathbf{\Sigma}$ $\mathbf{\Sigma}$ is a $U_{total} \times U_{total}$ Hermitian matrix

$\mathbf{z}$ $U_{total} \times 1$ vector

$\mathbf{R}_l$ autocorrelation function matrix of $R(\tau)$ associated to the l^{th} diversity branch

$\mathbf{\Psi}$ covariance matrix of $\mathbf{z}$

$\mathbf{\Lambda}$ diagonal matrix whose elements are the eigenvalues λ_i (i=1,..,U_{total}) of $\mathbf{\Sigma}'$

$\mathbf{\Phi}$ matrix whose columns are the orthogonal eigenvectors of $\mathbf{\Sigma}'$

List of Figures

Chapter 1

Introduction

1.1 Motivation an Scope

The growing demand for high speed wireless services and applications (especially those based on multimedia) has incited the rapid development of broadband wireless systems. A major challenge in design of this type of mobile communications systems is to overcome the effects of the mobile radio channel, assuring at the same time high power and spectral efficiencies. Therefore, to meet the high data rate requirements while dealing with severely time-dispersive channels effects, equalization techniques at the receiver side become necessary to compensate the signal distortion and guarantee good performance.

It is known that the Viterbi [1] equalizer is the optimum receiver to deal with time-dispersive channels. However, its complexity grows exponentially with the length of the Channel Impulsive Response (CIR).

An alternative technique used to minimize the channel frequency selectivity effects is time-domain equalization. In comparison with Viterbi equalizers, time-domain equalization techniques offer much lower implementation complexity. However, according to [2], conventional Single Carrier (SC) modulations suffer from a growing complexity with the length of channel response. Moreover, time-domain equalization normally needs a number of multiplications, per symbol, proportional to the maximum channel impulse response length [2].

It is known that nonlinear equalization, such as Decision Feedback Equalizer (DFE) [3], offers better performance for frequency-selective radio channels than linear equalization,

with just a small complexity increase. A nonlinear equalizer is implemented with a linear filter to remove a portion of Inter-Symbol Interference (ISI), followed by a filter that cancels the remaining interference, using previous detected data. Notwithstanding, when the time length of the channel response increases, conventional time-domain DFE receivers become too complex and more susceptible to error propagation problems.

Multi-Carrier (MC) modulation systems employing Frequency-Domain Equalization (FDE) are an alternative to SC modulation systems. One approach, OFDM, has become popular and widely used in a large number of wireless communications systems which operate in severely frequency-selective fading radio channels. For channels with severe delay spread, OFDM employs frequency domain equalization which is computationally less complex than the corresponding time domain equalization. This is because equalization is performed on a block of data at a time, and the operations on this block involve Discrete Fourier Transform (DFT) implemented by an efficient Fast Fourier Transform (FFT) [4] operation and a simple channel inversion operation.

More recently, SC modulations have recover the interest and became an alternative to MC, due to the use of nonlinear equalizer receivers implemented in the frequency-domain, employing FFTs, which allow better performances than the corresponding OFDM, while keep low the complexity of implementation. Furthermore, SC modulations have shown to be effective for block transmission schemes with cyclic prefix. Moreover, block transmission techniques employing FDE techniques, where each block includes a appropriate Cyclic Prefix (CP) (i.e., with a size that deals with the maximum channel delay), proved to be suitable for high data rate transmission over highly dispersive channels [5] [2], since they require simple FFT operations and the signal processing complexity grows logarithmically with the channel's impulsive response length.

Aspects as design complexity and power efficiency are very important, especially at the uplink transmission where low implementation complexity and power consumption at the mobile terminals are crucial to assure efficient battery preservation and the resort to low cost power amplifiers. Therefore, the power amplification complexity and processing charge can be concentrated in the base station, where power consumption and processing complexity are not a restriction.

1.2 Objectives

This thesis focus on the study of SC block transmission techniques with cycle prefix over severely frequency-selective fading radio channels.

It is investigated the impact of the number of multipath components as well as the diversity order on the asymptotic performance of SC-FDE schemes. The simulation's results show that, for a high number of multipath components, the system's asymptotic performance approaches the Matched Filter Bound (MFB), even without diversity. When diversity is considered, the performance approaches the MFB faster, even for a small number of multipath components.

We also made a characterization of the channel estimation problem, that includes the propose of a joint detection and channel estimation method, in which it is possible to combine the channel estimates, based on training sequences, with decision-directed channel estimates. These systems were evaluated through Monte-carlo simulations, and the obtained system performance results show the good performances allowed by these techniques, even without resort to high-power pilots or training blocks.

A research about the impact of the correlation factor estimation in the performance of IB-DFE receivers is also present. Since the correlation factor represents a key parameter to ensure the good performance of IB-DFE receivers, reliable estimates are needed in the feedback loop. We present several methods to estimate the correlation coefficient. We also propose a technique to compensate the inaccuracy of the correlation coefficient estimation.

1.3 Outline

After this introductory chapter, chapter 2 characterizes the basic principles of SC modulations and their relations with MC modulations. OFDM modulations and SC-FDE modulations with linear and nonlinear equalizer receivers are described, including transmitter and receiver schemes as well as the signal's representation in time and frequency domain.

Chapter 3 focus on the study of DFE iterative receivers. Here, the IB-DFE receiver parameters are defined and the turbo equalization method, based on the IB-DFE, is char-

acterized by employing in the equalizer's feedback loop the "soft decisions" at the channel decoded outputs. It is also investigated the impact of the number of multipath components and diversity order, on the asymptotic performance of IB-DFE schemes. For comparison purposes, are also derived the analytical expressions for the MFB, in a multipath environment, with or without diversity. Finally, some performance results are presented and discussed.

In chapter 4 it is proposed a joint detection and channel estimation approach for SC-FDE schemes, where a coarse channel estimate is obtained with the help of a training sequence. It employs iterative receivers, where for each iteration the data estimates are used to improve the channel estimates. To overcome the significant noise enhancement effects in the decision-directed channel estimation process, caused by large envelope fluctuations of the frequency-domain data blocks, it is proposed a channel estimation method that combines channel estimates based on the training sequence with decision-directed channel estimates. The results included at the end of the chapter support our assumptions.

Chapter 5 regards the impact of the correlation factor estimation in the performance of IB-DFE receivers. We present various methods to estimate the correlation coefficient as well as a technique to compensate the inaccuracy of the correlation coefficient estimation.

Lastly, chapter 6 presents the final conclusions and remarks of this thesis, as well as some future work perspectives.

Chapter 2

Block Transmission Techniques

A brief introduction to MC modulations and SC modulations is made in this chapter. This includes several aspects such as the analytical characterization of each modulation type, and some relevant properties of each modulation. For both modulations a special attention is given to the characterization of the transmission and receiver chains, with special emphasis on the transmitter and receiver performance structures. The chapter is organized as follows: In section 2.1, MC modulations and their relations with SC modulations are analyzed. Section 2.2 describes the OFDM modulation. Section 2.3 characterizes the basic aspects related with SC-FDE modulation including the linear and iterative FDE receivers. Finally, in section 2.4 we compare the performance of OFDM and SC-FDE for severely time-dispersive channels.

2.1 Multi-Carrier Modulations versus Single Carrier Modulations

Let us start by analyzing a conventional single carrier modulation. With SC schemes we transmit using a single carrier at a high symbol rate. It is a modulation where the energy of each symbol is distributed by the total transmission band. For a linear modulation, the complex envelope of an N-symbol burst (presuming that N is even) can be written as

$$s(t) = \sum_{n=0}^{N-1} s_n r(t - nT_s), \tag{2.1}$$

where s_n is a complex coefficient that corresponds to the n^{th} symbol, selected from a chosen constellation (for example, a Phase Shift Keying (PSK) constellation, or a Quadrature Amplitude Modulation (QAM)), according to a data sequence and a appropriated mapping rule, $r(t)$ denotes the support pulse and T_s refers the symbol duration. Applying the Fourier transform (FT) to (2.1) we may write

$$S(f) = \mathcal{F}\{s(t)\} = \sum_{k=0}^{N-1} s_n R(f) e^{-j2\pi f n T_s}. \tag{2.2}$$

Therefore from (2.2), results a transmission band for each data symbol s_n equal to the band occupied by $R(f)$, where $R(f)$ denotes the FT of $r(t)$.

By contrast, in a multi-carrier modulation the N symbols are sent in the frequency-domain, each one on a different sub-carrier during the same time interval T. Therefore, a multi-carrier burst has the following spectrum

$$S(f) = \sum_{k=0}^{N-1} S_k R(f - kF), \tag{2.3}$$

where N refers to the number of sub-carriers, S_k refers to the k^{th} frequency-domain symbol and $F = \frac{1}{T_s}$ denotes the spacing between sub-carriers. Applying the inverse Fourier transform to both sides of (2.3), leads to the dual of (2.2)

$$s(t) = \mathcal{F}^{-1}\{S(f)\} = \sum_{k=0}^{N-1} S_k r(t) e^{j2\pi k F t}, \tag{2.4}$$

that represents the complex envelope of the corresponding multi-carrier burst. Comparing the equations (2.1) with (2.3) and (2.2) with (2.4), becomes clear that the SC modulations are a dual version of the MC modulations and vice-versa.

The simplest multi-carrier modulation is the conventional Frequency Division Multiplexing (FDM) scheme, where the spectrum related to the different sub-carriers do not overlap. When the bandwidth of $R(f)$ is smaller then F[1], the bandwidth associated to each symbol S_k will be a fraction $\frac{1}{N}$ of the total transmission band, as shown in Fig. 2.1.

For a transmission without ISI (InterSymbol Interference), the pulses $r(t)$ must verify the

[1]Clearly, F is the bilateral bandwidth and $F/2$ is the unilateral bandwidth.

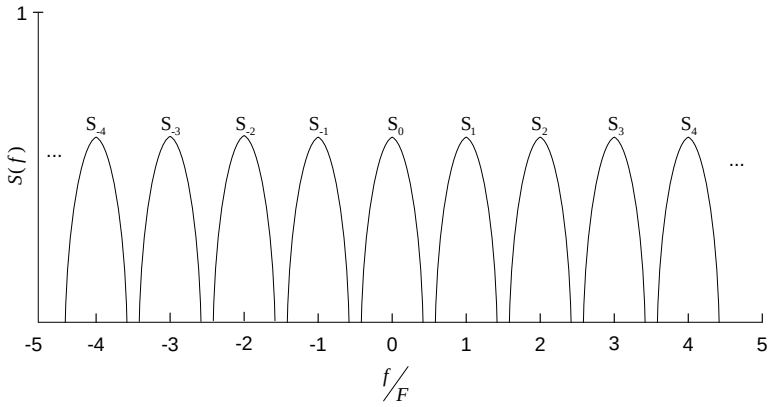

Figure 2.1: Conventional FDM

following orthogonality condition

$$\int_{-\infty}^{+\infty} r(t - nT_s)r^*(t - n'T_s)dt = 0, \quad n \neq n'. \tag{2.5}$$

Due to the duality property mentioned above, in the frequency domain, results the orthogonality condition between sub-carriers given by

$$\int_{-\infty}^{+\infty} R(f - kF)R^*(f - k'F)df = 0, \quad k \neq k'. \tag{2.6}$$

Using the Parseval's Theorem, we may write (2.6) as

$$\int_{-\infty}^{+\infty} |r(t)|^2 e^{-j2\pi(k-k')Ft}dt = 0, \quad k \neq k'. \tag{2.7}$$

For the particular case of linear SC modulations, the different pulses given by $r(t - nT_s)$ with $n = ..., -1, 0, 1, ...$, are still orthogonal even when exists overlap between them. For example, the pulse

$$r(t) = sinc\left(\frac{t}{T_s}\right), \tag{2.8}$$

with $sinc(x) \triangleq \frac{sen(\pi x)}{\pi x}$, verifies the condition (2.5). Similarly, for MC modulations the orthogonality is still preserved between the different sub-carriers even when the different $R(f - kF)$ overlap. For example, the orthogonality between sub-carriers (conditions (2.6)

and (2.7)) is verified when

$$R(f) = sinc\left(\frac{f}{F}\right), \tag{2.9}$$

that corresponds to have in time-domain a rectangular pulse $r(t)$, with duration $T = \frac{1}{F}$. In this case, the orthogonality condition (2.7) becomes

$$\int_0^{t_0+T} e^{-j2\pi(k-k')Ft}dt = 0, \quad k \neq k'. \tag{2.10}$$

2.2 OFDM Modulations

OFDM (Orthogonal Frequency Division Multiplexing) [6] is a multi-carrier modulation technique where data is transmitted simultaneously on N narrowband parallel sub-carriers. Each sub-carrier uses only a small portion of the total available bandwidth given by $N.F$, with a sub-carrier spacing of $F \geq \frac{1}{T_B}$, where T_B denotes the period of an OFDM block. By contrast to the SC modulation, the OFDM transmits N symbols as a block during each time interval T_B. Consequently, the period of an OFDM block, T_B, is N times bigger than the symbol period T_s. It can be viewed as a technique in many aspects similar to FDM, but in OFDM the sub-carriers are separated in frequency by the minimum distance required to fulfill the orthogonality condition between them.

The complex envelope of an OFDM signal is characterized by a sum of bursts (or blocks), with duration $T_B \geq T$ (where $T = \frac{1}{F}$ denotes the duration of the useful part of the block), and are transmitted at a rate $F \geq \frac{1}{T_B}$, i.e.,

$$s(t) = \sum_m \left[\sum_{k=0}^{N-1} S_k^{(m)} e^{j2\pi kFt}\right] r(t - mT_B). \tag{2.11}$$

It is important to point out that the N data symbols $\{S_k; k = 0, ..., N-1\}$ are sent during the m^{th} block, and that the group of complex sinusoids $\{e^{j2\pi kFt}; k = 0, ..., N-1\}$ denotes the sub-carriers.

Let us consider the m^{th} OFDM block. During the OFDM block interval, the transmitted signal can be expressed as

$$s^{(m)}(t) = \sum_{k=0}^{N-1} S_k^{(m)} r(t) e^{j2\pi kFt} = \sum_{k=0}^{N-1} S_k^{(m)} r(t) e^{j2\pi \frac{k}{T}t}, \tag{2.12}$$

with the pulse shape, $r(t)$, defined as

$$r(t) = \begin{cases} 1, & [-T_G, T] \\ 0, & \text{elsewhere} \end{cases}, \tag{2.13}$$

where $T = \frac{1}{F}$ and $T_G \geq 0$ denotes the duration of the "guard interval" used to compensate time-dispersive channels. Therefore $r(t)$ consists in a rectangular pulse, which duration should be greater then T ($T_B = T + T_G \geq T = \frac{1}{F}$) to be able to deal with the time-dispersive characteristics of the channels. The sub-carrier spacing $F = \frac{1}{T}$, guarantees the orthogonality between the sub-carriers over the OFDM block interval. In spite of the fact that (2.7) is not verified by the pulse given by (2.13), the different sub-carriers are still orthogonal during the interval $[0, T]$, which coincides with the effective detection interval, since

$$\int_0^T |r(t)|^2 e^{-j2\pi(k-k')Ft} dt = \int_0^T e^{-j2\pi(k-k')Ft} dt = \begin{cases} 1, & k = k', \\ 0, & k \neq k'. \end{cases} \tag{2.14}$$

Therefore, for each sampling instant, we may write (2.12) as

$$s^{(m)}(t) = \sum_{k=0}^{N-1} S_k e^{j2\pi kFt}, \quad 0 \leq t \leq T_B. \tag{2.15}$$

In spite of the overlap of the different sub-carriers, the mutual influence among them can be avoided. This implies a waveform that uses the available bandwidth with a very high bandwidth efficiency. Under these conditions, the bandwidth of each sub-carrier becomes small when compared with the coherence bandwidth of the channel (i.e., the individual sub-carriers experience flat fading, which allows simple equalization). This means that the symbol period of the sub-carriers must be longer than the delay spread of the time-dispersive radio channel.

From (2.4), we can say that the m^{th} "burst" (or block) should take the form

$$s^{(m)}(t) = \sum_{k=0}^{N-1} S_k^{(m)} e^{j2\pi kFt} = \sum_{k=0}^{N-1} S_k^{(m)} e^{j2\pi \frac{k}{T_B} t} = \sum_{k=0}^{N-1} S_k^{(m)} e^{j2\pi f_k t}, \quad 0 \leq t \leq T_B, \tag{2.16}$$

where $\{S_k^{(m)}; k = 0, ..., N-1\}$ represents the data symbols of the m^{th} burst, $\{e^{j2\pi f_k t}; k = 0, ..., N-1\}$ are the sub-carriers, $f_k = \frac{k}{T_B}$ is the center frequency of the k^{th} sub-carrier, and $r(t)$ is a rectangular pulse with duration superior to $\frac{1}{F}$, attending to the time dispersion conditions introduced by the channel. It is also assumed that $r(t) = 1$ in the interval $[-T_G, T]$.

By applying the inverse Fourier transform to both sides of (2.16), we obtain

$$S(f) = \mathcal{F}\{s(t)\} = \sum_{k=0}^{N-1} S_k^{(m)} sinc\left[\left(f - \frac{k}{T_B}\right)\right], \tag{2.17}$$

where the center frequency of the k^{th} sub-carrier is $f_k = \frac{k}{T_B}$, with a sub-carrier spacing of $\frac{1}{T_B}$, that assures the orthogonality during the block interval (as stated by (2.14)).

Fig. 2.2 depicts the Power Spectrum Density (PSD) of an OFDM signal, as well as the individual sub-carrier spectral shapes for $N = 16$ sub-carriers and data symbols. As we can see from Fig. 2.2, when the k^{th} sub-carrier PSD ($f_k = \frac{k}{T_B}$) has a maximum the adjacent sub-carriers have zero-crossings, which achieve null interference between carriers and improves the overall spectral efficiency.

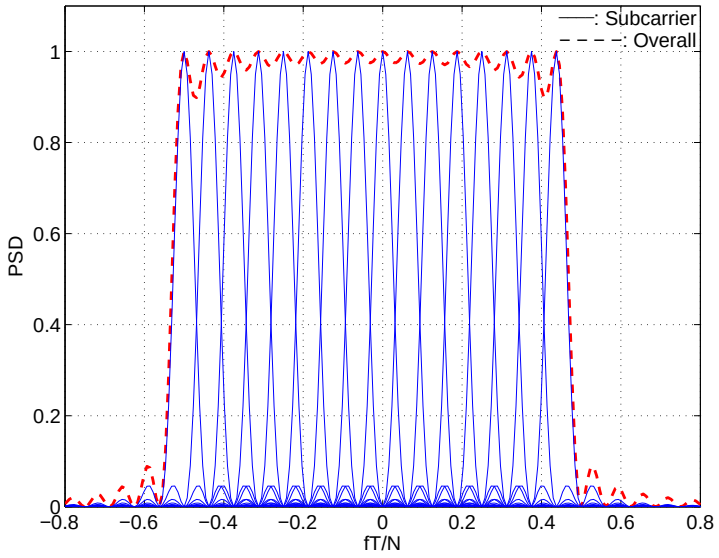

Figure 2.2: The power density spectrum of the complex envelope of the OFDM signal, with the orthogonal overlapping sub-carriers spectrum ($N = 16$).

Since the duration of each symbol is long, it is possible to insert a guard interval between the OFDM symbols, to eliminate Inter-Block Interference (IBI). If this guard interval is a

cyclic prefix instead of a zero interval, it can be shown that we also eliminate Inter-Carrier Interference (ICI) provided that we only use the useful part of the block for detection purposes [7]. Therefore, the equation (2.16) is a periodic function in t, with period T, and the complex envelope associated to the guard period can be regarded as a repetition of the MC bursts final part, as exemplified in Fig. 2.3. Thus, it is valid to write

$$s(t) = s(t+T), \quad -T_G \leq t \leq 0. \tag{2.18}$$

Consequently, the guard interval is a copy of the final part of the OFDM symbol which is added to the beginning of the transmitted symbol, making the transmitted signal periodic. The cyclic prefix, transmitted during the guard interval, consists of the end of the OFDM symbol copied into the guard interval, and the main reason to do that is on the receiver that integrates over an integer number of sinusoid cycles each multipath when it performs OFDM demodulation with the FFT [4].

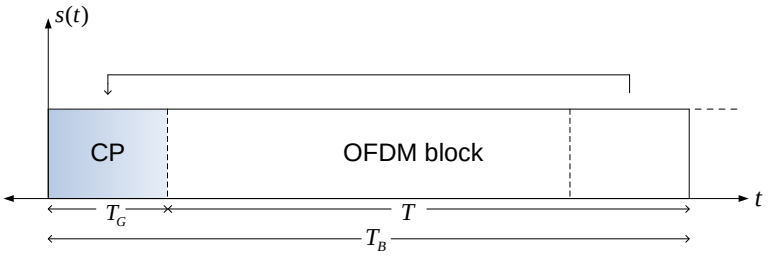

Figure 2.3: MC burst's final part repetition in the guard interval.

We may note that the guard interval also reduces the sensitivity to time synchronization problems.

2.2.1 Transmission Structure

Let us now focus on the transmission of an OFDM signal. For example purposes, we assume a noiseless transmission case. The incoming high data rate is split onto N rate sub-carriers by a serial/parallel converter. The data is therefore transmitted by blocks of size N, being $\{S_k; k = 0, ..., N-1\}$ a block of N complex data symbols chosen from a selected constellation (for example, a PSK constellation, or a QAM). From (2.16), and if we sample the OFDM signal with a interval of $T_a = \frac{T}{N}$ then we get the samples

$$s_n \equiv s(t)|_{t=nT_a} = s(t)\delta(t-nT_a) = \sum_{k=0}^{N-1} S_k e^{j2\pi \frac{k}{T} nT_a}, \quad n = 0, 1, ..., N-1, \tag{2.19}$$

where $F = \frac{1}{T}$. Consequently, (2.19) can be written as

$$s_n = \sum_{k=0}^{N-1} S_k e^{j\frac{2\pi kn}{N}} = IDFT\{S_k\}, \quad n = 0, 1, ..., N-1. \tag{2.20}$$

Hence, $\{s_n; n = 0, ..., N-1\} = IDFT\{S_k; k = 0, ..., N-1\}$. At the output of the Inverse Fast Fourier Transform (IFFT), a CP of N_G samples, is inserted at the beginning of each block of N IFFT coefficients. It consists in a time-domain cycle extension of the OFDM block, with size larger than the channel impulse response (i.e, the N_G samples assure that the CP length is equal or greater than the channel length N_H). The cycle prefix is appended between each block, in order to transform the multipath linear convolution in a circular one. Thus, the transmitted block is $\{s_n; n = -N_G, ..., N-1\}$, and the time duration of an OFDM symbol is $N_G + N$ times larger than the symbol of a SC modulation. Clearly, the CP is an overhead that costs power and bandwidth since it consists of additional redundant information data. Therefore, the resulting sampled sequence is described by

$$s_n = \sum_{k=0}^{N-1} S_k e^{j\frac{2\pi kn}{N}}, \quad n = -N_G, 1, ..., N-1. \tag{2.21}$$

After a parallel to serial conversion, this sequence is applied to a Digital-to-Analog Converter (DAC) whose output would be the signal $s(t)$. The signal is RF up converted and is sent through the channel. Therefore, an OFDM modulator can be based on a $N-$ point Inverse Discrete Fourier Transform (IDFT) on a block of N data symbols. The IDFT operation can be implemented through a IFFT which is more computational efficient, as shown in Fig. 2.4. The resulting IDFT samples are then submitted to a digital-to-analog conversion operation performed by a DAC.

The resort to the FFT algorithm allows an efficient way to implement the IDFT as well the DFT, by decreasing the number of complex multiplications operations from N^2 to $\frac{N}{2} log_2 N$, for an $N-$point IDFT or DFT.

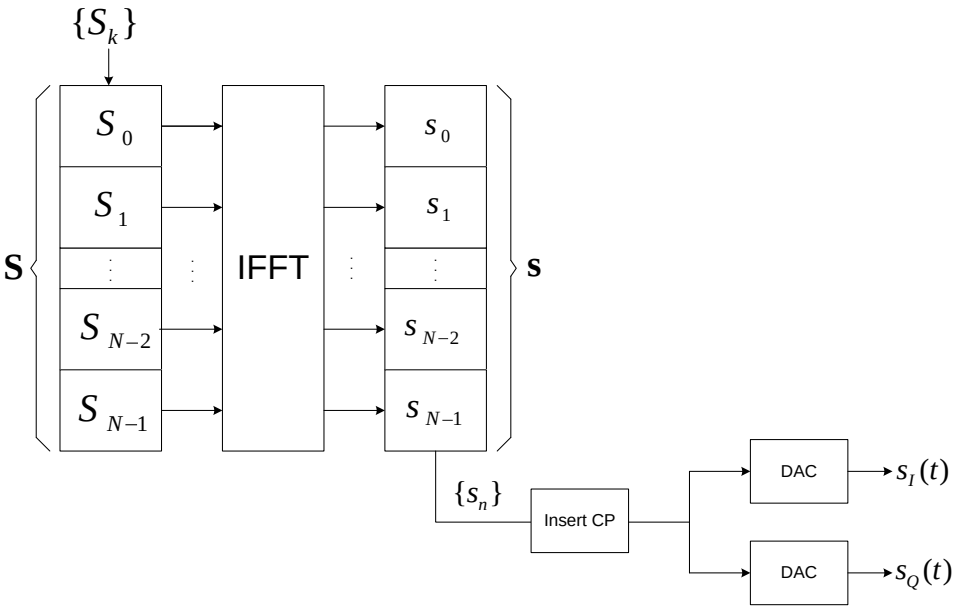

Figure 2.4: Basic OFDM transmitter block diagram.

2.2.2 Reception Structure

After the RF down conversion, at the channel output we have the received signal waveform $y(t)$ consisting of the convolution of $s(t)$ with the channel impulse response, $h(\tau, t)$, plus the noise signal $n(t)$,

$$y(t) = \int_{-\infty}^{+\infty} s(t-\tau)h(\tau,t)d\tau + n(t). \tag{2.22}$$

This $y(t)$ is then submitted to an Analog-to-Digital Converter (ADC), whose sequence at output $\{y_n; n = -N_G, ..., N-1\}$, corresponds to the sampled version of the received signal $y(t)$, for a sampling rate $T_a = \frac{T}{N}$. Therefore, the received sequence y_n consists in a set of $N + N_G$ samples, and since IBI only exists in the first N_G samples, they are extracted before the demodulation operation. The remaining samples $\{y_n; n = 0, ..., N-1\}$ are then demodulated through the DFT (performed by a FFT algorithm) to convert each block back to the frequency domain, followed by the baseband demodulation. The resulting frequency domain block $\{Y_k; k = 0, ..., N-1\}$, will be

$$Y_k = \sum_{k=0}^{N-1} y_n e^{-j\frac{2\pi kn}{N}}, \quad k = 0, 1, ..., N-1. \tag{2.23}$$

The OFDM receiver structure is implemented employing an N size DFT as shown in Fig. 2.5.

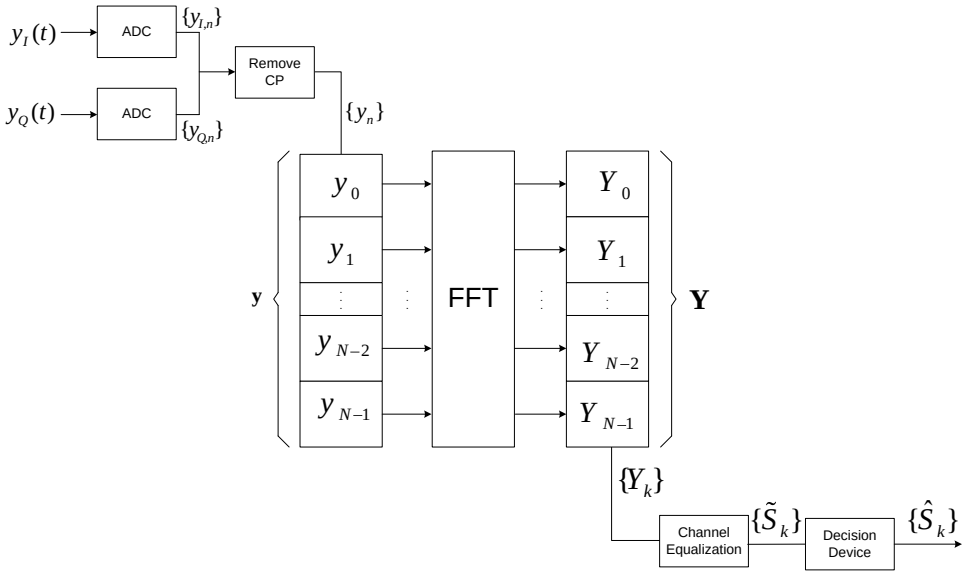

Figure 2.5: Basic OFDM receiver block diagram.

The OFDM signal detection is based on signal samples spaced by a period of duration T. Due to multipath propagation, the received data bursts overlap leading to a possible loss of orthogonality between the sub-carriers, as showed in Fig. 2.6(a). However, using a CP of duration T_G greater than overall channel impulse response, the overlapping bursts in received samples during the useful interval are avoided, as shown in Fig. 2.6(b).

Since IBI can be prevented through the CP inclusion, each sub-carrier can be regarded individually. Moreover, assuming flat fading on each sub-carrier and null ISI, the received symbol is characterized in the frequency-domain by

$$Y_k = H_k S_k + N_k, \quad k = 0, 1, ..., N-1, \tag{2.24}$$

where H_k denotes the overall channel frequency response for the k^{th} sub-carrier and N_k represents the additive Gaussian channel noise component.

On the other hand, the frequency-selective channel's effect, as the fading caused by multipath propagation, can be considered constant (flat) over an OFDM sub-carrier if it has a narrow bandwidth (i.e., when the number of sub-channels is sufficiently large). Under these conditions, the equalizer only has to multiply each detected sub-carrier (each

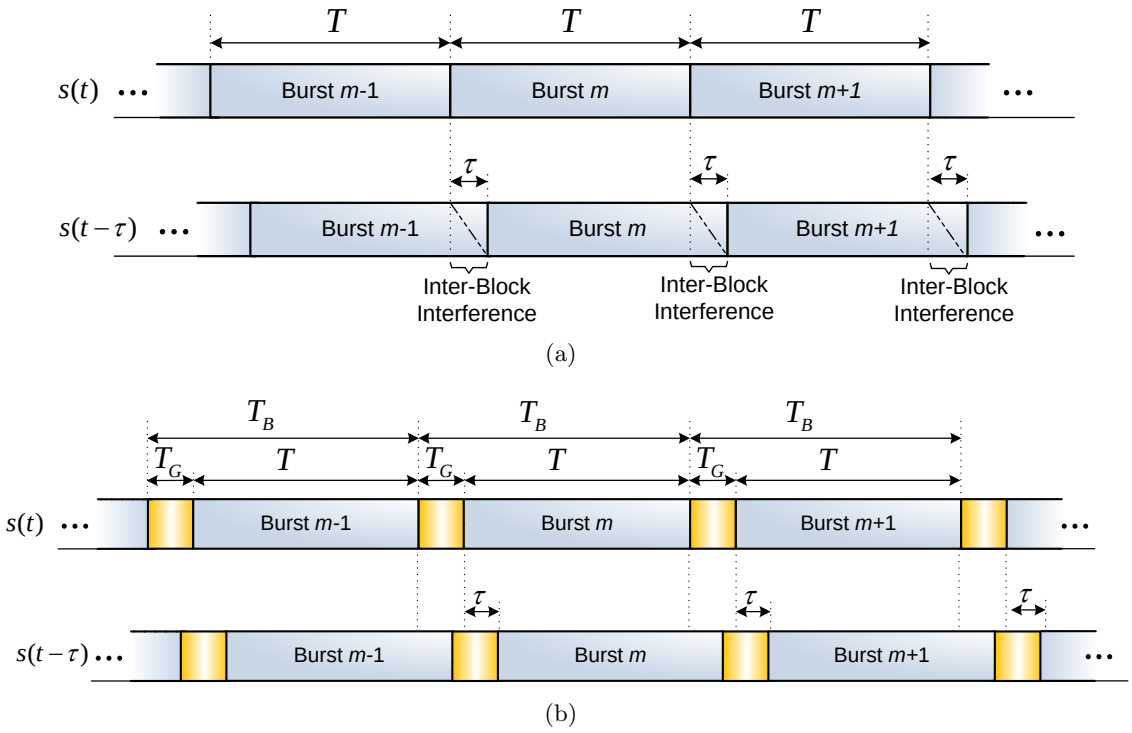

Figure 2.6: (a) Overlapping bursts due to multipath propagation; (b) IBI cancelation by implementing the cyclic prefix.

Fourier coefficient) by a constant complex number. This makes equalization far simpler at the OFDM receiver in comparison to conventional single-carrier modulation case. Also, from the point of view of computational effort, frequency-domain equalization is simpler than the corresponding time-domain equalization, since it only requires an FFT and a simple channel inversion operation. After acquiring the Y_k samples, the data symbols are obtained by processing each one of the N samples (in the frequency domain) with a FDE followed by a decision device. Consequently, the FDE is a simple one-tap equalizer [3]. Hence, the channel distortion effects (for an uncoded OFDM transmission) can be compensated by the receiver depicted in Fig. 2.7(a), where the equalization process can be accomplished by a FDE optimized under the ZF criterion, with the equalized frequency-domain samples at the k^{th} sub-carrier given by

$$\tilde{S}_k = F_k Y_k. \tag{2.25}$$

In (2.25) $\tilde{S}_k$ represents the estimated data symbols which are acquired with the set of

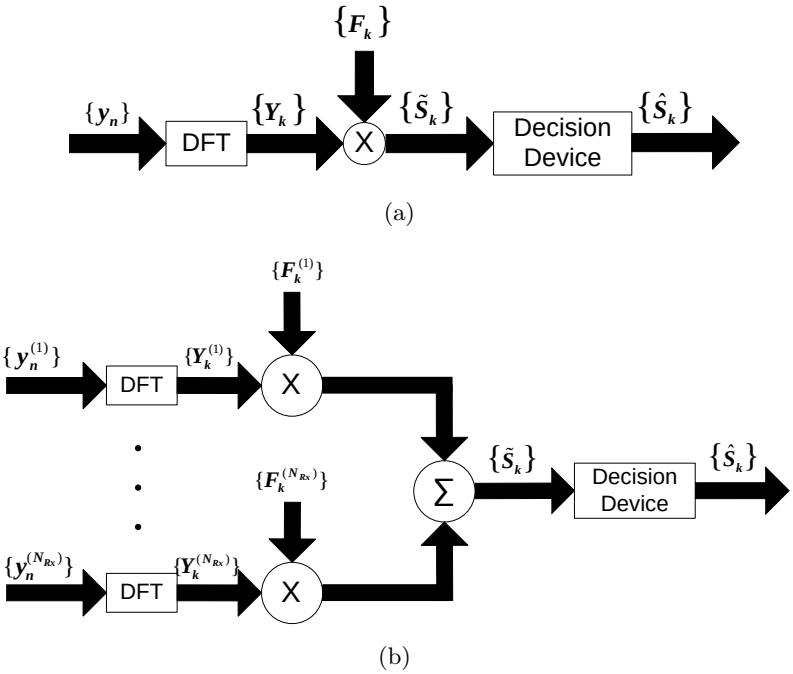

Figure 2.7: (a) OFDM Basic FDE structure block diagram with no space diversity; (b) and with an N_{Rx}-order space diversity.

coefficients $\{F_k; = k = 0, 1, ..., N-1\}$, expressed by

$$F_k = \frac{1}{H_k} = \frac{H_k^*}{|H_k|^2}. \tag{2.26}$$

Naturally, the decision on the transmitted symbol in a sub-carrier k can be based on $\tilde{S}_k$. Let us consider the case in which we have N_{Rx}-order space diversity. In Fig. 2.7(b) a Maximal-Ratio Combining (MRC) [8] diversity scheme is implemented for each sub-carrier k. Therefore, the received sample for the l^{th} receive antenna and the k^{th} sub-carrier is denoted by

$$Y_k^{(l)} = S_k H_k^{(l)} + N_k^{(l)}, \tag{2.27}$$

with $H_k^{(l)}$ denoting the overall channel frequency response between the transmit antenna and the l^{th} receive antenna for the k^{th} frequency, S_k denoting the frequency-domain of the transmitted blocks and $N_k^{(l)}$ denoting the corresponding channel noise. The equalized samples is $\{\tilde{S}_k; k = 0, 1, \ldots, N-1\}$, are

$$\tilde{S}_k = \sum_{l=1}^{N_{Rx}} F_k^{(l)} Y_k^{(l)}, \tag{2.28}$$

where $\{F_k^{(l)}; k = 0, 1, \ldots, N-1\}$ is the set of FDE coefficients related to the l^{th} diversity branch, denoted by

$$F_k^{(l)} = \frac{H_k^{(l)*}}{\sum_{l'=1}^{N_{Rx}} \left| H_k^{(l')} \right|^2}. \tag{2.29}$$

Finally, applying (2.27) and (2.29) to (2.28), the corresponding equalized samples can then be given by

$$\tilde{S}_k = S_k + \frac{\sum_{l=1}^{N_{Rx}} H_k^{(l)*}}{\sum_{l'=1}^{N_{Rx}} \left| H_k^{(l')} \right|^2} N_k^{(l)}. \tag{2.30}$$

2.3 SC-FDE Modulations

One drawback of the OFDM modulation is the high envelope fluctuations of frequency-domain data blocks. Consequently, these signals are more susceptible to nonlinear distortion effects namely those associated to a nonlinear amplification at the transmitter. Instead, when a SC modulation is employed with the same signals and constellation, the envelope fluctuations of the transmitted signal will be much lower. Thus, SC modulations are especially adequate for the uplink transmission (i.e., transmission from the mobile terminal to the base station), allowing cheaper user terminals with more efficient high-power amplifiers. Nevertheless, if conventional SC modulations are employed in digital communications systems requiring transmission bit rates of Mbits/s, over severely time-dispersive channels, high signal distortion levels can arise. Therefore, the transmission bandwidth becomes much higher than the channels's coherence bandwidth. As consequence, high complexity receivers will be required to overcome this problem [3].

2.3.1 Transmission Structure

In a SC-FDE modulation, data is transmitted in blocks of N useful modulation symbols $\{s_n; n = 0, ..., N-1\}$, resulting from a direct mapping of the original data into a selected signal constellation, for example QPSK. Posteriorly, a cyclic prefix with length longer

that the channel impulse response is appended, resulting the transmitted signal $\{s_n; n = -N_G, ..., N-1\}$. The transmission structure of an SC-FDE scheme is depicted in Fig. 2.8. As we can see the receiver is quite simple since it does not implements an DFT/IDFT operation. The discrete versions of in-phase (s_n^I) and quadrature (s_n^Q) components, are then converted by a DAC onto continuous signals $s^I(t)$ and $s^Q(t)$, which are then combined to generate the transmitted signal $s(t)$

$$s(t) = \sum_{n=-N_G}^{N-1} s_n r(t - nT_s), \tag{2.31}$$

where $r(t)$ is the support pulse and T_s denotes the symbol period.

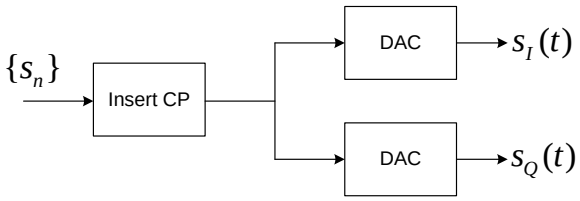

Figure 2.8: Basic SC-FDE transmitter block diagram.

2.3.2 Reception Structure

The received signal is sampled at the receiver and the CP samples are removed, leading in the time-domain the samples $\{y_n; n = 0, ..., N-1\}$. As with OFDM modulations, after a size-N DFT results the corresponding frequency-domain block $\{Y_k; k = 0, ..., N-1\}$, with Y_k given by

$$Y_k = H_k S_k + N_k, \quad k = 0, 1, ..., N-1, \tag{2.32}$$

where H_k denotes the overall channel frequency response for the k^{th} frequency of the block, and N_k represents channel noise term in the frequency-domain.
After the equalizer we get for the k^{th} subcarrier the frequency-domain samples $\tilde{S}_k$ given by

$$\tilde{S}_k = F_k Y_k. \tag{2.33}$$

For a ZF equalizer the coefficients F_k are given by (2.26), i.e.,

$$F_k = \frac{1}{H_k} = \frac{H_k^*}{|H_k|^2}. \tag{2.34}$$

From (2.34) and (2.32), we may write (2.33) as

$$\tilde{S}_k = F_k Y_k = \frac{Y_k}{H_k} = S_k + \frac{N_k}{H_k} = S_k + \epsilon_k. \tag{2.35}$$

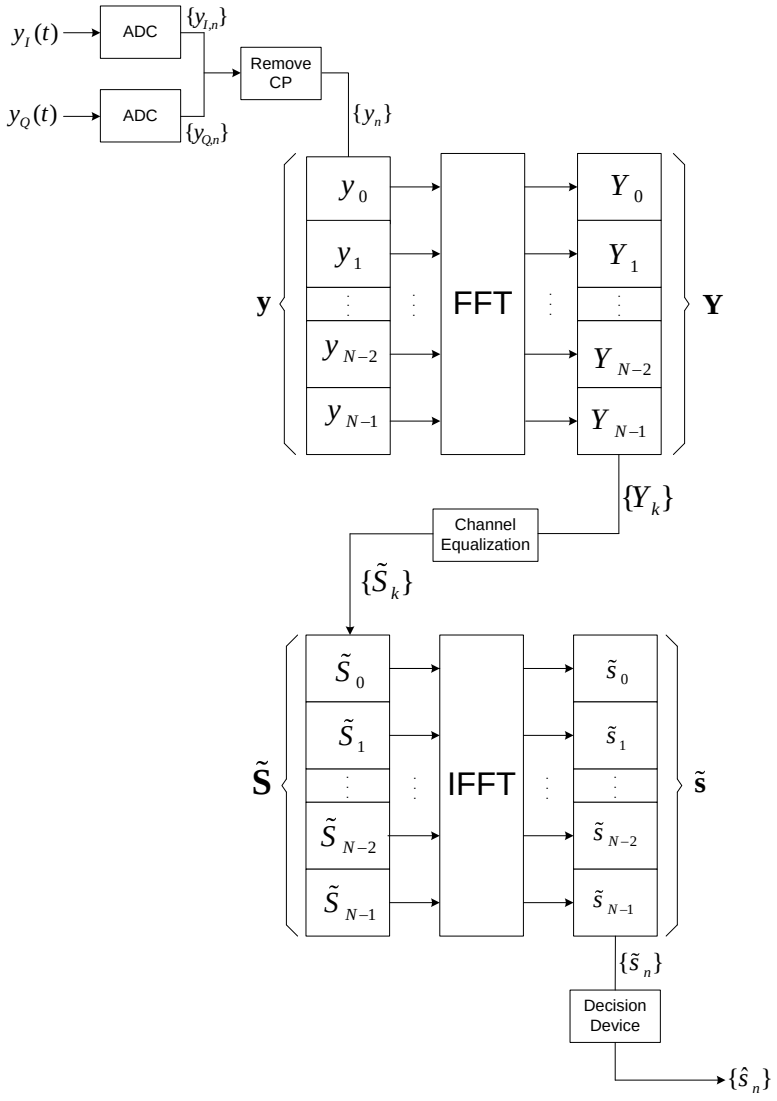

Figure 2.9: Basic SC-FDE receiver block diagram.

The receiver structure is depicted in Fig. 2.9. This means that the channel will be completely inverted. However, noise enhancement problems may arise, in the presence of a typical frequency-selective channel, caused by eventual deep notches in the channel

frequency response. The consequence, can be a diminution of the Signal to Noise Ratio (SNR).

Optimizing the coefficients F_k under the MMSE criterion avoids this. Although the MMSE does not attempt to fully invert the channel effects in the presence of deep fades, the optimization of the F_k coefficients under the MMSE criterion allows to minimize the combined effect of ISI and channel noise, allowing better performances.

The Mean Square Error (MSE), in time-domain, can be described by

$$\Theta(k) = \frac{1}{N^2} \sum_{k=0}^{N-1} \Theta_k, \tag{2.36}$$

where

$$\Theta_k = E\left[\left|\tilde{S}_k - S_k\right|^2\right] = E\left[|Y_k F_k - S_k|^2\right]. \tag{2.37}$$

The minimization of Θ_k in order to F_k, requires the MSE minimization for each k , which corresponds to impose the condition

$$min_{F_k}\left(E\left[|Y_k F_k - S_k|^2\right]\right), \quad k = 0, 1, ..., N-1, \tag{2.38}$$

that results in the set of optimized FDE coefficients $\{F_k; k = 0, 1, ..., N-1\}$ [9]

$$F_k = \frac{H_k^*}{\alpha + |H_k|^2}. \tag{2.39}$$

In (2.39) α denotes the inverse of the SNR, given by

$$\alpha = \frac{\sigma_N^2}{\sigma_S^2}, \tag{2.40}$$

where $\sigma_N^2 = \frac{E\left[|N_k|^2\right]}{2}$ represents the variance of the real and imaginary parts of the channel noise components $\{N_k; k = 0, 1, ..., N-1\}$, and $\sigma_S^2 = \frac{E\left[|S_k|^2\right]}{2}$ represents the variance of the real and imaginary parts of the data samples components $\{S_k; k = 0, 1, ..., N-1\}$. α is a noise-dependent term that avoids noise enhancement effects for very low values of the channel frequency response.

For SC modulations, once that the data contained in a block is transmitted in the time-

domain, the equalized samples in the frequency-domain $\{\tilde{S}_k; k = 0, 1, ..., N-1\}$, must be converted to the time-domain through an IDFT operation, with the decisions on the transmitted symbols made on the resulting equalized samples $\{\tilde{s}_n; n = 0, 1, ..., N-1\}$.
It is possible to extend the SC-FDE receiver for space diversity scenarios. Fig. 2.10(b) shows a SC-FDE receiver structure with an N_{Rx}-branch space diversity, where a MRC combiner is applied to each sub-carrier k. For comparison purposes, in Fig.2.10(a) it is also shown the basic SC-FDE receiver without diversity. Considering the N_{Rx}-order

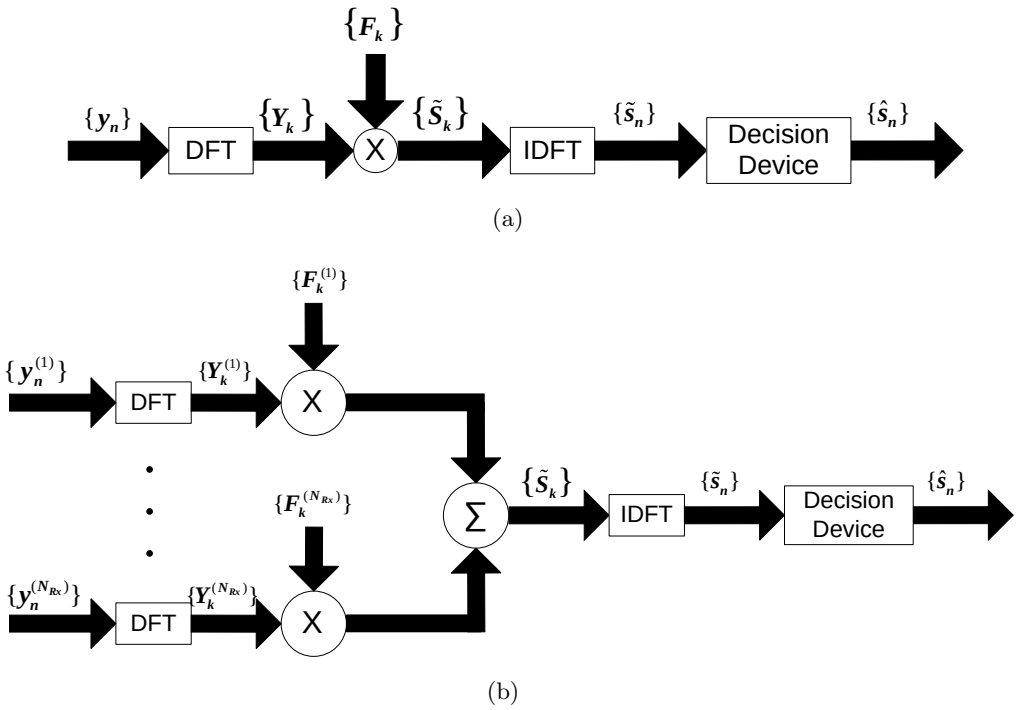

Figure 2.10: (a) Basic SC-FDE structure block diagram with no space diversity; (b) and with an N_{Rx}-order space diversity.

diversity receiver, the equalized samples at the FDE's output, are given by

$$\tilde{S}_k = \sum_{l=1}^{N_{Rx}} F_k^{(l)} Y_k^{(l)} \tag{2.41}$$

where $\{F_k^{(l)}; k = 0, 1, \ldots, N-1\}$ is the set of FDE coefficients related to the l^{th} diversity, which are given by

$$F_k^{(l)} = \frac{H_k^{(l)*}}{\alpha + \sum_{l'=1}^{N_{Rx}} \left| H_k^{(l')} \right|^2}, \tag{2.42}$$

with $\alpha = \frac{1}{SNR}$.

2.3.3 IB-DFE Receivers

It is well-known that nonlinear equalizers outperform linear ones [3] [10] [11]. Among nonlinear equalizers the DFE is a popular choice since it provides a good tradeoff between complexity and performance. Clearly, the previously described SC-FDE receiver is a linear FDE. Therefore, it would be desirable to design nonlinear FDEs, namely a DFE FDE. An efficient way of doing this is by replacing the linear FDE by an IB-DFE. The IB-DFE scheme was proposed in [10] and extended to diversity scenarios in [11]. It is an iterative DFE for SC-FDE where the feedforward and feedback operations are implemented in the frequency domain, as depicted in Fig. 2.11.

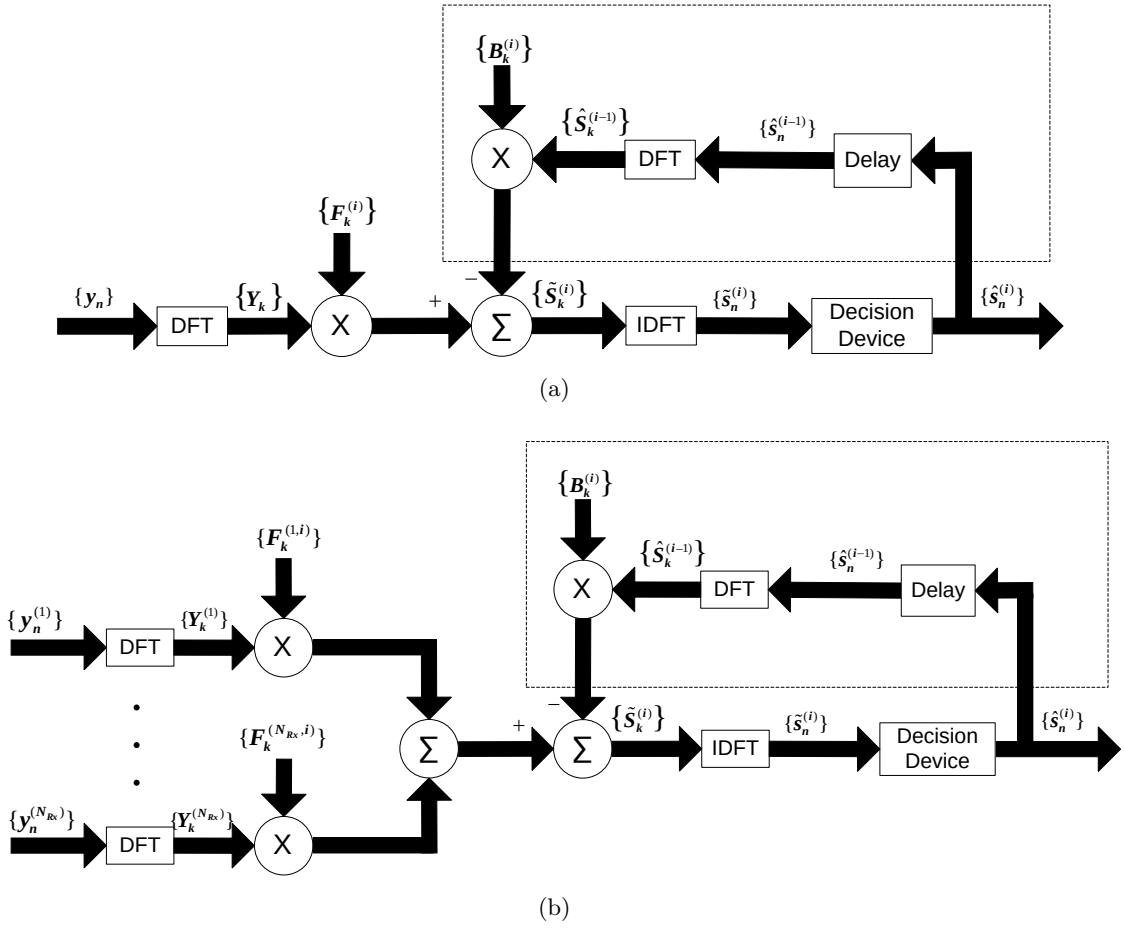

Figure 2.11: (a) Basic IB-DFE structure block diagram with no space diversity; (b) and with an N_{Rx}-order space diversity.

In the case where a N_{Rx}-order space diversity IB-DFE receiver is considered, for the

i^{th} iteration, the frequency-domain block at the output of the equalizer is $\{\tilde{S}_k^{(i)}; k = 0, 1, \ldots, N-1\}$, with

$$\tilde{S}_k^{(i)} = \sum_{l=1}^{N_{Rx}} F_k^{(l,i)} Y_k^{(l)} - B_k^{(i)} \hat{S}_k^{(i-1)}, \tag{2.43}$$

where $\{F_k^{(l,i)}; k = 0, 1, \ldots, N-1\}$ are the feedforward coefficients associated to the lth diversity antenna and $\{B_k^{(i)}; k = 0, 1, \ldots, N-1\}$ are the feedback coefficients. $\{\hat{S}_k^{(i-1)}; k = 0, 1, \ldots, N-1\}$ denotes the DFT of the "hard-decision" block $\{\hat{s}_n^{(i-1)}; n = 0, 1, \ldots, N-1\}$ from previous iteration, related with the transmitted block $\{s_n; n = 0, 1, \ldots, N-1\}$.
Both the forward and backward IB-DFE coefficients are chosen in order to maximize the Signal to Interference-plus-Noise Ratio (SINR). Considering an IB-DFE with "hard-decisions", the optimum feedback coefficients are [12]

$$B_k^{(i)} = \rho^{(i-1)} \left(\sum_{l'=1}^{N_{Rx}} F_k^{(l',i)} H_k^{(l')} - 1 \right), \tag{2.44}$$

and the feedforward coefficients are given by

$$F_k^{(l,i)} = \frac{H_k^{(l)*}}{\alpha + \left(1 - \left(\rho_m^{(i-1)}\right)^2\right) \sum_{l'=1}^{N_{Rx}} \left| H_k^{(l')} \right|^2}, \tag{2.45}$$

with α given by (2.40) and the correlation coefficient $\rho^{(i-1)}$ is defined as

$$\rho^{(i-1)} = \frac{E[\hat{s}_n^{(i-1)} s_n^*]}{E[|s_n|^2]} = \frac{E[\hat{S}_k^{(i-1)} S_k^*]}{E[|S_k|^2]}, \tag{2.46}$$

where the block $\{\hat{s}_n^{(i-1)}; n = 0, 1, \ldots, N-1\}$ denotes the data estimates associated to the previous iteration, i.e., the hard decisions associated to the time-domain block at the output of the FDE, $\{\tilde{s}_n^{(i)}; n = 0, 1, \ldots, N-1\} = \text{IDFT } \{\tilde{S}_k^{(i)}; k = 0, 1, \ldots, N-1\}$. The correlation coefficient ρ represents a crucial parameter to ensure a good receiver performance, since it supplies a blockwise reliability measure of the estimates employed in the feedback loop. This is done in the feedback loop by taking into account the hard-decisions for each block plus the overall block reliability, which reduces error propagation problems.

Clearly, the IB-DFE techniques outperform the non-iterative methods, since they can achieve better performances [10] [11]. With a conventional IB-DFE receiver the log-likelihood values are computed on a symbol-by-symbol basis (i.e., we do not need to perform the channel decoding in the feedback loop). Therefore, conventional IB-DFE receivers can be considered as low complexity turbo equalizers when the feedback loop employs the equalizer outputs rather than the channel decoder outputs. For the first iteration, no information exists about s_n, which means that $\rho = 0$, $B_k^{(0)} = 0$, and $F_k^{(0)}$ coefficients are given by (2.39) (in this situation the IB-DFE receiver is reduced to a linear FDE). After the first iteration, the feedback coefficients can be applied to reduce a major part of the residual interference (considering that the residual Bit Error Rate (BER) doesn't assume a high value). After several iterations and for a moderate-to-high SNR, the correlation coefficient will be $\rho \approx 1$ and the residual ISI will be almost totally cancellated. In Fig. 2.12 is shown the average BER performance evolution for a fading channel. We considered a transmission system, with SC uncoded modulation, that uses an IB-DFE receiver with 1, 2, 3 and 4 iterations. Also, for sake of comparison, are included the corresponding performances of the MFB and Additive White Gaussian Noise (AWGN) channel.

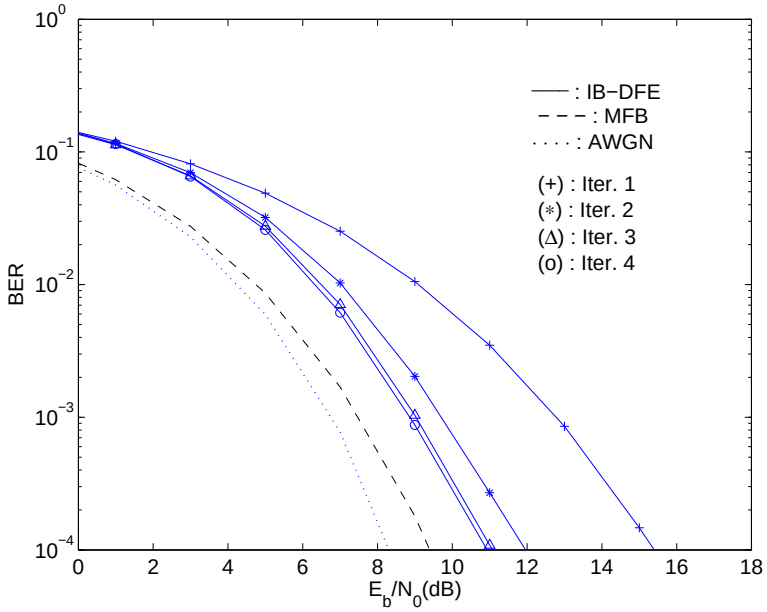

Figure 2.12: Uncoded BER perfomance for an IB-DFE receiver with four iterations.

From the results, we can see that the E_b/N_0 required for BER=10^{-4} is arround 15.5 dB

for the 1^{st} iteration (that corresponds to the linear SC-FDE), descending to 11 dB after only three iterations, being clear that the use of the iterative receiver allows a significative performance improvement. Also, the asymptotic BER performance becomes close to the MFB after a few iterations.

2.4 Comparisons Between OFDM and SC-FDE

In order to compare OFDM and SC-FDE, we will start looking to the transmission chains of both modulation systems, depicted in Fig. 2.13. Clearly, the transmission chains for OFDM and SC-FDE are essentially the same, except in the place where is performed the IFFT operation. In the OFDM, the IFFT is placed at the transmitter side to divide the data in different parallel sub-carriers. For the SC-FDE, the IFFT is placed in the receiver to convert into the time-domain the symbols at the FDE output. Although the lower complexity of the SC-FDE transmitter (it does not need the IDFT block), it requires a more complex receiver than OFDM. Consequently, from the point of view of overall processing complexity (evaluated in terms of the number of DFT/IDFT blocks), both schemes are equivalent [13].

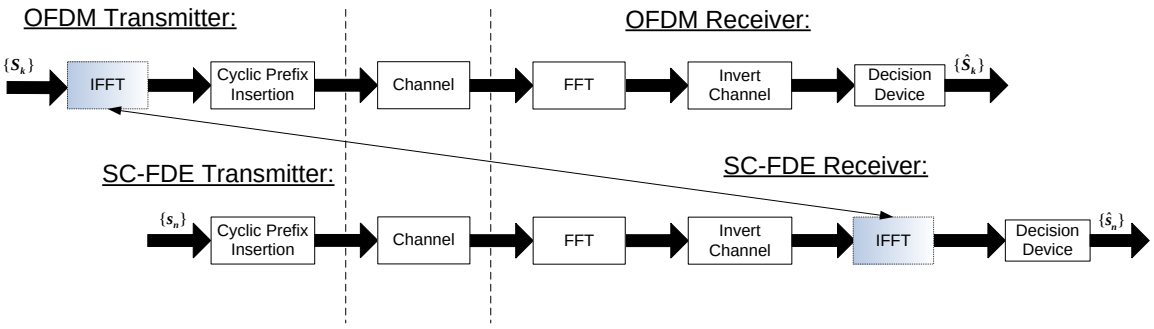

Figure 2.13: Basic transmission chain for OFDM and SC-FDE.

Moreover, for the same equalization effort, SC-FDE schemes have better uncoded performance and lower envelope fluctuations than OFDM.

Fig. 2.14 presents a example of the performance results regarding uncoded OFDM modulations and uncoded SC-FDE modulations with ZF and MMSE equalization, for QPSK signals. The blocks are composed by $N = 256$ data symbols with a cycle prefix of 32 symbols. For simulation purposes, we consider a severely time dispersive channel with 32

equal power taps, with uncorrelated rayleigh fading on each tap.

Without channel coding, the performance of the OFDM is very close to SC-FDE with ZF equalization. Moreover, SC-FDE has better uncoded performance under the same conditions of average power and complexity demands [5]. We should note that these results can not be interpreted as if OFDM has poor performance, since the OFDM is severely affected by deep-faded sub-carriers. Therefore, when combined with error correction codes, OFDM has a higher gain code when compared with SC-FDE [5].

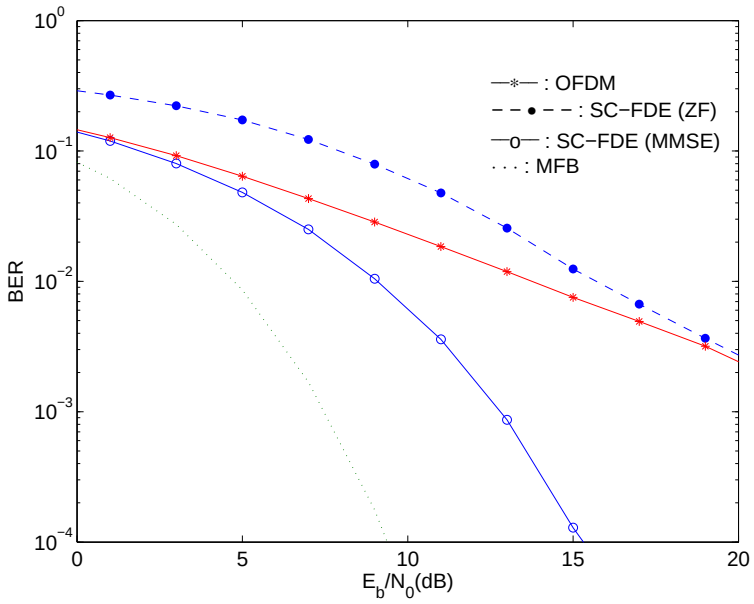

Figure 2.14: Performance result for uncoded OFDM and SC-FDE.

Moreover, OFDM symbols are affected by strong envelope fluctuations and excessive Peak-to-Mean Envelope Power Ratio (PMEPR) which causes difficulties related to power amplification and requires the use of linear amplification at the transmitter. On the other hand, the lower envelope fluctuation of SC signals allows a more efficient amplification. This is a very important aspect for the uplink transmission, where it is desirable to have low-cost and low-consumption power amplifiers. For downlink transmission, since that the implementation complexity is gathered at the base stations where the costs and high power consumption are not major constraints, the OFDM schemes are a good option. Considering that both schemes are compatible, it is possible to have a dual-mode system where the user terminal employs an SC-FDE transmitter and a OFDM receiver, while the base station employs an OFDM transmitter and an SC-FDE receiver. Obviously, from

Fig. 2.13, it becomes clear that this approach allows very low complexity mobile terminals where we implement the simpler SC transmissions and MC reception schemes.

Chapter 3

DFE Iterative Receivers

In chapter 2 it was shown that block transmission techniques, with appropriate cyclic prefixes and employing FDE techniques, are suitable for high data rate transmission over severely time dispersive channels. Typically, the receiver for SC-FDE schemes is a linear FDE. However, it is known that nonlinear equalizers outperform linear equalizers [3] [10] [11]. IB-DFE is a promising iterative FDE technique, for SC-FDE. The IB-DFE receiver can be regarded as an iterative FDE receiver where the feedforward and the feedback operations are implemented in the frequency domain. Due to the iteration process it tends to offer higher performance than non-iterative receiver. These receivers can be regarded as low-complexity turbo FDE schemes [14], [15], where the channel decoder is not involved in the feedback. True turbo FDE schemes can also be designed based on the IB-DFE concept [16], [12]. In this chapter we present a detailed study of schemes employing iterative frequency domain equalization.

This chapter is organized as follows: In section 3.1 a detailed analysis on the IB-DFE techniques is carried out and the receiver parameters are defined. In section 3.2 the receive system based in "soft decisions" is described and and the new receiver parameters are also defined. It includes the derivation of the turbo equalization based on IB-DFE receivers by employing "soft decisions" from the channel decoder outputs, in the equalizer feedback loop. Section 3.3 analyzes the impact of the number of multipath components and the diversity order on the asymptotic performance of IB-DFE schemes. Analytical expressions for the MFB, when we have multipath propagation and diversity, are also defined. It is

also shown that, for a high number of multipath components the asymptotic performance approaches the MFB even without diversity. When we have diversity, the performance approaches the MFB faster, even for a small number of multipath components.

3.1 IB-DFE with Hard Decisions

This section focus on analytical characterization of the receiver parameters for IB-DFE without or with diversity. The feedback and feedforward coefficients defined in chapter 2, are reproduced by convenience in (3.1) and (3.2), respectively.

$$B_k^{(i)} = \rho^{(i-1)} \left(\sum_{l'=1}^{N_{Rx}} F_k^{(l',i)} H_k^{(l')} - 1 \right), \tag{3.1}$$

$$F_k^{(l,i)} = \frac{H_k^{(l)*}}{\alpha + \left(1 - \left(\rho^{(i-1)}\right)^2\right) \sum_{l'=1}^{N_{Rx}} \left| H_k^{(l')} \right|^2}. \tag{3.2}$$

To calculate the receiver parameters was assumed that the global channel frequency response is

$$\sum_{l=1}^{N_{Rx}} F_k^{(l,i)} H_k^{(l)}. \tag{3.3}$$

The residual ISI component, in the frequency-domain, is related with the difference between the global channel frequency response given by (3.3) and

$$\gamma^{(i)} = \frac{1}{N} \sum_{k=0}^{N-1} \sum_{l=1}^{N_{Rx}} F_k^{(l,i)} H_k^{(l)}. \tag{3.4}$$

Clearly, $\gamma^{(i)}$ can be regarded as the average overall channel frequency response at the i^{th} iteration, after combining the outputs of the N_{Rx} output filters.

Nevertheless, if the estimates of the transmitted block are reliable, the feedback filter can be employed to eliminate the residual ISI. The equalized samples related to each iteration, in the frequency-domain, are then given by

$$\tilde{S}_k^{(i)} = \gamma^{(i)} S_k + \varepsilon_k^{(i)}, \tag{3.5}$$

where $\varepsilon_k^{(i)} = \tilde{S}_k^{(i)} - \gamma^{(i)} S_k$, represents the global error consisting of the residual ISI plus the channel noise.

As referred in chapter 2, the feedforward and feedback IB-DFE coefficients are chosen with the objective to maximize the SINR, denoted as

$$SINR^{(i)} = \frac{\left|\gamma^{(i)}\right|^2 E\left[\left|S_k\right|^2\right]}{E\left[\left|\varepsilon_k^{(i)}\right|^2\right]}. \tag{3.6}$$

It can be shown that the frequency-domain data estimates, $\hat{S}_k^{(i)}$, are given by

$$\hat{S}_k^{(i)} = \rho^{(i)} S_k + \Delta_k^{(i)}, \tag{3.7}$$

where the correlation factor $\rho^{(i)}$ is defined as

$$\rho^{(i)} = \frac{E\left[\hat{s}_n^{(i)} s_n^*\right]}{E\left[\left|s_n\right|^2\right]} = \frac{E\left[\hat{S}_k^{(i)} S_k^*\right]}{E\left[\left|S_k\right|^2\right]}, \tag{3.8}$$

measures the blockwise reliability of the decisions used in the feedback loop, and $\Delta_k^{(i)}$ denotes a zero-mean error term for the k^{th} frequency-domain "hard decision" estimate [12]. By, assuming that $E\left[\Delta_k^{(i)}\right] = 0$ and $E\left[\Delta_k^{(i)} S_{k'}^{(i)*}\right] \approx 0$ for $k' \neq k$, then

$$E\left[\left|\Delta_k^{(i)}\right|^2\right] \approx \left(1 - \left(\rho^{(i)}\right)^2\right) E\left[\left|S_k\right|^2\right]. \tag{3.9}$$

Therefore, it is possible to combine (2.27), (2.43) and (3.7) to write

$$\begin{aligned} \tilde{S}_k^{(i)} &= \sum_{l=1}^{N_{Rx}} F_k^{(l,i)} \left(S_k H_k^{(l)} + N_k^{(l)}\right) - B_k^{(i)} \left(\rho^{(i-1)} S_k + \Delta_k^{(i-1)}\right) \\ &= \gamma^{(i)} S_k + \left(\sum_{l=1}^{N_{Rx}} F_k^{(l,i)} H_k^{(l)} - \gamma^{(i)} - \rho^{(i-1)} B_k^{(i)}\right) S_k - B_k^{(i)} \Delta_k^{(i-1)} \\ &+ \sum_{l=1}^{N_{Rx}} F_k^{(l,i)} N_k^{(l)}. \end{aligned} \tag{3.10}$$

It can be seen from (3.17) that $\tilde{S}_k^{(i)}$ has the following components:

- The first term, $\gamma^{(i)} S_k$, denotes the useful signal component.
- The second term, $\left(\sum_{l=1}^{N_{Rx}} F_k^{(l,i)} H_k^{(l)} - \gamma^{(i)} - \rho^{(i-1)} B_k^{(i)} \right) S_k$, denotes the residual ISI component.
- The third term, $B_k^{(i)} \Delta_k^{(i-1)}$, denotes the noise originated by feedback errors (i.e., errors in the decision estimates $\hat{s}_n^{(i-1)}$ that are reintroduced in the system).
- The fourth term, $\sum_{l=1}^{N_{Rx}} F_k^{(l,i)} N_k^{(l)}$, denotes the channel noise.

Hence $\tilde{S}_k^{(i)}$ has three noise components and can be rewritten as

$$\tilde{S}_k^{(i)} = \gamma^{(i)} S_k + \varepsilon_k^{Eq(i)}, \tag{3.11}$$

where $\varepsilon_k^{Eq(i)}$ denotes the overall error for the k^{th} frequency-domain symbol, and is given by

$$\varepsilon_k^{Eq(i)} = \left(\sum_{l=1}^{N_{Rx}} F_k^{(l,i)} H_k^{(l)} - \gamma^{(i)} - \rho^{(i-1)} B_k^{(i)} \right) S_k - B_k^{(i)} \Delta_k^{(i-1)} + \sum_{l=1}^{N_{Rx}} F_k^{(l,i)} N_k^{(l)}. \tag{3.12}$$

From [11] ,the maximization of the SINR results in the optimum values of the feedback and feedforward coefficients given by

$$B_k^{(i)} = \rho^{(i-1)} \left(\sum_{l'=1}^{N_{Rx}} F_k^{(l',i)} H_k^{(l')} - \gamma^{(i)} \right), \tag{3.13}$$

and

$$F_k^{(l,i)} = \frac{\mathrm{SNR} \left(1 - \left(\rho_m^{(i-1)} \right)^2 \right) \gamma^{(i)} H_k^{(l)*}}{1 + \mathrm{SNR} \left(1 - \left(\rho_m^{(i-1)} \right)^2 \right) \sum_{l'=1}^{N_{Rx}} \left| H_k^{(l')} \right|^2}, \tag{3.14}$$

respectively, where $\mathrm{SNR} = \frac{E_s}{2\sigma_N^2}$ with $E_s = E\left[|s_n|^2 \right]$ denoting the average symbol energy. Since that the multplication of all the $F_k^{(l,i)}$ feedforward coefficients by a constant does not alter the SINR, we may write

$$F_k^{(l,i)} = \frac{\kappa^{(i)} H_k^{(l)*}}{\frac{1}{\text{SNR}} + \left(1 - \left(\rho_m^{(i-1)}\right)^2\right) \sum_{l'=1}^{N_{Rx}} \left|H_k^{(l')}\right|^2}. \tag{3.15}$$

where $\kappa^{(i)}$ is selected to ensure that $\gamma^{(i)} = 1$.

It is important to remark that, for the first iteration ($i = 0$), no information exists about $S_k; k = 0, 1, ..., N-1$ and the correlation coefficient $\rho = 0$, $B_k^{(0)} = 0$. Under these conditions, $F_k^{(l,0)}$ coefficients are given by

$$F_k^{(l,0)} = \frac{H_k^{(l)*}}{\alpha + \sum_{l'=1}^{N_{Rx}} \left|H_k^{(l')}\right|^2}. \tag{3.16}$$

Therefore, for the first iteration the IB-DFE receiver is simply reduced in a linear FDE. It is also worth mentioning that without diversity, the IB-DFE parameters are easily derived from the same equations above defined assuming $N_{Rx} = 1$.

3.2 IB-DFE with Soft Decisions

To improve the IB-DFE performance it is possible to use "soft decisions", $\overline{s}_n^{(i)}$, instead of "hard decisions", $\hat{s}_n^{(i)}$. Consequently, the "blockwise average" is substituted by "symbol averages". Under these assumptions the equation (2.43) can take the form

$$\tilde{S}_k^{(i)} = F_k^{(i)} Y_k - B_k^{(i)} \overline{S}_k^{(i-1)}, \tag{3.17}$$

in which

$$\overline{S}_k^{(i-1)} = \rho^{(i-1)} \hat{S}_k^{(i-1)}. \tag{3.18}$$

Being $\rho^{(i-1)}$ a measure of the blockwise reliability of the estimates expressed by $\hat{S}_k^{(i-1)}$, then $\overline{S}_k^{(i-1)}$ represents the overall block average of $S_k^{(i-1)}$ at the FDE's output.

Assuming that the transmitted symbols are selected from a QPSK constellation, under a Gray mapping rule, then $s_n = \pm 1 \pm j = s_n^I + s_n^Q$, in which $s_n^I = \text{Re}\{s_n\}$ and $s_n^Q = \text{Im}\{s_n\}$

(where the same applies to $\tilde{s}_n$, $\hat{s}_n$ and $\overline{s}_n$). Thus, the LLRs (LogLikelihood Ratios) of the "in-phase bit" and the "quadrature bit", associated to s_n^I and s_n^Q, respectively, are given by

$$L_n^{I(i)} = \frac{2}{\sigma_i^2}\tilde{s}_n^{I(i)}, \tag{3.19}$$

and

$$L_n^{Q(i)} = \frac{2}{\sigma_i^2}\tilde{s}_n^{Q(i)}, \tag{3.20}$$

respectively, with the total variance of channel and interference noise, σ_i^2, given by

$$\sigma_i^2 = \frac{1}{2}E[|s_n - \tilde{s}_n^{(i)}|^2] \approx \frac{1}{2N}\sum_{n=0}^{N-1}|\hat{s}_n^{(i)} - \tilde{s}_n^{(i)}|^2. \tag{3.21}$$

Therefore, the conditional expectations associated with the data symbols are

$$\overline{s}_n^{(i)} = \tanh\left(\frac{L_n^{I(i)}}{2}\right) + j\tanh\left(\frac{L_n^{Q(i)}}{2}\right) = \rho_n^I\hat{s}_n^I + j\rho_n^Q\hat{s}_n^Q, \tag{3.22}$$

with the signs of L_n^I and L_n^Q defining the hard decisions $\hat{s}_n^I = \pm 1$ and $\hat{s}_n^Q = \pm 1$, respectively. In (3.22), ρ_n^I and ρ_n^Q denote the reliabilities related to the "in-phase bit" and the "quadrature bit" of the n^{th} symbol, are given by

$$\rho_n^{I(i)} = \left|\tanh\left(\frac{L_n^{I(i)}}{2}\right)\right|, \tag{3.23}$$

and

$$\rho_n^{Q(i)} = \left|\tanh\left(\frac{L_n^{Q(i)}}{2}\right)\right|. \tag{3.24}$$

Obviously, for the first iteration $\rho_n^{I(0)} = \rho_n^{Q(0)} = 0$, and consequently $\overline{s}_n = 0$.

Therefore, the correlation coefficient employed in the feedforward coefficients will be given

by

$$\rho^{(i)} = \frac{1}{2N} \sum_{n=0}^{N-1} (\rho_n^{I(i)} + \rho_n^{Q(i)}). \tag{3.25}$$

The receiver structure for the IB-DFE with "soft decisions", is illustrated in Fig. 3.1. We may note that the receiver that employs "blockwise reliabilities" is referred as IB-DFE with "hard decisions", while the receiver that employs "symbol reliabilities" is referred as IB-DFE with "soft decisions". The feedforward coefficients used in both types of IB-DFE receivers are given by (3.15) but the feedback loop of the IB-DFE with "hard decisions" uses the estimated data block, weighted by a reliability coefficient common to the entire block, while for IB-DFE with "soft decisions" the feedback loop uses a different reliability coefficient for each symbol. From the performances results shown in Fig. 3.2, we have clear BER improvements when we adopte "soft decisions" instead of "hard decisions" in IB-DFE receivers.

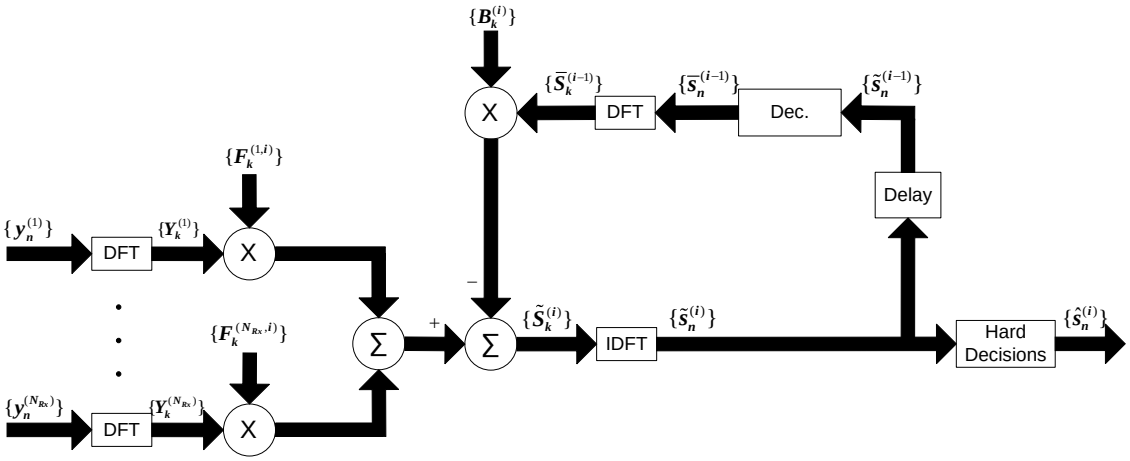

Figure 3.1: IB-DFE receiver structure employing "soft decisions" from the FDE output in the feedback loop.

3.2.1 Turbo FDE Receiver

The most common way to perform detection in digital transmission systems with channel coding, is to consider separately the channel equalization and channel decoding operations. Using a different approach in which both operations are executed in conjunction, it is pos-

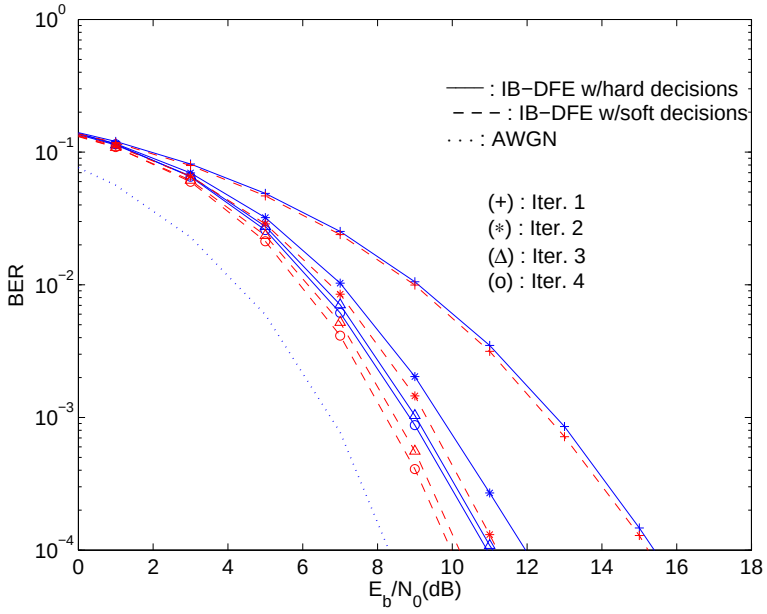

Figure 3.2: Improvements in uncoded BER perfomance accomplished by employing "soft decisions" in an IB-DFE receiver with four iterations.

sible to achieve better performance results. This can be done employing turbo-equalization systems where channel equalization and channel decoding processes are repeated in a iterative way, with "soft decisions" being passed through them. Turbo equalizers were firstly proposed for time-domain receivers. However, turbo equalizers can be implemented in the frequency-domain that, as conventional turbo equalizers, use "soft decisions" from the channel decoder output in the feedback loop.

An alternative to the conventional IB-DFE receivers, we can use IB-DFE receivers where we use in the feedback loop the "soft decisions" from the channel decoder output instead the uncoded "soft decisions" from the FDE output. The main difference between conventional IB-DFE and turbo IB-DFE relies on the decision device: in the first case the decision device is a symbol-by-symbol soft-decision (for QPSK constellation this corresponds to the hyperbolic tangent, as in (3.22)); For turbo IB-DFE we employ a Soft-In, Soft-Out (SISO) channel decoder in the feedback loop. The SISO block can be implemented as defined in [17], and provides the LLRs of both the "information bits" and the "coded bits". The input of the SISO block are the LLRs of the "coded bits" at the FDE output, given by (3.19) and (3.20). It should be noted that the data bits must be encoded, interleaved and mapped into symbols before transmission. The receiver scheme is illustrated in Fig. 3.3.

At the receiver side the equalized samples are demapped by a soft demapper followed by a deinterleaver providing the LLRs of the "coded bits" to the SISO channel decoder. The SISO operation is proceeded by a interleaver and after that a soft mapper provides the desired "soft decisions".

Figure 3.3: SISO channel decoder soft decisions

3.3 Impact of Multipath Propagation and Diversity in IB-DFE

3.3.1 Analytical Computation of the MFB

In this section we present an analytical approach for obtaining the MFB when no channel coding is employed. Since for the case with channel coding it is very difficult to obtain analytical BER expressions, even for an ideal Additive White Gaussian Noise (AWGN) channel, the MFB needs to be computed by simulation.

We will derive the MFB using an approach similar to [18]. Let us consider the case of a transmission over an multipath Rayleigh fading channel with N_{Rx} diversity branches, where all branches can have different fading powers or can be correlated. Assuming a discrete multipath channel for each diversity branch l, composed of U_l discrete taps, where the magnitude of each tap i has a mean square value of $\Omega_{i,l}^2$, the respective response at time t to an impulse, applied at t-τ, can be modeled as

$$c_l(\tau, t) = \sum_{i=1}^{U_l} \varphi_{i,l}(t)\, \delta(\tau - \tau_{i,l}), \quad l = 1...N_{Rx}, \tag{3.26}$$

with $\varphi_{i,l}(t)$ being a zero-mean complex Gaussian random process, $\tau_{i,l}$ the respective delay (assumed constant) and $\delta(t)$ is the Dirac function. For the derivation of the MFB we assume a transmission of one pulse $s \cdot g(t)$, where s is a symbol of an QPSK constellation and $g(t)$ is the impulse response of the transmit filter.

Assuming a slowly time-varying channel, the sum of the sampled outputs, from the

matched filters of the diversity branches, can be written as

$$y\left(t=t_0\right)=s\cdot\sum_{l=1}^{N_{Rx}}\sum_{i=1}^{U_l}\sum_{i'=1}^{U_l}\varphi_{i,l}\varphi_{i',l}^{*}R\left(\tau_{i,l}-\tau_{i',l}\right)+\sum_{l=1}^{N_{Rx}}\nu_l, \tag{3.27}$$

where ν_l represents AWGN samples with power spectral density N_0 and $R(\tau)$ is the autocorrelation function of the transmit filter. The instantaneous received signal to noise power ratio is given by $SNR=\frac{2E_b}{N_0}\kappa$, where E_b denotes the average bit energy and κ is defined as

$$\kappa=\sum_{l=1}^{N_{Rx}}\sum_{i=1}^{U_l}\sum_{i'=1}^{U_l}\varphi_{i,l}\varphi_{i',l}^{*}R\left(\tau_{i,l}-\tau_{i',l}\right)=\mathbf{z}^{H}\mathbf{\Sigma}\mathbf{z}. \tag{3.28}$$

In (3.28), $\mathbf{z}$ represents a $U_{total}\times 1$ (with $U_{total}=\sum_{l=1}^{N_{Rx}}U_l$) vector containing the random variables $\varphi_{i,l}$ and $\mathbf{z}^H$ denotes the conjugate transpose of $\mathbf{z}$. $\mathbf{\Sigma}$ is a $U_{total}\times U_{total}$ Hermitian matrix constructed as

$$\mathbf{\Sigma}=\begin{bmatrix}\mathbf{R}_1 & \cdots & \mathbf{0}\\ \vdots & \ddots & \vdots\\ \mathbf{0} & \cdots & \mathbf{R}_{N_{Rx}}\end{bmatrix}, \tag{3.29}$$

where $\mathbf{R}_l$ is a matrix associated to the l^{th} diversity branch, defined as

$$\mathbf{R}_l=\begin{bmatrix}R(0) & \cdots & R\left(\tau_{U_l,l}-\tau_{1,l}\right)\\ \vdots & \ddots & \vdots\\ R\left(\tau_{1,l}-\tau_{U_l,l}\right) & \cdots & R(0)\end{bmatrix}. \tag{3.30}$$

For a QPSK constellation, the instantaneous BER can be written as

$$P_b\left(\kappa\right)=\frac{1}{2}erfc\left(\sqrt{\frac{E_b}{N_0}\kappa}\right), \tag{3.31}$$

where erfc(x) is the complementary error function. To obtain the probability density

function (PDF) of κ we will write κ as a sum of uncorrelated random variables with known PDFs. Denoting $\mathbf{\Psi}$ as the covariance matrix of $\mathbf{z}$ ($\mathbf{\Psi} = Cov[\mathbf{z}]$), which is Hermitian and positive-semidefinite, it is possible to decompose $\mathbf{\Psi}$ into $\mathbf{\Psi} = \mathbf{Q}\mathbf{Q}^H$. In fact, if we apply the Cholesky decomposition, $\mathbf{Q}$ will be a lower triangular matrix. Moreover, using this matrix we can define a new vector $\mathbf{z}' = \mathbf{Q}^{-1}\mathbf{z}$, whose components will be uncorrelated unit-variance complex Gaussian variables and κ becomes

$$\kappa = \mathbf{z}'^H \mathbf{Q}^H \mathbf{\Sigma} \mathbf{Q} \mathbf{z}' = \mathbf{z}'^H \mathbf{\Sigma}' \mathbf{z}', \tag{3.32}$$

with

$$\mathbf{\Sigma}' = \mathbf{Q}^H \mathbf{\Sigma} \mathbf{Q} = \mathbf{\Phi} \mathbf{\Lambda} \mathbf{\Phi}^H, \tag{3.33}$$

where $\mathbf{\Lambda}$ is a diagonal matrix whose elements are the eigenvalues λ_i (i=1,..,U_{total}) of $\mathbf{\Sigma}'$ and $\mathbf{\Phi}$ is a matrix whose columns are the orthogonal eigenvectors of $\mathbf{\Sigma}'$. The decomposition of $\mathbf{\Sigma}'$ in (3.33) is possible due to its Hermitian property. We can then rewrite (3.32) as

$$\kappa = \mathbf{z}'^H \mathbf{\Phi} \mathbf{\Lambda} \mathbf{\Phi}^H \mathbf{z}' = \mathbf{z}''^H \mathbf{\Lambda} \mathbf{z}'' = \sum_{i=1}^{U_{total}} \lambda_i \left| z_i'' \right|^2, \tag{3.34}$$

where we have defined two more vectors, $\mathbf{z}''^{\mathbf{H}} = \mathbf{z}'^{\mathbf{H}} \mathbf{\Phi}$ and $\mathbf{z}'' = \mathbf{\Phi}^H \mathbf{z}'$, whose components are still uncorrelated unit-variance complex Gaussian variables. According to (3.34), κ can be expressed as a sum of independent random variables with exponential distributions whose characteristic function is

$$E\left\{e^{-j\upsilon\kappa}\right\} = \prod_{i=1}^{U_{total}} \frac{1}{1 + j\lambda_i \upsilon}. \tag{3.35}$$

If there are U' distinct eigenvalues, each with a multiplicity of q_i, i=1...U', we can apply the inverse Fourier transform to (3.35) and obtain the PDF of κ as

$$p(\kappa) = \sum_{i=1}^{U'} \sum_{c=1}^{q_i} \frac{A_{i,c}}{\lambda_i^{q_i} (q_i - c)! (c-1)!} \kappa^{c-1} e^{-\frac{\kappa}{\lambda_i}}, \tag{3.36}$$

with

$$A_{i,c} = \left[\frac{\partial^{q_i - c}}{\partial s^{q_i - c}} \left(\prod_{\substack{j=1 \\ j \neq i}}^{U'} \frac{1}{(1 + s\lambda_j)^{q_j}} \right) \right]_{s=-\frac{1}{\lambda_i}} . \tag{3.37}$$

It is easy to verify that the average BER can be obtained as

$$P_{b_{av}} = \int_{-\infty}^{+\infty} P_b(\kappa)\, p(\kappa)\, d\kappa = \sum_{i=1}^{U'} \sum_{m=1}^{q_i} \frac{A_{i,m}}{\lambda_i^{q_i - m}\,(q_i - m)!} \left[\frac{1-\mu_i}{2}\right]^m \cdot \sum_{r=0}^{m-1} \binom{m-1+r}{r} \left[\frac{1+\mu_i}{2}\right]^r ,$$

where

$$\mu_i = \sqrt{\frac{\frac{E_s}{N_0}\lambda_i}{1 + \frac{E_s}{N_0}\lambda_i}}. \tag{3.38}$$

3.3.2 Performance Results

Here, we present a set of performance results concerning the impact of the number of multipath components and the diversity on the performance of IB-DFE receivers as well as the correspondent MFB. We consider FFT-blocks with $N = 256$ data symbols, selected from a QPSK constellation under a Gray mapping rule. Similar results were observed for other values of N, provided that $N >> 1$.

The channel is characterized by one of the following PDPs (Power Delay Profile):

- Uniform PDP, with $U = U_1 = ... = U_{N_{Rx}}$ equal-power symbol-spaced multipath components, for all diversity branches.
- Exponential PDP, with $U = U_1 = ... = U_{N_{Rx}}$ symbol-spaced multipath components, for all diversity branches, but with an exponential decay such as the last component is 20dB below the first one.

We also assume that both channels, have uncorrelated Rayleigh fading on the different multipath components and diversity branches.

For each channel, we considered uncoded and coded transmissions. The channel encoder is based on a convolutional code with the polynomials generators $1 + D^2 + D^3 + D^5 + D^6$ and $1 + D + D^2 + D^3 + D^6$ and the coded bits are interleaved before being mapped into the constellation points and distributed by the symbols of the block. We assumed a linear power amplification at the transmitter and perfect synchronization and channel estimation at the receiver. All performance results are expressed as function of E_b/N_0, where N_0 is the one-sided power spectral density of the noise and E_b is the energy of the transmitted bits (i.e., the degradation due to the useless power spent on the cyclic prefix is not included). Fig. 3.4 shows the typical behavior of the BER for an IB-DFE with uncoded channel, for the case without diversity ($N_{Rx} = 1$), while Figs. 3.5 and 3.6 show the cases with two ($N_{Rx} = 2$) and four ($N_{Rx} = 4$) branch diversity, respectively. Clearly, there is a significant performance improvement with the iteration number, being the asymptotic BER closer to the MFB for 4 iterations. However, these improvements are much lower for low-to-moderate values of E_b/N_0. For this reason, the IB-DFE iterations yield only marginal gains when we consider channel coding, as depicted in Fig. 3.7 for the case without diversity ($N_{Rx} = 1$), and in Figs. 3.8 and 3.9 for the cases with two ($N_{Rx} = 2$) and four ($N_{Rx} = 4$) branch diversity, respectively. On the other hand, for the turbo IB-DFE, where the channel decoding is involved in the feedback loop, the gains are much higher with the performance results closer to the MFB.

Next we will present the required values of E_b/N_0 for a specific BER (10^{-4} in the uncoded case and 10^{-5} in the coded case), for the MFB and for each iteration of the IB-DFE. These results are expressed as a function of the number of multipath components U. Are considered three cases: without diversity ($N_{Rx} = 1$); two-branch diversity ($N_{Rx} = 2$); four-branch diversity ($N_{Rx} = 4$).

Let us first consider the uniform PDP. Figs. 3.10 and 3.11 show the results without and with channel coding, respectively. As we can see, for a high number of multipath components we can be very close to the MFB after a few iterations, in all cases (naturally, for $U = 1$ the BER is identical to the MFB, although the performance is very poor, since this corresponds to a flat fading channel). The improvements introduced by the iterations are higher without diversity and for the uncoded case. This is also the case where an

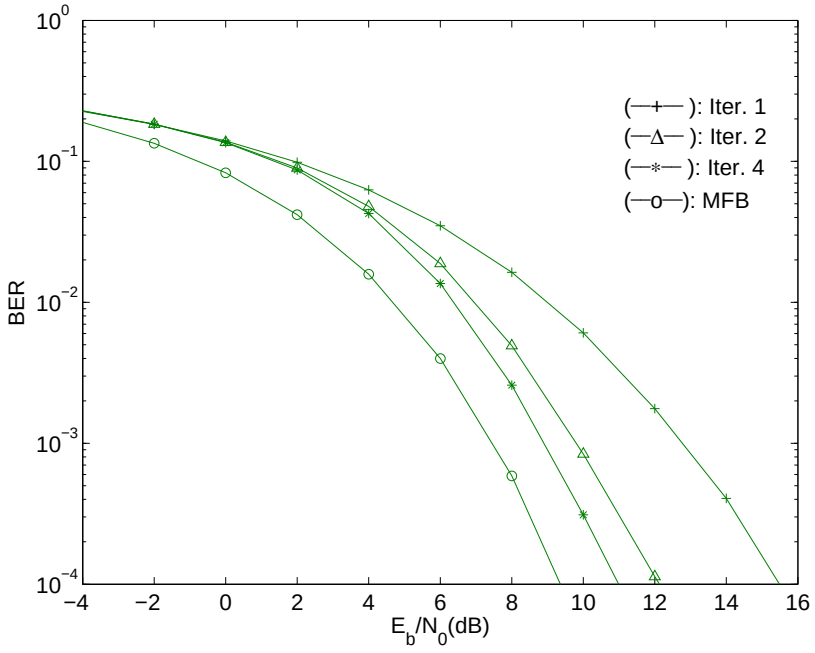

Figure 3.4: BER performance for an IB-DFE without channel coding for $N_{Rx} = 1$.

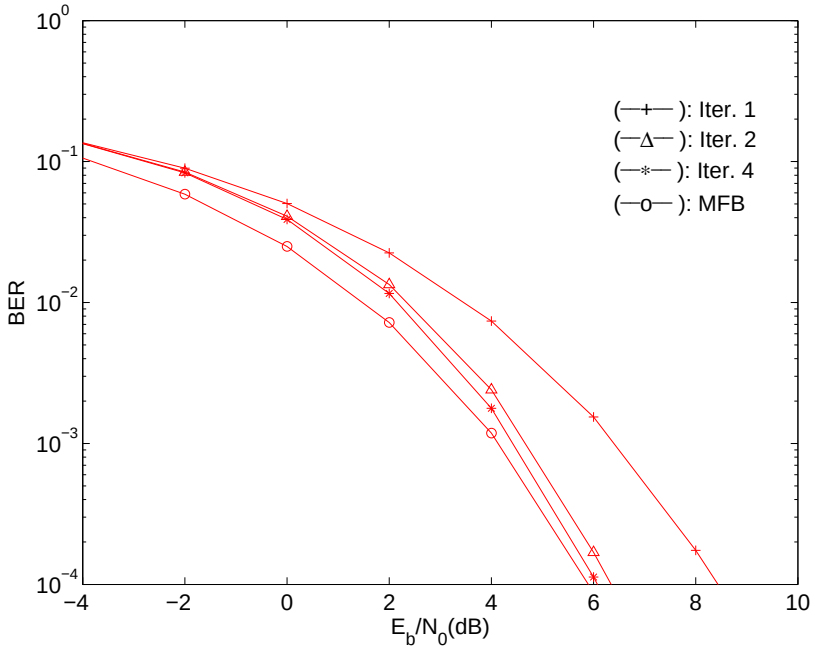

Figure 3.5: BER performance for an IB-DFE without channel coding for $N_{Rx} = 2$.

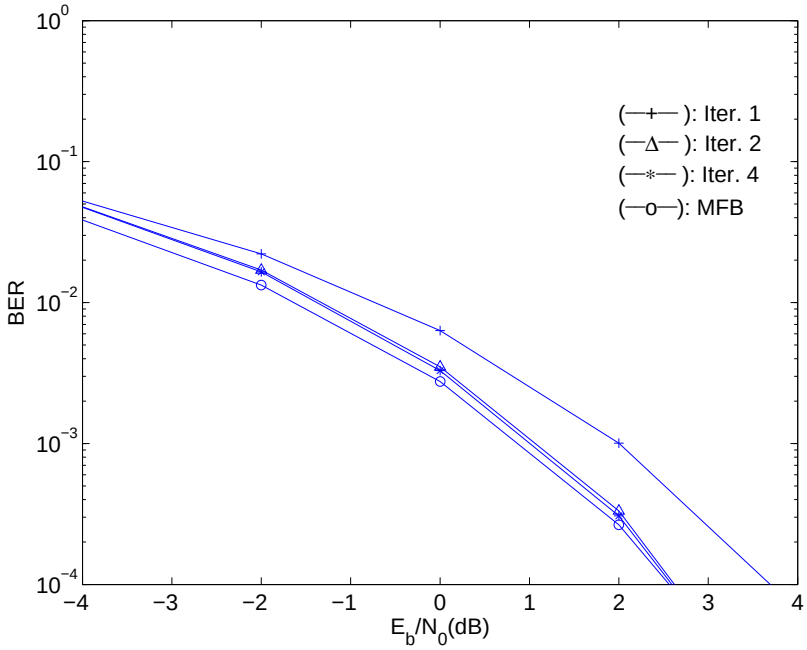

Figure 3.6: BER performance for an IB-DFE without channel coding for $N_{Rx} = 4$.

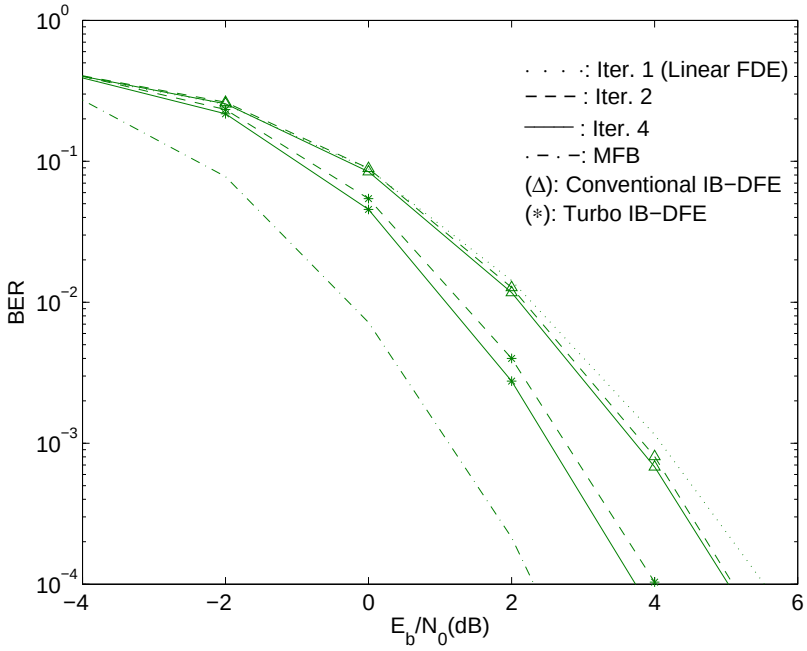

Figure 3.7: BER performance for a conventional IB-DFE with channel coding, as well as a turbo IB-DFE for $N_{Rx} = 1$.

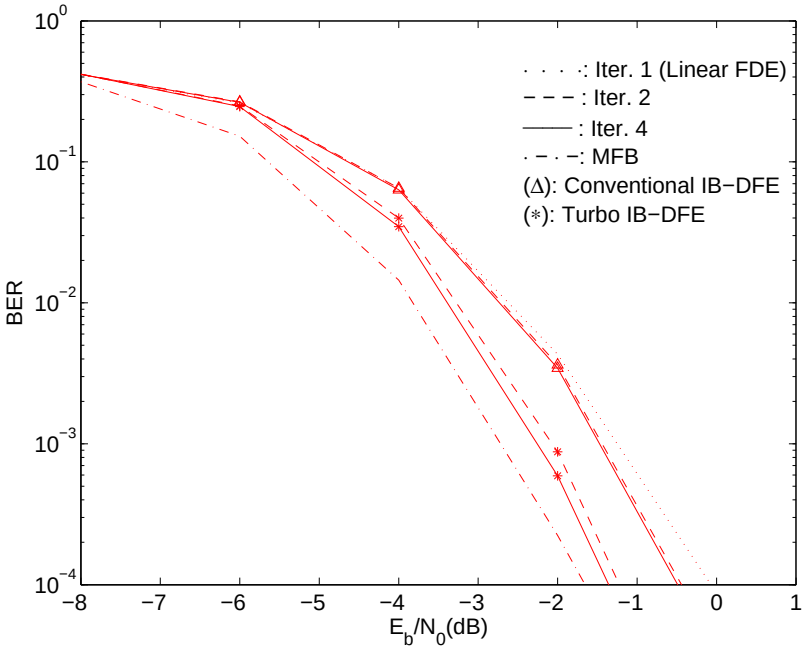

Figure 3.8: BER performance for a conventional IB-DFE with channel coding, as well as a turbo IB-DFE for $N_{Rx} = 2$.

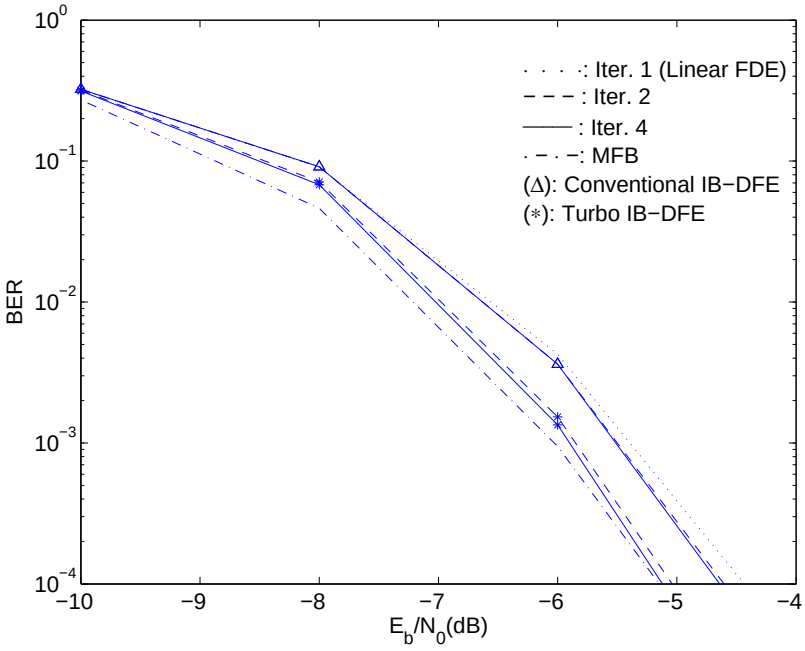

Figure 3.9: BER performance for a conventional IB-DFE with channel coding, as well as a turbo IB-DFE for $N_{Rx} = 4$.

higher number of multipath components is required to allow performances close to the MFB (about $U = 60$).

Let us consider now the exponential PDP. For Figs. 3.12 and 3.13 are shown the results without channel coding and with channel coding, respectively. By comparing these figures with the corresponding ones related with the uniform PDP, we can observe a similar behavior. The major difference is on the higher number of multipath components in the exponential PDP needed to have results similar to the ones of the uniform PDP. This is due to the fact that the number of relevant multipath components is lower for the exponential PDP, since the last ones have much lower power.

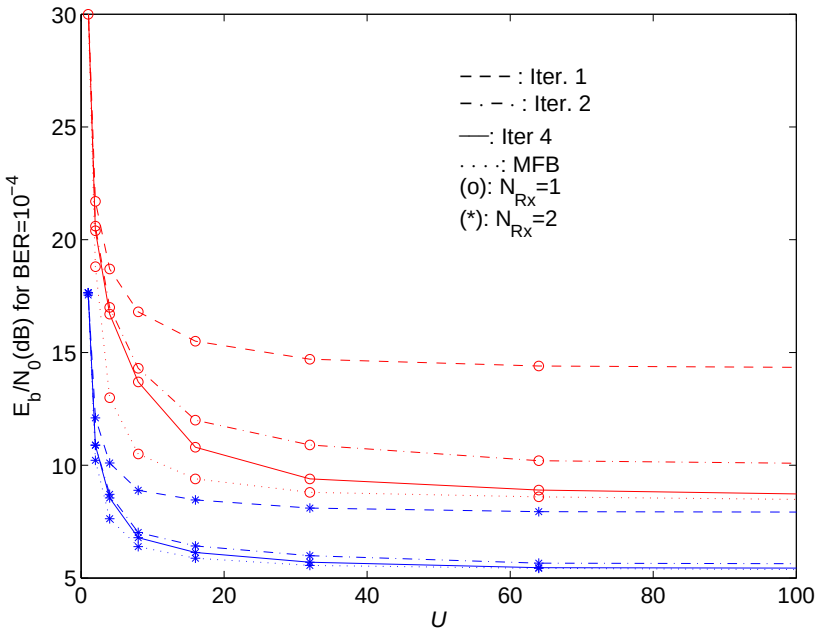

Figure 3.10: Required E_b/N_0 to achieve $BER = 10^{-4}$ without convolutional code and uniform PDP, as function of the number of multipath components: IB-DFE with 1, 2 and 4 iterations; MFB (dashed lines).

As shown in Fig. 3.14, for the uncoded case without diversity, the required values of E_b/N_0 for a BER $= 10^{-4}$ are independent of the number of symbols N of each transmitted block. Consequently, for a high number of separable multipath components, the performance can be very close to the MFB, even without diversity. In presence of diversity the performance approaches MFB faster, even for a small number of separable multipath components. These results apply to both conventional IB-DFE schemes and turbo IB-DFE schemes.

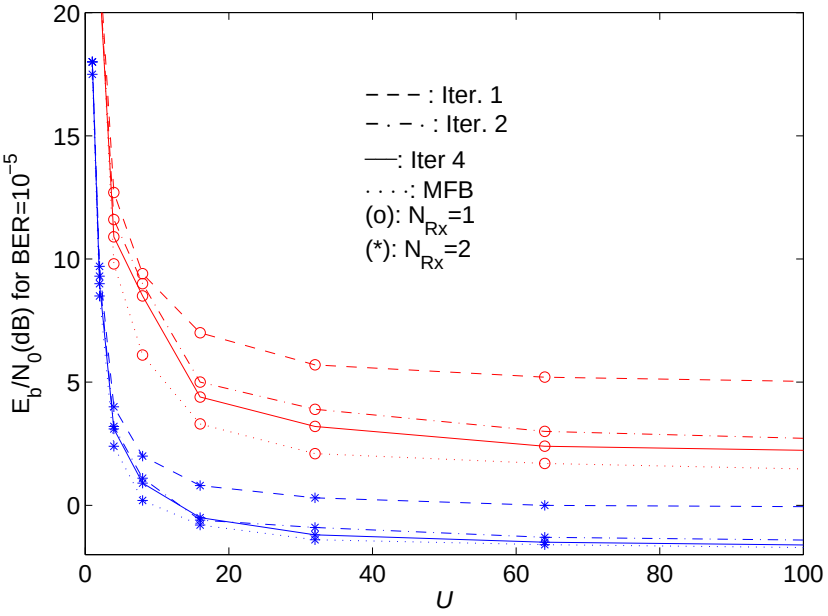

Figure 3.11: Required E_b/N_0 to achieve $BER = 10^{-5}$ with convolutional code for uniform PDP, as function of the number of multipath components: IB-DFE with 1, 2 and 4 iterations; MFB (dashed lines).

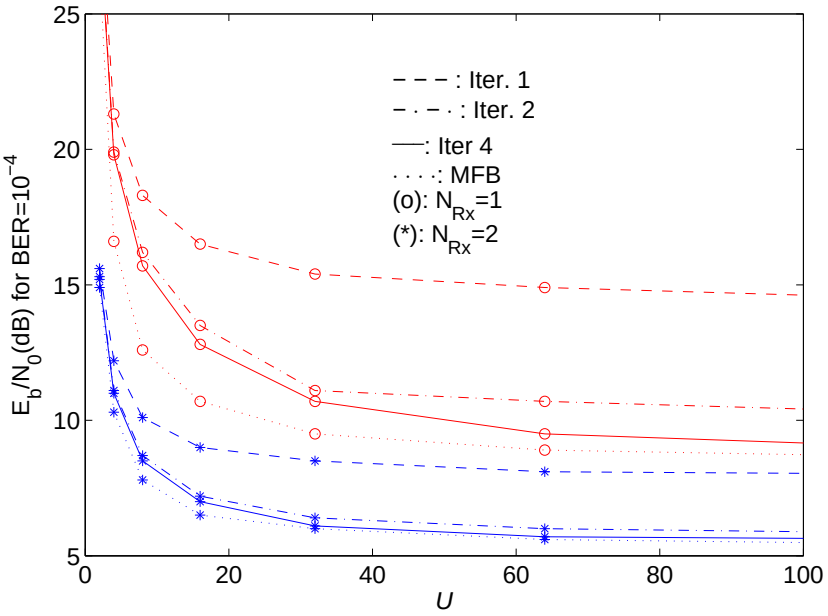

Figure 3.12: Required E_b/N_0 to achieve $BER = 10^{-4}$ without convolutional code for exponential PDP, as function of the number of multipath components: IB-DFE with 1, 2 and 4 iterations; MFB (dashed lines).

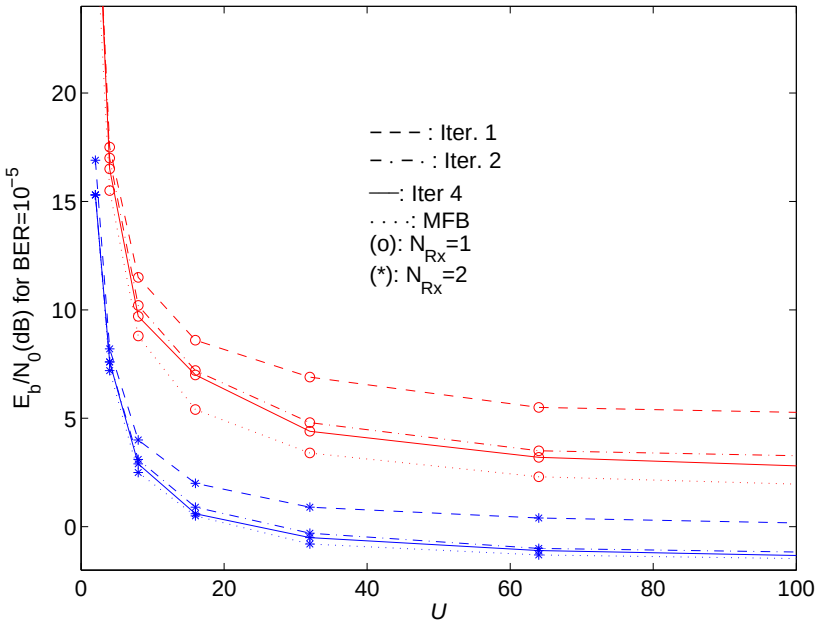

Figure 3.13: Required E_b/N_0 to achieve $BER = 10^{-5}$ with convolutional code for exponential PDP, as a function of the number of multipath components: IB-DFE with 1, 2 and 4 iterations; MFB (dashed line).

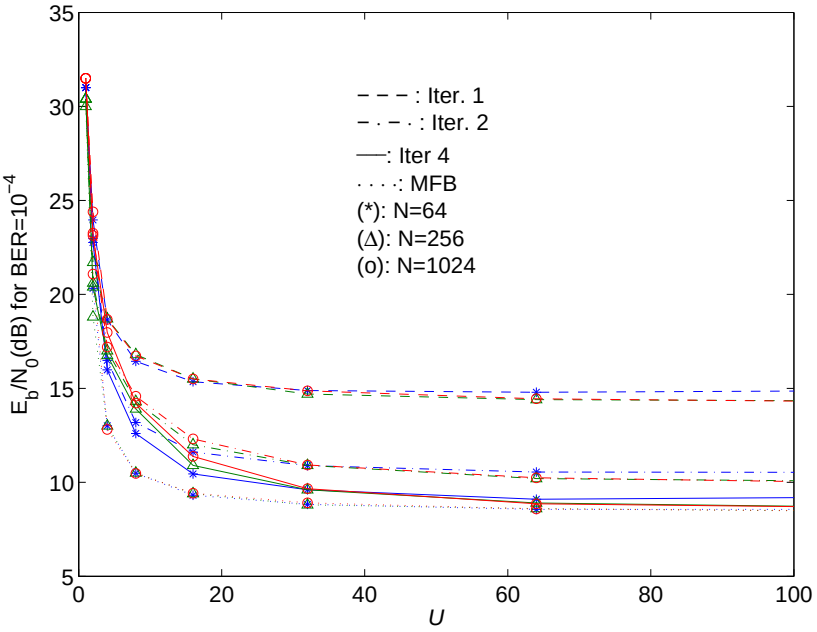

Figure 3.14: Required E_b/N_0 to achieve $BER = 10^{-4}$ without convolutional code for uniform PDP, without diversity, as a function of the number of multipath components: IB-DFE with 1, 2 and 4 iterations; MFB (dashed line).

Chapter 4

Joint Detection and Channel Estimation

In this chapter we consider joint detection and channel estimation for iterative SC-FDE schemes, where a coarse channel estimate is obtained with the help of a training sequence and in each iteration the data estimates are used to improve the channel estimates. Since the absolute value of the frequency-domain samples can have large envelope fluctuations, a decision-directed channel estimation may have significant noise enhancement effects. To overcome this problem, it is possible to combine the channel estimates based on the training sequence with decision-directed channel estimates. It will be shown that these techniques allow good performances without requiring high-power pilots or training blocks. This chapter is organized as follows: section 4.2 describes the proposed receiver with joint detection and channel estimation for SC-FDE. A set of performance results is presented in section 4.3.

4.1 System Characterization

As noted in the previous chapter, our receiver can be regarded as a modified turbo FDE [14, 12]. This implies only a marginal complexity increase in the receiver compared with conventional turbo receivers. For joint detection and channel estimation we consider a frame structure, as depicted in Fig. 4.1, with a training bock followed by N_D data blocks. Both the training and the data blocks are preceded by a cyclic prefix whose duration T_{CP}

is longer than the duration of the overall channel impulse response (including the channel effects and the transmit and receive filters). The duration of the data blocks is T_D, each one corresponding to a size-N DFT block, and the duration of the training blocks is T_{TS}, which can be equal or smaller than T_D. For the sake of simplicity it is assumed that $T_{TS} = T_D/L$, where L is a power of 2, which means that the training sequence will be formally equivalent to have one pilot for each L subcarriers when the channel is static over. Given that, results a overall frame duration $T_F = (N_D + 1)T_{CP} + T_{TS} + N_D T_D$.

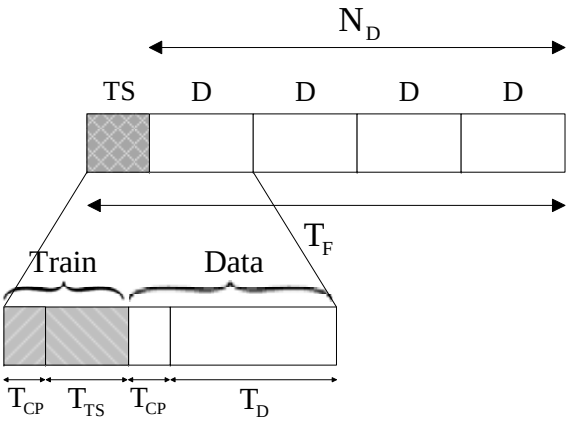

Figure 4.1: Frame structure.

When the channel variations are small within the frame duration, the training block can provide the channel frequency response for the subsequent N_D data blocks. If we can afford a delay near to half the frame duration the training block can be used to estimate the channel for the $N_D/2$ blocks, before and after the training, grossly duplicating the robustness to channel variations. For fast-varying channels it is necessary to interpolate the channel estimates obtained using different training sequences, although increasing significantly the delay (we might need delays of several frames). With an ideal interpolation pulse $sinc()$, the maximum Doppler frequency is around $1/(2T_F)$.

The signal associated to the m^{th} data block has the form

$$s^{(m)}(t) = \sum_{n=-N_{CP}}^{N-1} s_n^{(m)} h_T(t - nT_S), \tag{4.1}$$

where T_s denotes the symbol duration ($T_D = NT_s$), $N_{CP} = T_{CP}/T_s$ denotes the number of samples at the cyclic prefix and $h_T(t)$ is the adopted pulse shaping filter. For SC-FDE

schemes the symbols to be transmitted, $\{s_n^{(m)}; n = 0, 1, \ldots, N-1\}$, are directly selected from a suitable constellation (e.g., a QPSK constellation), under an appropriate mapping rule.

The signal $s^{(m)}(t)$ is transmitted over a time-dispersive channel, leading after cyclic prefix removal to the time-domain block $\{y_n^{(m)}; n = 0, 1, \ldots, N-1\}$. The corresponding frequency-domain block, after an size-N DFT operation, is $\{Y_k^{(m)}; k = 0, 1, \ldots, N-1\}$, where $Y_k^{(m)}$ can be written as

$$Y_k^{(m)} = S_k^{(m)} H_k^{(m)} + N_k^{(m)}, \tag{4.2}$$

where $H_k^{(m)}$ denotes the overall channel frequency response for the k^{th} frequency of the m^{th} time block, and $N_k^{(m)}$ denotes the corresponding channel noise. Without loss of generality, we will assume a slow-varying channel, i.e., $H_k^{(m)} = H_k$.

4.1.1 Channel Estimation

Since the optimum FDE coefficients are a function of the channel frequency response, accurate channel estimates are required at the receiver. The channel estimates are usually obtained with the help of pilot symbols and/or training sequences multiplexed with data symbols [19]. Therefore, a way to improve the channel estimation performance is to perform a joint detection and channel estimation [20, 21]. To avoid performance degradation, the power of pilots should be similar or higher than the power associated to the data. However there is always some performance degradation when we consider the power spent to transmit each block, i.e., the power of pilots plus data. As with data blocks, the training signal has the form

$$s^{TS}(t) = \sum_{n=-N_{CP}}^{N_{TS}-1} s_n^{TS} h_T(t - nT_s), \tag{4.3}$$

where s_n^{TS} denotes the n^{th} symbol of the training sequence, and the corresponding time-domain block at the receiver, after cyclic prefix removal, will be $\{y_n^{TS}; n = 0, 1, \ldots, N_{TS} - 1\}$. The corresponding frequency-domain block $\{Y_k^{TS}; k = 0, 1, \ldots, N_{TS} - 1\}$ is the size-

N_{TS} DFT of $\{y_n^{TS}; n = 0, 1, \ldots, N_{TS} - 1\}$. Since $N_{TS} = N/L$, we may write

$$Y_k^{TS} = S_k^{TS} H_{kL} + N_k^{TS}, \; k = 0, 1, ..., N_{TS} - 1, \tag{4.4}$$

with $\{S_k^{TS}; k = 0, 1, \ldots, N_{TS} - 1\}$ denoting the size-N_{TS} DFT of $\{s_n^{TS}; n = 0, 1, \ldots, N_{TS} - 1\}$ and N_k^{TS} denoting the channel noise. We could estimate the channel frequency response as follows:

$$\tilde{H}_{kL} = \frac{Y_k^{TS}}{S_k^{TS}} = H_{kL} + \frac{N_k^{TS}}{S_k^{TS}} = H_{kL} + \epsilon_{kL}^{H}, \tag{4.5}$$

where the channel estimation error, ϵ_{kL}^{H} is Gaussian-distributed, with zero-mean.

It should be noted that, when $L > 1$, will be necessary to interpolate the channel estimates. In this case, we just need to form the block $\{\tilde{H}_k^{TS}; k = 0, 1, \ldots, N - 1\}$, where $\tilde{H}_k^{TS} = 0$ if k is not a multiple of L (i.e., for the subcarriers that do not have estimates given by (4.5)) and compute its IDFT, to derive $\{\tilde{h}_n^{TS}; n = 0, 1, \ldots, N - 1\}$. Provided that the channel impulse response is restricted to the first N_{CP} samples, the interpolated channel frequency response is $\{\hat{H}_k^{TS}; k = 0, 1, \ldots, N - 1\} = \text{DFT } \{\hat{h}_n^{TS} = \tilde{h}_n^{TS} w_n; n = 0, 1, \ldots, N - 1\}$, where $w_n = 1$ if the n^{th} time-domain sample is inside the cyclic prefix (first N_{CP} samples) and 0 otherwise. Figs. 4.2 and 4.3 illustrate the impulsive and frequency response of the channel as well the enhanced estimates.

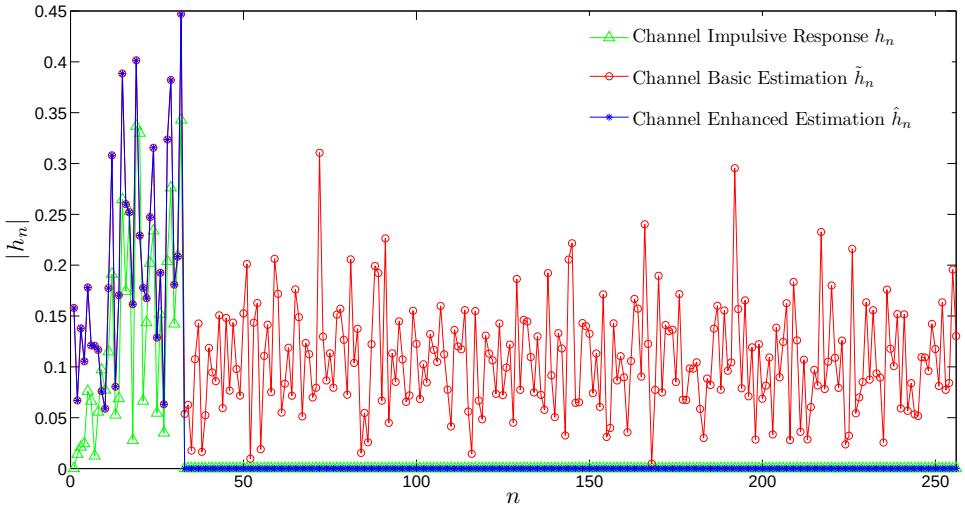

Figure 4.2: Impulsive response of the channel estimation.

Naturally,

$$\hat{H}_k^{TS} = H_k + \epsilon_k^{TS}, \tag{4.6}$$

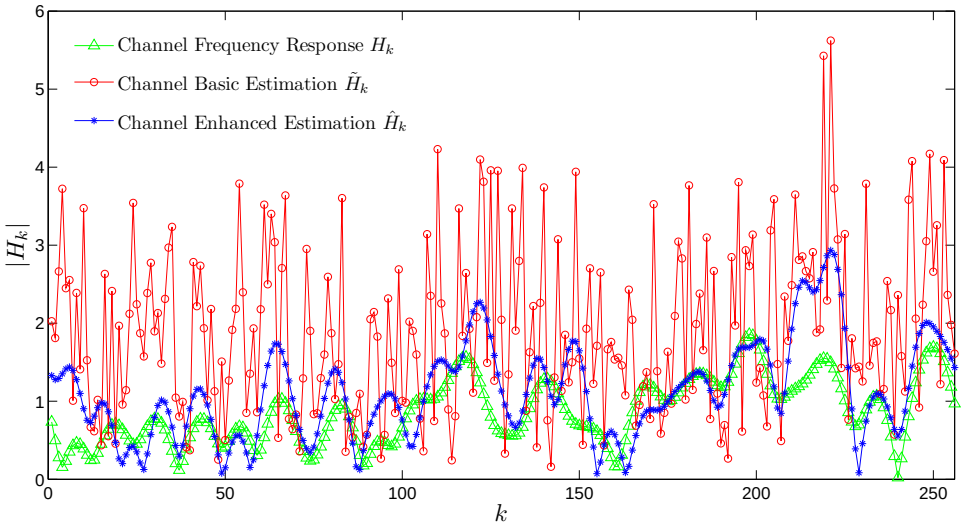

Figure 4.3: Frequency response of the channel estimation.

where ϵ_k^{TS} represents the channel estimation error after the interpolation. It can be shown that ϵ_k^{TS} is Gaussian-distributed, with zero-mean and

$$E[|\epsilon_k^{TS}|^2] = \sigma_{H,TS}^2 = \sigma_N^2 |S_k^{TS}|^2, \tag{4.7}$$

assuming $|S_k^{TS}|$ constant.

Since the power assigned to the training block is proportional to $E[|S_k^{TS}|^2] = \sigma_T^2$ and $E\left[1/|S_k^{TS}|^2\right] \geq 1/E[|S_k^{TS}|^2]$, with equality for $|S_k^{TS}|$ constant, the training blocks should have $|S_k^{TS}|^2 = \sigma_T^2$ for all k. By contrast, if we want to minimize the envelope fluctuations of the transmitted signal $|s_n^{TS}|$ should also be constant. This condition can be achieved by employing Chu sequences, which have both $|s_{n,m}^{TS}|$ and $|S_{k,m}^{TS}|$ constant [22].

When the training sequence has the same duration of the data block ($N = N_{TS}$), typically much longer than duration of the channel impulse response, we could use the enhanced $\{\hat{H}_k^{TS}; k = 0, 1, \ldots, N-1\} = \text{DFT}\ \{\hat{h}_n^{TS} = \tilde{h}_n^{TS} w_n; n = 0, 1, \ldots, N-1\}$, with w_n defined as above and $\{\tilde{h}_n^{TS}; n = 0, 1, \ldots, N-1\} = \text{IDFT}\ \{\tilde{H}_k^{TS} = Y_k^{TS}/S_k^{TS}; k = 0, 1, \ldots, N-1\}$. In this case, the variance of the noise in the channel estimates, $\sigma_{H,TS}^2$, is improved by a factor N/N_{CP}. Naturally, the system's spectral efficiency decreases (due to the use of longer training sequences) and the overall power spent in the training sequence increases, although the power per subcarrier and the peak power remain the same.

4.2 Decision-Directed Channel Estimation

The channel estimation methods, described above, are based on training sequences multiplexed with data. To avoid performance degradation, due to channel estimation errors, the required average power for these sequences should be several dB above the data power[1]. In the present section we will show that is possible to use a decision-directed channel estimation to improve the accuracy of channel estimates without resort to high-power training sequences.

If we knew the transmitted symbols for a set of N_D data blocks $\{S_k^{(m)}; k = 0, 1, , ..., N-1\}$ $(m = 1, 2, ..., N_D)$ we could estimate the channel as follows:

$$\tilde{H}_k^D = \frac{\sum_{m=1}^{N_D} Y_k^{(m)} S_k^{(m)*}}{\sum_{m=1}^{N_D} |S_k^{(m)}|^2} = H_k + \frac{\sum_{m=1}^{N_D} N_k^{(m)} S_k^{(m)*}}{\sum_{m=1}^{N_D} |S_k^{(m)}|^2}. \tag{4.8}$$

This basic channel estimates $\{\tilde{H}_k^D; k = 0, 1, \ldots, N-1\}$ can be enhanced as described for the case where $N_{TS} = N$: from $\{\tilde{h}_n^D; n = 0, 1, \ldots, N-1\} = \text{IDFT}\ \{\tilde{H}_k^D; k = 0, 1, \ldots, N-1\}$ we obtain $\{\hat{H}_k^D; k = 0, 1, \ldots, N-1\} = \text{DFT}\ \{\hat{h}_n^D = \tilde{h}_n^D w_n; n = 0, 1, \ldots, N-1\}$, with w_n defined as above. In the following, the term "enhanced channel estimates" will be employed to characterize this procedure (starting with estimates for all subcarriers, passing to the time domain where the impulse response is truncated to N_{CP} samples and back to the frequency domain). Therefore, we may write

$$\hat{H}_k^D = H_k + \epsilon_k^D, \tag{4.9}$$

with

$$E[|\epsilon_k^D|^2] = \sigma_D^2 = \frac{N_{CP}\sigma_N^2}{N \sum_{m=1}^{N_D} |S_k^{(m)}|^2}. \tag{4.10}$$

Once again we have channel estimates obtained from the training sequence, $\tilde{H}_k^{TS} = H_k + \epsilon_k^{TS}$, with variance $\sigma_{TS}^2 = \sigma_N^2/|S_k^{TS}|^2$ (for the sake of simplicity, we will assume a duration of the training sequences equal to the duration of the channel impulse response, i.e., $T_{CP} = T_D/L$, with L a power of 2). As described in Appendix A, we can combine $\tilde{H}_k^{TS}$

[1] As mentioned above, the resort to training blocks longer than the channel impulse response (e.g., with the duration of data blocks), can improve the accuracy of the channel estimates, but reduces the system's spectral efficiency.

and $\tilde{H}_k^D$ to provide the normalized channel estimates, with minimum error variance, given by

$$\tilde{H}_k^{TS,D} = \frac{\sigma_D^2 \tilde{H}_k^{TS} + \sigma_{TS}^2 \tilde{H}_k^D}{\sigma_D^2 + \sigma_{TS}^2} = H_k + \epsilon_k^{TS,D}, \tag{4.11}$$

with $E[|\epsilon_k^{TS,D}|^2] = \sigma_{TS,D}^2 = \dfrac{\sigma_D^2 \sigma_{TS}^2}{\sigma_D^2 + \sigma_{TS}^2}$.

In Fig. 4.4 we show the block diagram regarding the combination process between the $\tilde{H}_k^{TS}$ and $\tilde{H}_k^D$ channel estimates. For the first iteration, the detection of the transmitted data blocks is done using the channel estimation $\tilde{H}_k^{TS}$, resulting from detection of the training sequence. A basic channel estimation $\tilde{H}_k^D$ is then obtained by (4.8), combined with $\tilde{H}_k^{TS}$ by equation (4.11) being the resulting estimation $\tilde{H}_k^{TS,D}$ used in the detection of transmitted symbols in the next iteration. For each iteration, $\tilde{H}_k^{TS}$ and $\tilde{H}_k^D$ are combined to remove the undesirable signal components. Therefore, enhanced channel estimates are obtained by considering the data symbols as an "extended" training, and the estimation and detection phases of each iteration use the signal's most updated version.

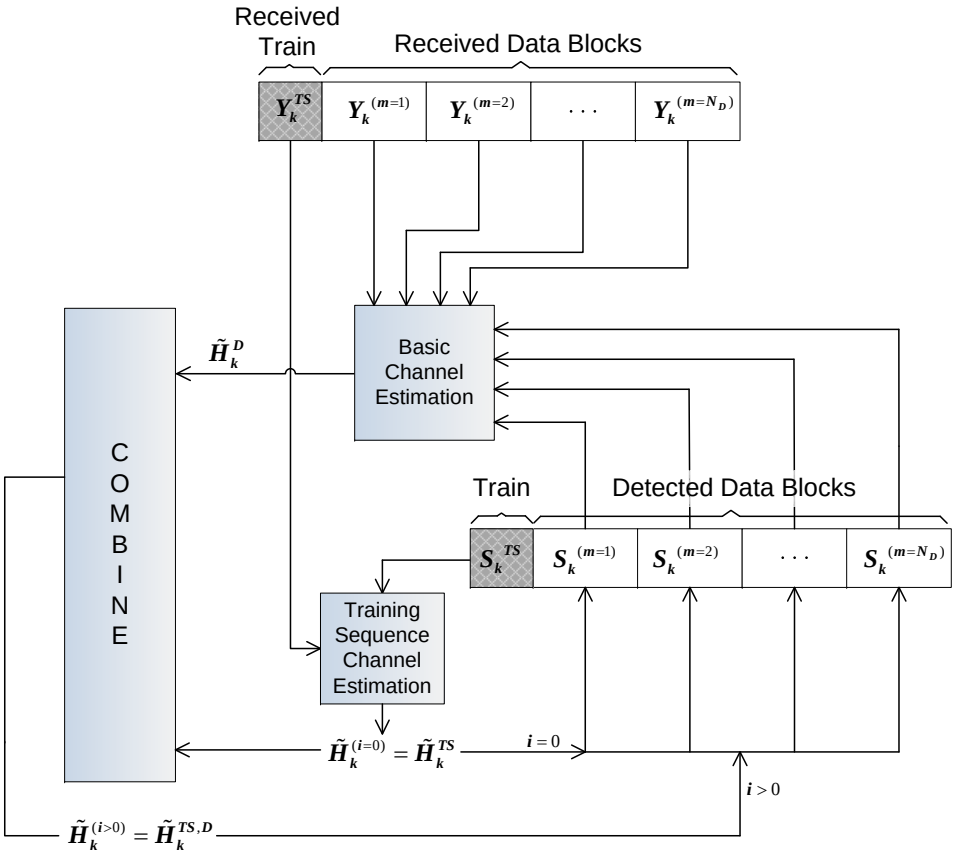

Figure 4.4: Combination scheme between $\tilde{H}_k^{TS}$ and $\tilde{H}_k^D$ channel estimates.

Of course, in realistic conditions we do not know the transmitted symbols. To overcome this problem, we may use a decision-directed channel estimation where the estimated blocks are used $\{\hat{S}_k^{(m)}; k = 0, 1, , ..., N-1\}$ in place of the transmitted blocks $\{S_k^{(m)}; k = 0, 1, , ..., N-1\}$ (naturally, for SC-FDE schemes the estimated frequency-domain block $\{\hat{S}_k^{(m)}; k = 0, 1, , ..., N-1\}$ is the DFT of the estimated time-domain block $\{\hat{s}_n^{(m)}; n = 0, 1, , ..., N-1\}$). Even so, we should take into account possible decisions errors in the data estimates. This can be done by noting that $\hat{S}_k^{(m)} \approx \rho_m S_k^{(m)} + \Delta_k^{(m)}$, with $\Delta_k^{(m)}$ uncorrelated with $S_k^{(m)}$ and $E[|\Delta_k^{(m)}|^2] = \sigma_S^2(1-\rho_m^2)$ [11]. This means that the "enhanced channel estimates" $\hat{H}_k^D$ will be based on

$$\tilde{H}_k^D = \frac{1}{\xi_k} \sum_{m=1}^{N_D} Y_k^{(m)} \hat{S}_k^{(m)*}, \tag{4.12}$$

with

$$\xi_k = \sum_{m=1}^{N_D} |\rho_m \hat{S}_k^{(m)}|^2. \tag{4.13}$$

Replacing $\hat{S}_k^{(m)}$ and $Y_k^{(m)}$ in (4.12) results

$$\begin{aligned}\tilde{H}_k^D =& \frac{1}{\xi_k} \sum_{m=1}^{N_D} (S_k^{(m)} H_k + N_k^{(m)})(\rho_m S_k^{(m)} + \Delta_k^{(m)})^* \\ =& \frac{H_k}{\xi_k} \sum_{m=1}^{N_D} \rho_m |S_k^{(m)}|^2 + \frac{1}{\xi_k}(H_k \sum_{m=1}^{N_D} S_k^{(m)} \Delta_k^{(m)*} + \sum_{m=1}^{N_D} N_k^{(m)} \rho_m S_k^{(m)*} + \sum_{m=1}^{N_D} N_k^{(m)} \Delta_k^{(m)*}).\end{aligned} \tag{4.14}$$

It can easily be shown that $\hat{H}_k^D = H_k + \epsilon_k^D$, with

$$\begin{aligned}E[|\epsilon_k^D|^2] =& \sigma_D^2 = \frac{1}{\xi_k^2}(|H_k|^2 \sum_{m=1}^{N_D} |S_k^{(m)}|^2(1-\rho_m^2)\sigma_S^2 + \sum_{m=1}^{N_D} \sigma_N^2 \rho_m^2 |S_k^{(m)}|^2 + \sum_{m=1}^{N_D} \sigma_N^2(1-\rho_m^2)\sigma_S^2) \\ \approx& \frac{1}{\xi_k^2}(|\hat{H}_k|^2 \sum_{m=1}^{N_D} |\hat{S}_k^{(m)}|^2(1-\rho_m^2)\sigma_S^2 + \sum_{m=1}^{N_D} \sigma_N^2 \rho_m^2 |\hat{S}_k^{(m)}|^2 + \sum_{m=1}^{N_D} \sigma_N^2(1-\rho_m^2)\sigma_S^2)\end{aligned} \tag{4.15}$$

As seen from Fig. 4.5, the channel estimates can be significantly improved with the combination of the decision-directed estimates with estimates based on the training sequence.

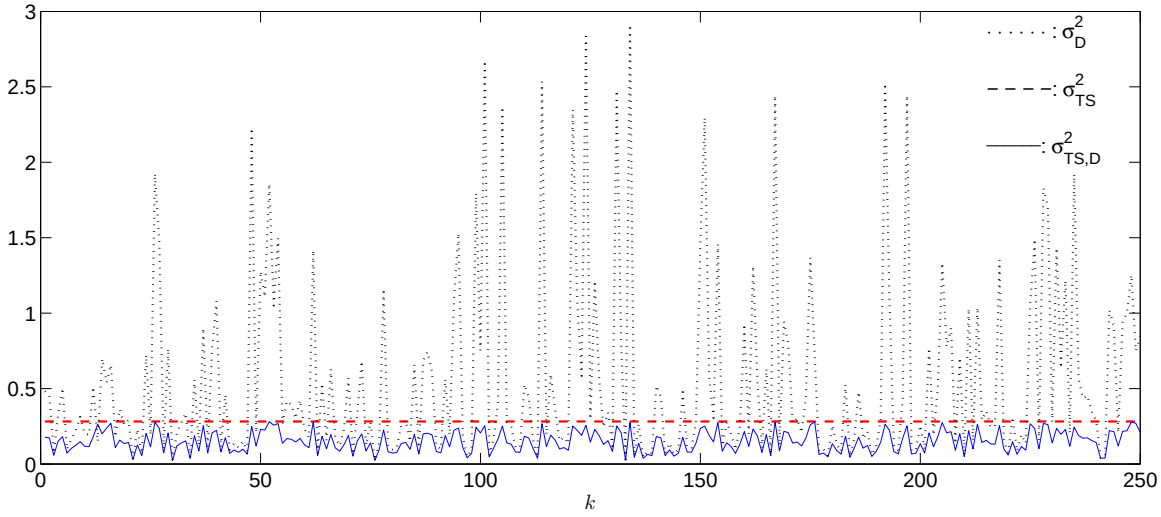

Figure 4.5: Variance of the channel estimates for the k subcarriers, with $E_b/N_0 = 20$.

4.3 Performance Results

This section presents a set of performance results concerning the proposed IB-DFE channel estimation for QPSK signals. We consider blocks of $N = 256$ data symbols and cycle prefix of 32 symbols. As channel model, is adopted a strong time dispersive channel with 32 equal power taps, with uncorrelated rayleigh fading on each tap (similar results were observed for other severely time-dispersive channels). We also assume a linear power amplification at the transmitter and perfect synchronization at the receiver.

Both uncoded and coded transmissions are considered. Once again, the channel encoder is based on a convolutional code with the polynomials generators $1 + D^2 + D^3 + D^5 + D^6$ and $1 + D + D^2 + D^3 + D^6$ and the coded bits are interleaved before being mapped into the constellation points and distributed by the symbols of the block. The receiver employed in the coded transmission is the turbo FDE defined in subsection 3.2.1.

In the following figures, we present performance results regarding channel estimation, based on a training sequence (denoted "TS" in the figures), and channel estimation using training sequence plus decision-directed channel estimation (denoted "TS+DD" in the figures). For comparison purposes, we also include the BER performance results for perfect channel estimation and for a "genie" decision-directed channel estimation (i.e., the receiver knows the transmitted symbols).

Figs. 4.6 and 4.7 show the uncoded BER performance for $N_D = 1$ and $N_D = 4$, respectively. Figs. 4.8 and 4.9 show the corresponding coded performances for a turbo FDE (i.e., an IB-DFE that used the channel decoder in the feedback loop). As expected, the IB-DFE outperforms the linear FDE (corresponding to the first iteration of the IB-DFE). In fact, the channel estimates are more accurate for higher values of N_D (i.e., when we use more data blocks in the decision-directed estimation). This is a consequence of the higher power of the overall signals, as well as the lower probability of having $\sum_{m=1}^{N_D} |S_k^{(m)}|^2 \approx 0$ when N_D is high.

Fig. 4.10 shows the required value of E_b/N_0 for BER=10^{-4}, that includes the power spent on the training sequence and cyclic prefix, for both the training and the data when N_D=1. Let β denote the relation between the average power of the training sequences, and the data power. From this figure, we can conclude that the optimum value is $\beta \approx 1$. The lower probability of $\sum_{m=1}^{N_D} |S_k^{(m)}|^2 \approx 0$, for higher values of N_D, also justifies the power gain of 1dB of $N_D = 4$ over $N_D = 1$ for 4 iterations. From Fig. 4.11, regarding the coded case, results an optimum value of $\beta \approx 2$.

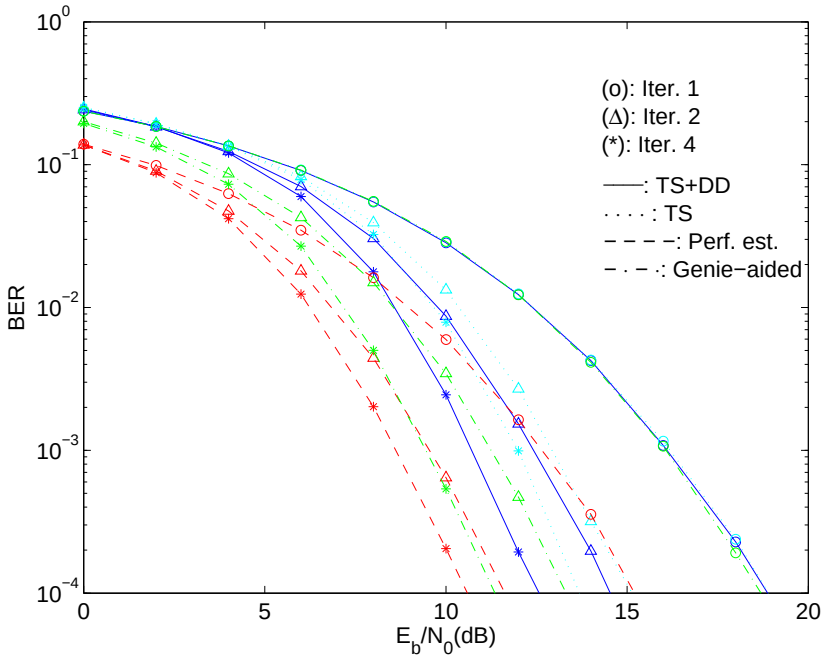

Figure 4.6: BER performance for uncoded SC-FDE with $N_D = 1$ block and $\beta = 1$.

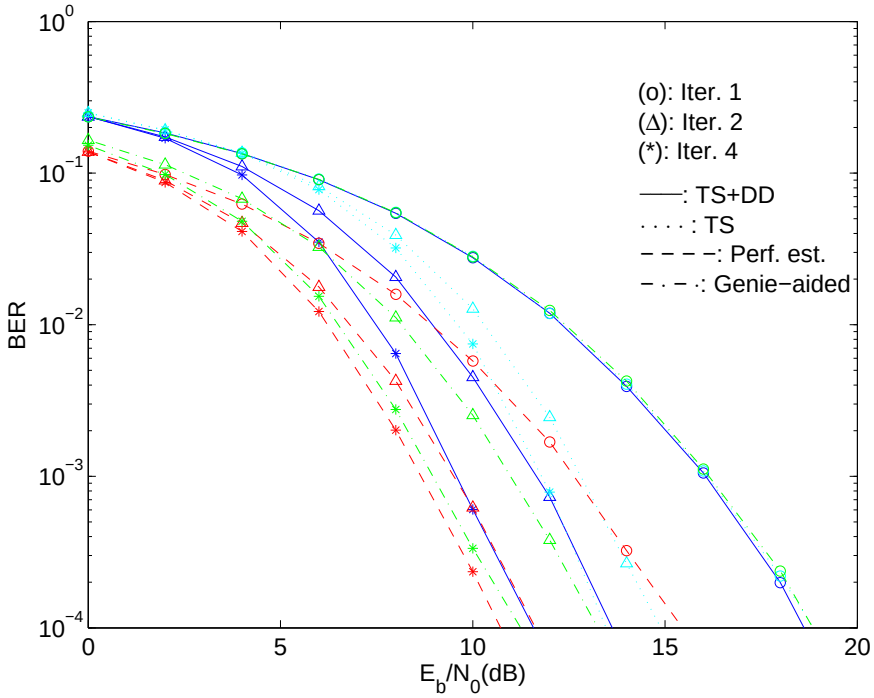

Figure 4.7: BER performance for uncoded SC-FDE with $N_D = 4$ blocks and $\beta = 1$.

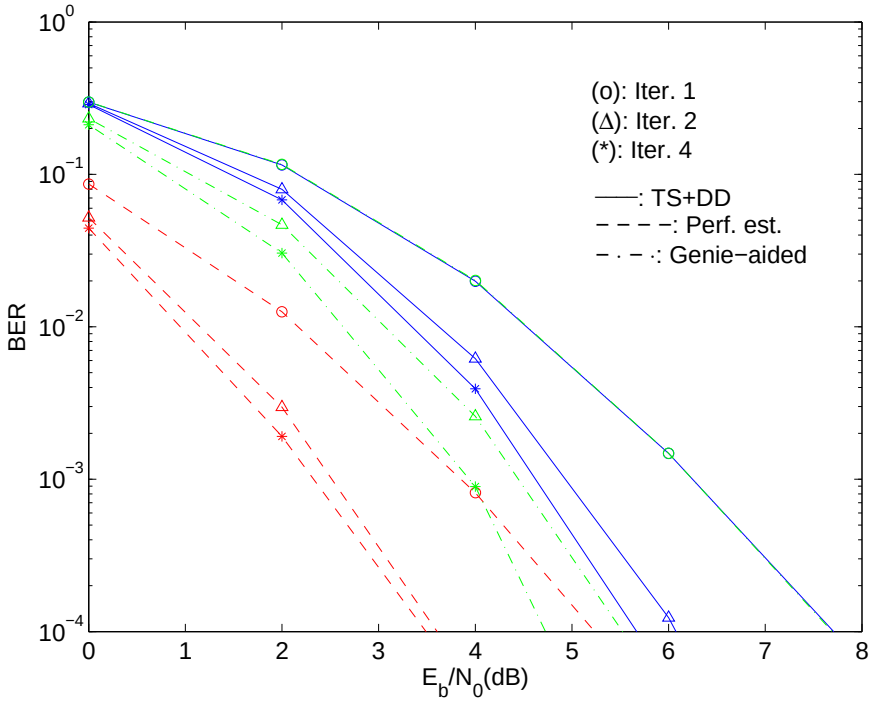

Figure 4.8: BER performance for coded SC-FDE with $N_D = 1$ block and $\beta = 2$.

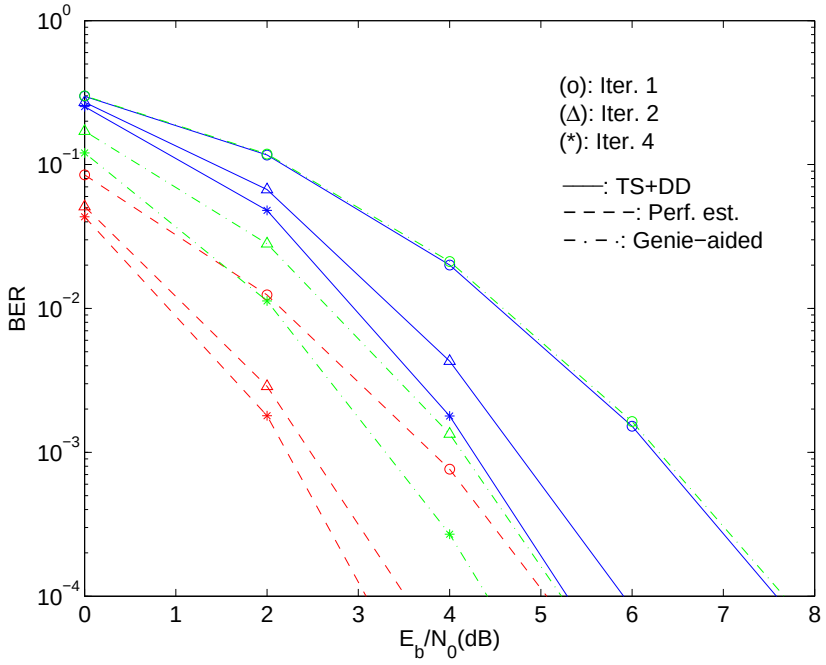

Figure 4.9: BER performance for coded SC-FDE with $N_D = 4$ blocks and $\beta = 2$.

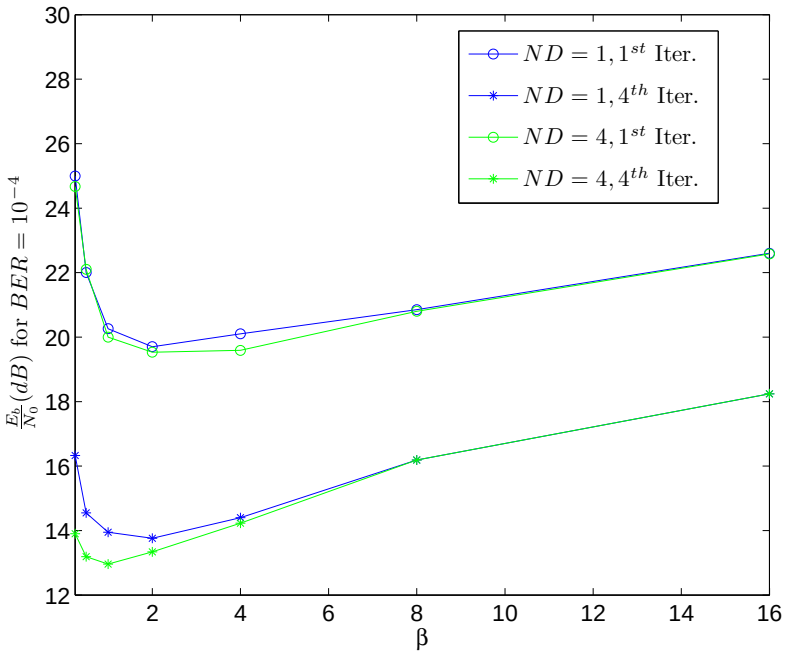

Figure 4.10: Required E_b/N_0 to achieve $BER = 10^{-4}$ without convolutional code, as function of β: IB-DFE with 1 and 4 iterations.

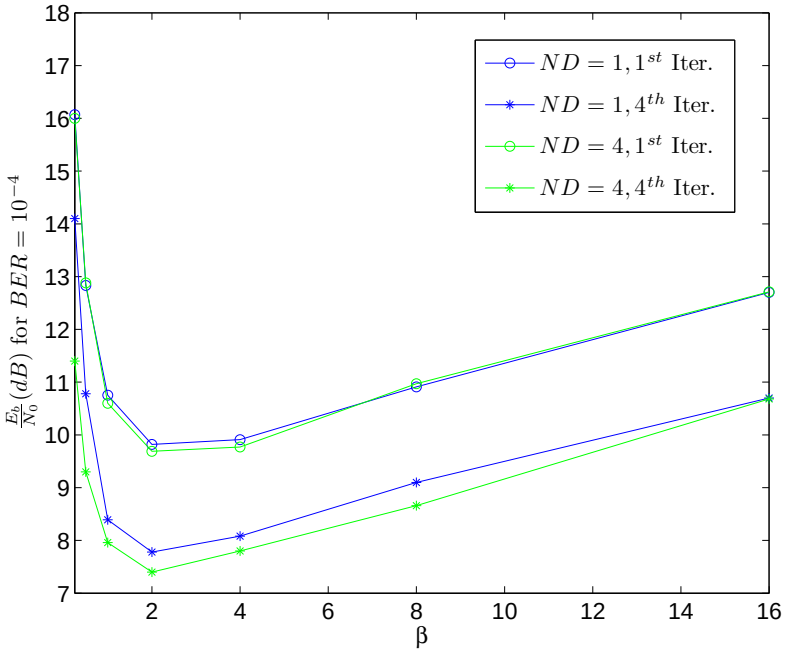

Figure 4.11: Required E_b/N_0 to achieve $BER = 10^{-4}$ with convolutional code, as function of β: IB-DFE with 1 and 4 iterations.

Chapter 5

Correlation Coefficient Estimation

As shown in the previous chapters, the correlation factor is a key parameter for the good performance of IB-DFE receivers. However, contrarily to the channel frequency response, it changes from block to block and iteration to iteration. Therefore, it cannot be computed using reference blocks and needs to be obtained from the equalized output.

In this chapter we present several methods to estimate the correlation coefficient. The correlation coefficient $\rho^{(i-1)}$ was defined in (3.8), and is reproduced here in (5.1) by convenience (for the sake of simplicity, the iteration number i will be ignored in the following equations)

$$\rho = \frac{E\left[\hat{s}_n s_n^*\right]}{E\left[|s_n|^2\right]} = \frac{E\left[\hat{S}_k S_k^*\right]}{E\left[|S_k|^2\right]}. \tag{5.1}$$

Let us consider the transmitted symbols $\{s_n; n = 0, ..., N-1\}$ corresponding to a QPSK constellation, under a Gray mapping rule. Therefore, the s_n may be written as

$$s_n = s_n^I + s_n^Q = \pm d \pm jd, \tag{5.2}$$

in which

$$s_n^I = \mathrm{Re}\{s_n\}, \tag{5.3}$$

is the "in-phase" component of s_n, and

$$s_n^Q = \mathrm{Im}\{s_n\}, \tag{5.4}$$

is the "quadrature" component of s_n. Also, d is given by

$$d = \frac{D}{2}, \tag{5.5}$$

where D denotes the minimum Euclidean distance between two constellation symbols. Under these conditions,

$$E\left[|s_n|^2\right] = \frac{D^2}{4}. \tag{5.6}$$

The time-domain samples at the FDE's output are given by

$$\tilde{s}_n = \tilde{s}_n^I + \tilde{s}_n^Q = s_n + \theta_n, \tag{5.7}$$

where θ_n denotes the global error term, which is Gaussian-distributed, with zero-mean. The symbol estimates are then given by

$$\hat{s}_n = s_n + \vartheta_n^I + j\vartheta_n^Q, \tag{5.8}$$

where ϑ_n^I denotes the error coefficient in $\hat{s}_n^I$ and ϑ_n^Q denotes the error coefficient in $\hat{s}_n^Q$. Clearly, if $\hat{s}_n^I$ and $\hat{s}_n^Q$ have no errors, then ϑ_n^I and ϑ_n^Q are null. On the other hand, if there are errors then the value of ϑ_n^I and/or ϑ_n^Q will be $\pm D$. Consequently, ϑ_n^I and ϑ_n^Q are random variables, with values 0, $+D$ and $-D$ with probabilities $1 - 2P_e$, P_e and P_e respectively, where P_e denotes the bit error rate. Therefore, it can be shown that

$$\rho = 1 - 2P_e. \tag{5.9}$$

Naturally, in practice we do not know the transmitted symbols $\{s_n; n = 0, ..., N-1\}$.

5.1 Method I: Estimation based on the BER estimate

The total variance of the overall noise plus residual ISI, σ^2_{Eq}, is given by

$$\sigma^2_{Eq} = \frac{1}{2}E\left[\left|s_n - \tilde{s}_n\right|^2\right]. \tag{5.10}$$

The exact value of σ^2_{Eq} can not be used in practice, because we do not know the transmitted symbols $\{s_n; n = 0, ..., N-1\}$. Therefore, we may use an approximated value of σ^2_{Eq}, given by

$$\hat{\sigma}^2_{Eq} = \frac{1}{2N}\sum_{n=0}^{N-1}|\hat{s}_n - \tilde{s}_n|^2. \tag{5.11}$$

Provided that the numbers of decision errors in $\hat{s}_n$ is small and N is high, we have

$$\sigma^2_{Eq} \approx \hat{\sigma}^2_{Eq}. \tag{5.12}$$

For a QPSK constellation, the estimated BER, denoted by $\hat{P}_e$, can be approximated by

$$\hat{P}_e \approx Q\left(\frac{1}{\hat{\sigma}_{Eq}}\right), \tag{5.13}$$

where $Q(x)$ denotes the Q function, and from (5.9), the estimated value of ρ will be

$$\hat{\rho} = 1 - 2\hat{P}_e. \tag{5.14}$$

In the following, we present a set of results obtained during the research of the impact of the correlation coefficient estimation on the performance of IB-DFE receivers, for 10 iterations, for a given channel realization. We consider uncoded transmissions of FFT-blocks with $N = 1024$ data symbols, selected from a QPSK constellation under a Gray mapping rule. Similar results were observed for other values of N, provided that $N >> 1$. Fig. 5.1 presents the evolution of the correlation coefficient for values of E_b/N_0. The results show the differences between the ideal value of the correlation coefficient (obtained with (5.1)), and the estimated value (obtained by (5.14)). As we can see, the $\hat{\rho}$ curve suffered a deviation from the curve corresponding to the evolution of the optimum (true) correlation coefficient. This deviation is due to the use of optimistic estimates of the

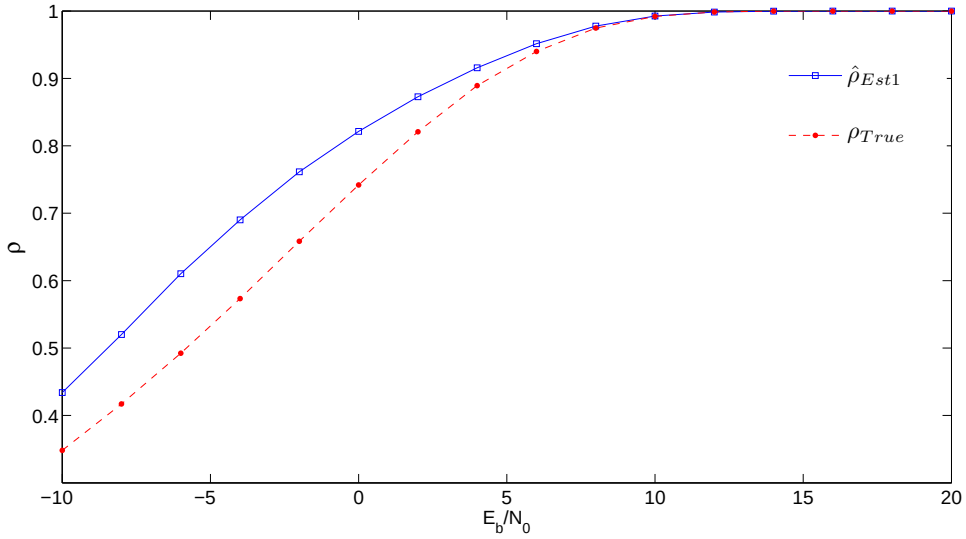

Figure 5.1: Evolution of ρ as function of the E_b/N_0 for method I.

transmitted symbols in the feedback loop, due to the optimistic P_e derivation, in its turn calculated with resort to the approximated value $\hat{\sigma}_{Eq}$. Fig. 5.2 shows the evolution of the variance σ_{Eq}, for values of the corresponding BER. From the figure it is obvious that $\hat{\sigma}_{Eq}$ has lower values relatively to the optimum σ_{Eq}. Fig. 5.3 presents the evolution of the variance σ_{Eq}, for values of the corresponding E_b/N_0, and the results illustrate the inaccuracy of the approximated $\hat{\sigma}_{Eq}$.

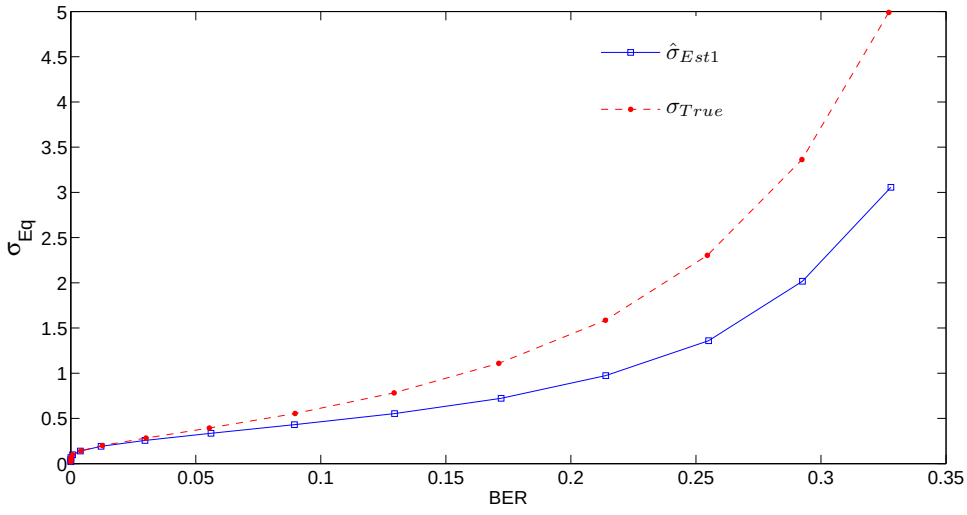

Figure 5.2: Evolution of σ_{Eq} as function of the BER for method I.

In Fig. 5.4 we present the performance results, expressed as function of E_b/N_0, where N_0 is the one-sided power spectral density of the noise and E_b is the energy of the transmit-

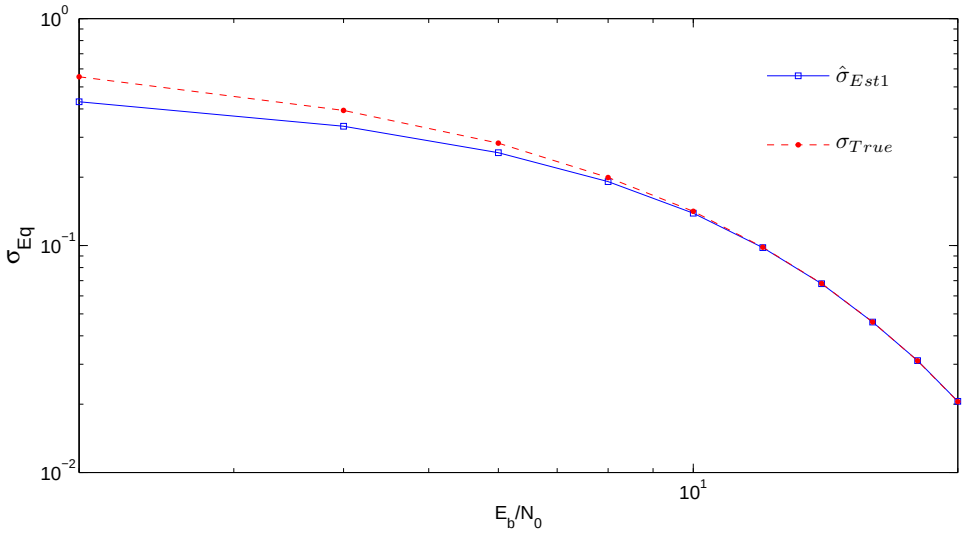

Figure 5.3: Evolution of σ_{Eq} as function of the E_b/N_0 for method I.

ted bits (i.e., the degradation due to the useless power spent on the cyclic prefix is not included). We present performance results corresponding to a scenario where the IB-DFE suffers from error propagation.

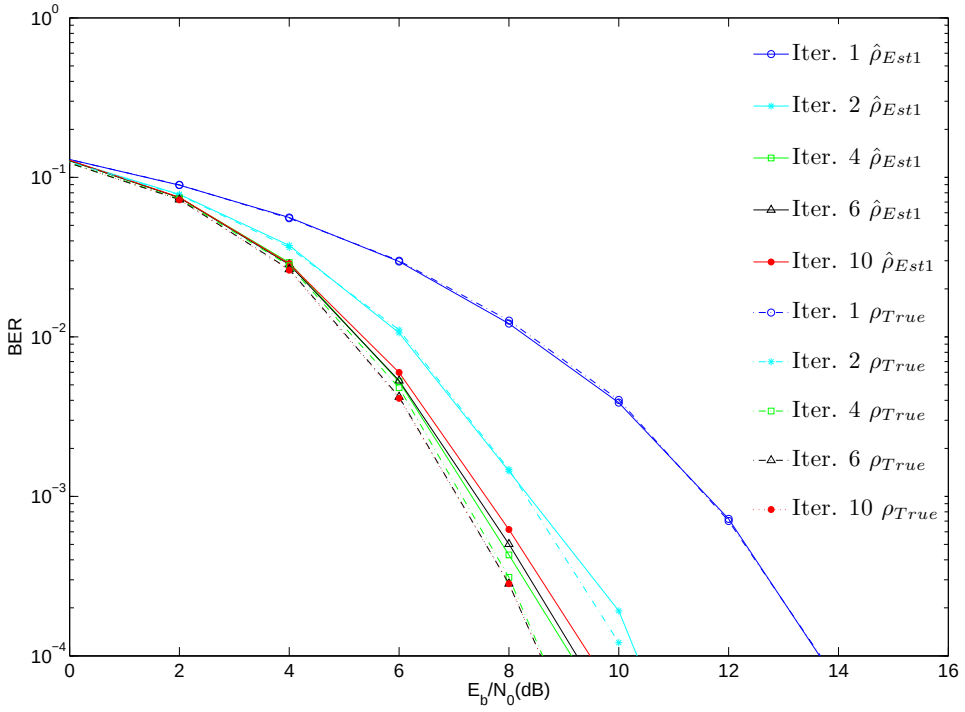

Figure 5.4: BER perfomance for method I.

Fig. 5.5 presents the required BER to achieve $E_b/N_0 = 9$ (dB) as a function of the iterations number. Clearly, there is a performance degradation after a few iterations.

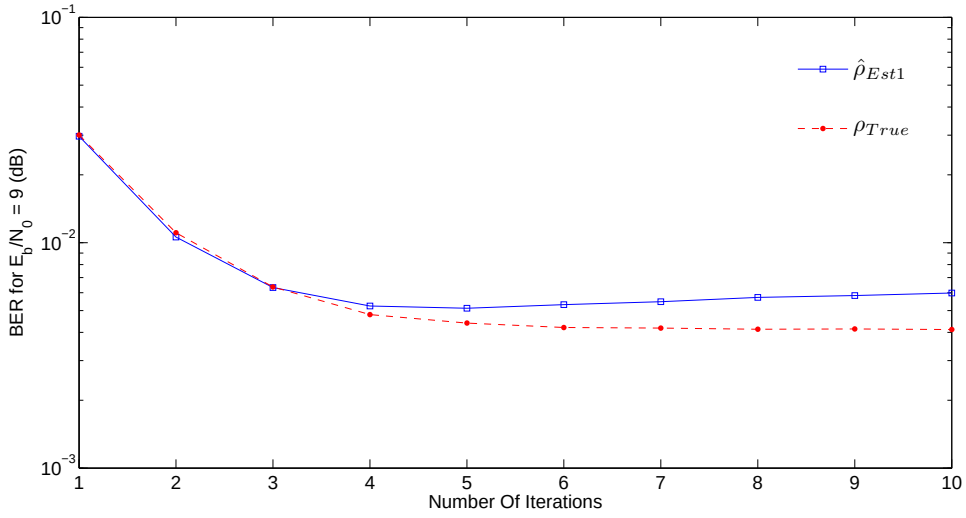

Figure 5.5: Required BER to achieve $E_b/N_0 = 9$ (dB) as a function of the iterations number for method I.

Although the approximation in (5.12) may seem reliable, the true value of σ^2_{Eq} is in fact higher than the estimated one due to decision errors. Consequently, the estimated BER, $\hat{P}_e$, is lower then the true bit error rate, P_e, leading to,

$$\hat{\rho} \geq \rho, \tag{5.15}$$

i.e., we are assuming that the estimates used in the feedback loop are more reliable then what they are in fact.

It should be pointed out that while underestimating ρ (i.e., using $\hat{\rho} < \rho$) leads to a slower convergence of the IB-DFE, overestimating ρ (i.e., using $\hat{\rho} > \rho$) leads to a fast convergence but worse BER values.

5.2 Method II: Estimation based on the LLR

This technique consists in the estimation of the correlation coefficient with resort to the LLRs (Log-Likelihood Ratio), as derived in chapter 3. However, as in method I, an approximated value for the variance of channel and interference noise is considered, instead of the optimum value.

$$\hat{\sigma}_{Eq}^2 = \frac{1}{2N}\sum_{n=0}^{N-1}|\hat{s}_n - \tilde{s}_n|^2. \tag{5.16}$$

The calculation of the LLRs of the "in-phase bit" and the "quadrature bit", associated to s_n^I and s_n^Q, respectively, are based in, $\hat{\sigma}_{Eq}^2$, and given by

$$\hat{L}_n^I = \frac{2}{\hat{\sigma}_{Eq}^2}\tilde{s}_n^I, \tag{5.17}$$

and

$$\hat{L}_n^Q = \frac{2}{\hat{\sigma}_{Eq}^2}\tilde{s}_n^Q. \tag{5.18}$$

The reliabilities related to the "in-phase bit" and the "quadrature bit" of the n^{th} symbol, are given by

$$\hat{\rho}_n^I = \left|\tanh\left(\frac{\hat{L}_n^I}{2}\right)\right|, \tag{5.19}$$

and

$$\hat{\rho}_n^Q = \left|\tanh\left(\frac{\hat{L}_n^Q}{2}\right)\right|. \tag{5.20}$$

Therefore, the estimated value of the correlation coefficient will be given by

$$\hat{\rho} = \frac{1}{2N}\sum_{n=0}^{N-1}(\hat{\rho}_n^I + \hat{\rho}_n^Q). \tag{5.21}$$

We now present a set of results referring to this method, obtained during the research on the impact of the correlation coefficient estimation on the performance of IB-DFE receivers, for 10 iterations, and employing the same simulation parameters as in method I.

Fig. 5.6 presents the evolution of the correlation coefficient for values of E_b/N_0. As for the method I, the deviation on the $\hat{\rho}$ curve relatively to the optimum (true) ρ curve indicates the inaccuracy of the reliability measure used in the feedback loop, caused by a approximated version of σ_{Eq} used in the calculation of LLRs. Fig. 5.7 shows the evolution of the variance σ_{Eq} for values of the corresponding BER. Also for this method, the figure shows that $\hat{\sigma}_{Eq}$ has lower values when compared to the optimum σ_{Eq}. Fig. 5.8 presents

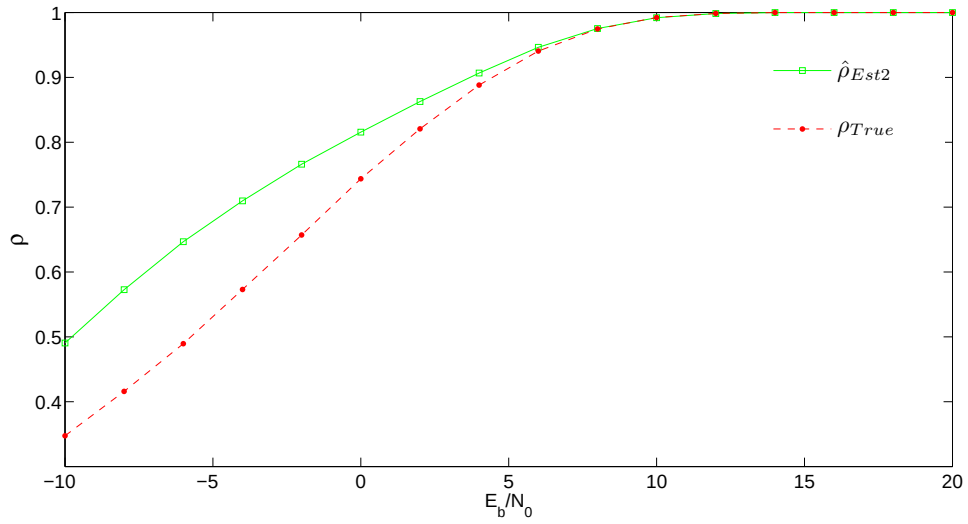

Figure 5.6: Evolution of ρ as function of the E_b/N_0 for method II.

the evolution of the variance $\hat{\sigma}_{Eq}$, for values of the corresponding E_b/N_0, and as expected the results show the inaccuracy of the approximated $\hat{\sigma}_{Eq}$.

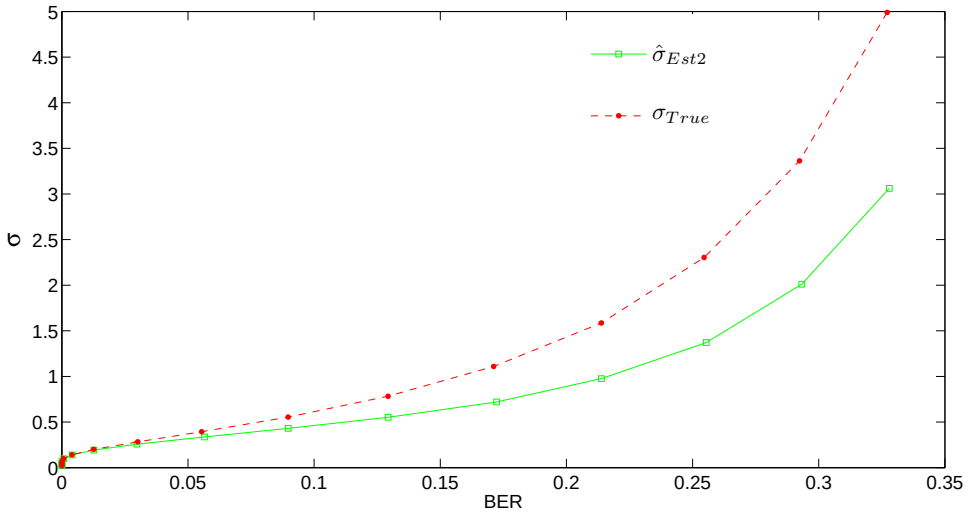

Figure 5.7: Evolution of σ_{Eq} as function of the BER for method II.

In Fig. 5.9 we present the performance results, expressed as function of E_b/N_0, where N_0 is the one-sided power spectral density of the noise and E_b is the energy of the transmitted bits (i.e., the degradation due to the useless power spent on the cyclic prefix is not included). We present performance results corresponding to a scenario where the IB-DFE suffers from error propagation. Fig. 5.10 presents the required BER to achieve $E_b/N_0 = 9$ (dB) as a function of the iterations number. As in method I, there is a performance degradation after a few iterations.

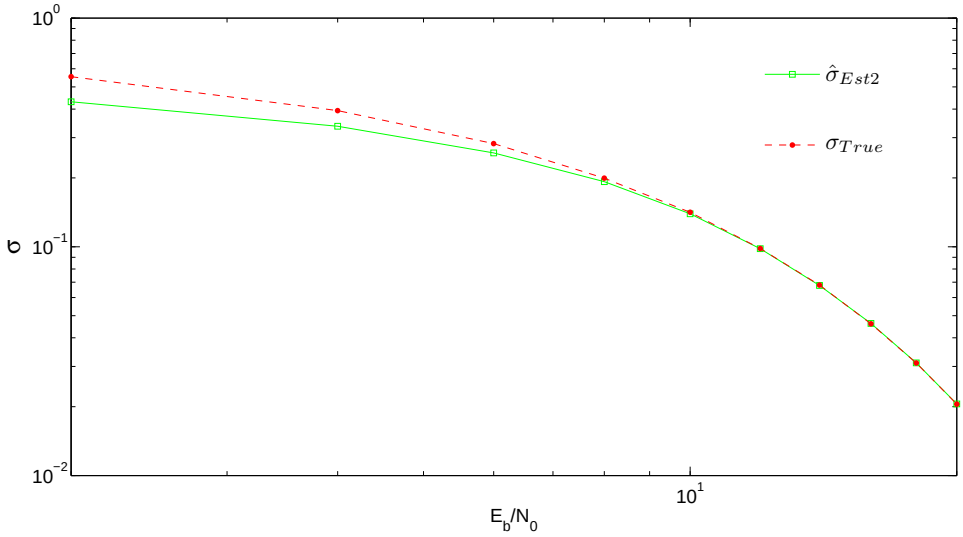

Figure 5.8: Evolution of σ_{Eq} as function of the E_b/N_0 for method II.

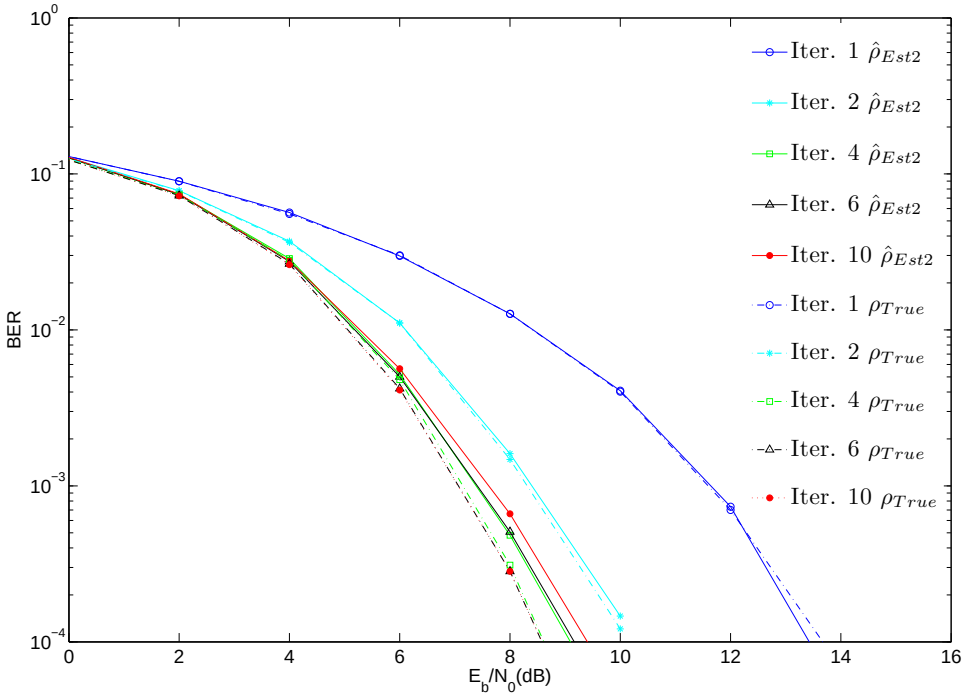

Figure 5.9: BER perfomance for method II.

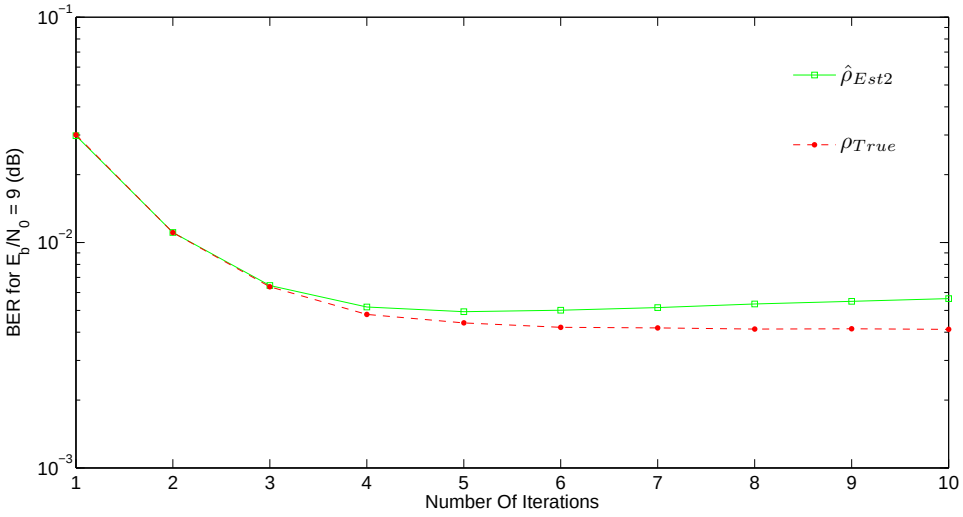

Figure 5.10: Required BER to achieve $E_b/N_0 = 9$ (dB) as a function of the iterations number for method II.

5.3 Method III: Estimation based on the MSE

This estimation method is based on the same technique employed in the method I, given by equation (5.13). However, unlike method I, the BER calculation employs the MSE (Mean-Squared Error) of the equalized samples, instead of an approximated value for the channels variance's and interference noise. Therefore, in method III the estimated bit error rate denoted by $\hat{P}_e$, is given by

$$\hat{P}_e = Q\left(\sqrt{\frac{|\gamma|^2 \cdot E\left[|S_k|^2\right]}{\sigma^2_{\text{MSE}}}}\right). \tag{5.22}$$

Once again, assuming a QPSK constellation with a Gray mapping and $s_n = \pm 1 \pm j$, then (5.22) can be written as

$$\hat{P}_e = Q\left(\frac{|\gamma|}{\sqrt{\sigma^2_{\text{MSE}}}}\right), \tag{5.23}$$

where σ^2_{MSE} corresponds to the MSE, defined in (2.36), and reproduced here for convenience in (5.24),

$$\sigma^2_{\text{MSE}} = \frac{1}{N^2} \sum_{k=0}^{N-1} \Theta_k, \tag{5.24}$$

where

$$\Theta_k = E\left[|\tilde{S}_k - S_k|^2\right]. \tag{5.25}$$

By combining (2.32), (3.7), (3.17) and (3.18), and assuming that $E\left[|N_k \cdot \Delta_k^*|\right] = 0$, $E\left[|N_k \cdot S_k^*|\right] = 0$ and $E\left[|S_k \cdot \Delta_k^*|\right] = 0$, we can rewrite (5.25) as

$$\begin{aligned}
\Theta_k &= E\left[|\tilde{S}_k - S_k|^2\right] \\
&= E\left[|F_k S_k H_k + F_k N_k - B_k \rho \hat{S}_k - S_k|^2\right] \\
&= E\left[|F_k H_k - B_k \rho^2 - 1|^2\right] 2\sigma_S^2 + E\left[|F_k|^2\right] 2\sigma_N^2 + E\left[|B_k|^2\right] \rho^2 (1-\rho^2) 2\sigma_S^2,
\end{aligned} \tag{5.26}$$

where the variance of the transmitted frequency-domain data symbols is given by

$$\sigma_S^2 = \frac{E\left[|S_k|^2\right]}{2},$$

the variance of the channel noise is obtained by

$$\sigma_N^2 = \frac{E\left[|N_k|^2\right]}{2},$$

and the expected value of the error term for the k^{th} frequency-domain "hard decision" estimate is defined as

$$\sigma_S^2(1-\rho^2) = E\left[|\Delta_k|^2\right],$$

and the estimated value of ρ can be expressed by

$$\hat{\rho} = 1 - 2\hat{P}_e, \tag{5.27}$$

with $\hat{P}_e$ given by (5.23).

We now present a set of results referring to this method, obtained during the research on the impact of the correlation coefficient estimation on the performance of IB-DFE re-

ceivers, for 10 iterations, and employing the same simulation parameters as in the previous methods.

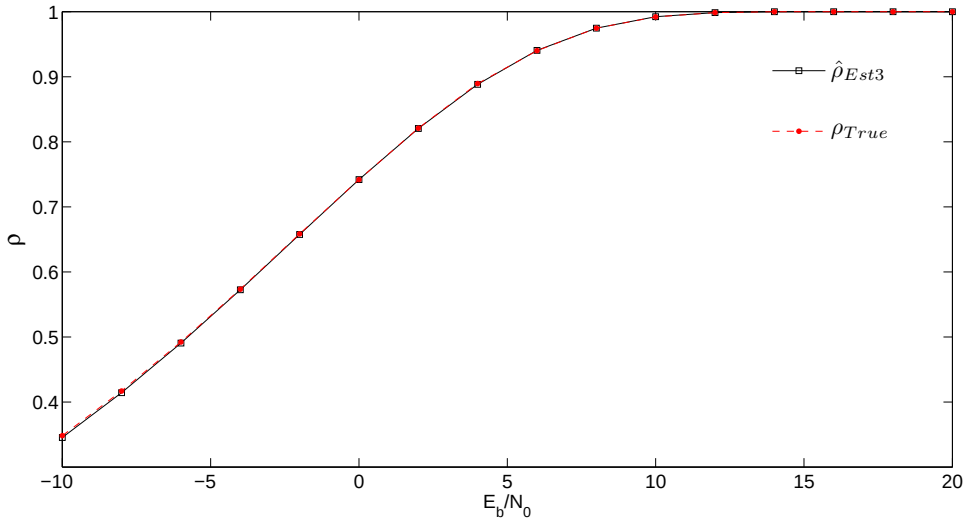

Figure 5.11: Evolution of ρ as function of the E_b/N_0 for method III.

Fig. 5.11 presents the evolution of the correlation coefficient for values of E_b/N_0. Unlike methods I and II, now the $\hat{\rho}$ curve is very close to the optimum (true) ρ curve. This means that the reliability measure estimation, with resort to the MSE, used in the feedback loop is very accurate. Figs. 5.12 and 5.13 are presented for comparison purposes only, since that the variance of channel and interference noise estimation, $\hat{\sigma}_{Eq}$, is not considered in the estimation process of method III.

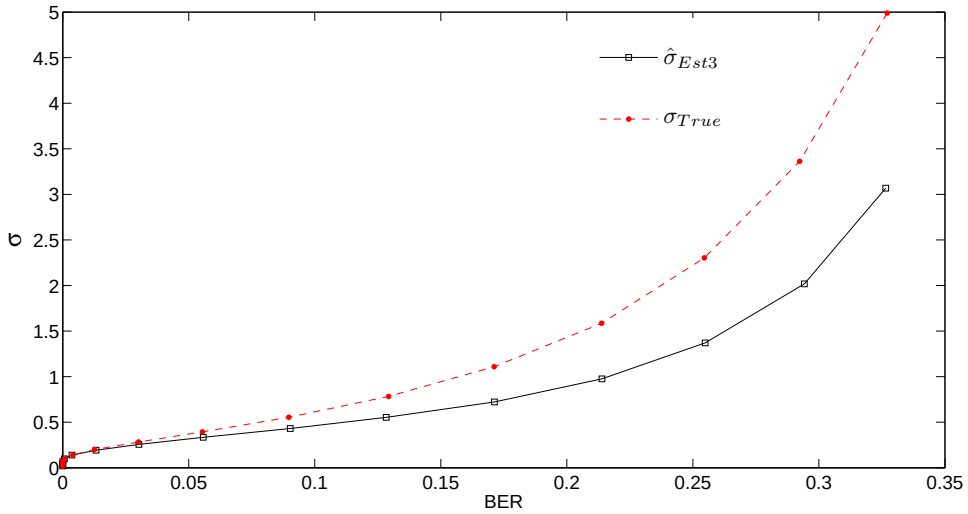

Figure 5.12: Evolution of σ_{Eq} as function of the BER for method III.

In Fig. 5.14 we present the performance results, expressed as function of E_b/N_0, where

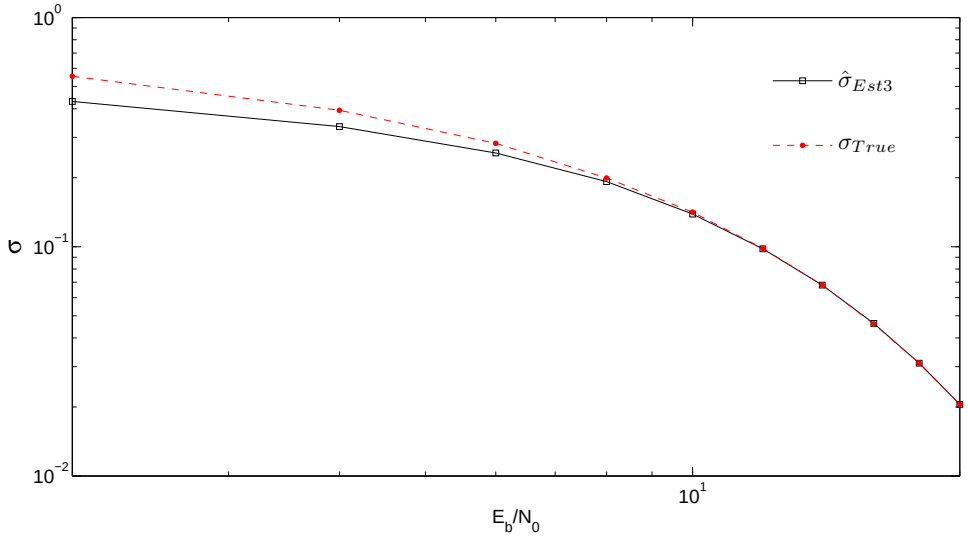

Figure 5.13: Evolution of σ_{Eq} as function of the E_b/N_0 for method III.

N_0 is the one-sided power spectral density of the noise and E_b is the energy of the transmitted bits (i.e., the degradation due to the useless power spent on the cyclic prefix is not included). We present performance results corresponding to a scenario where the IB-DFE suffers from error propagation.

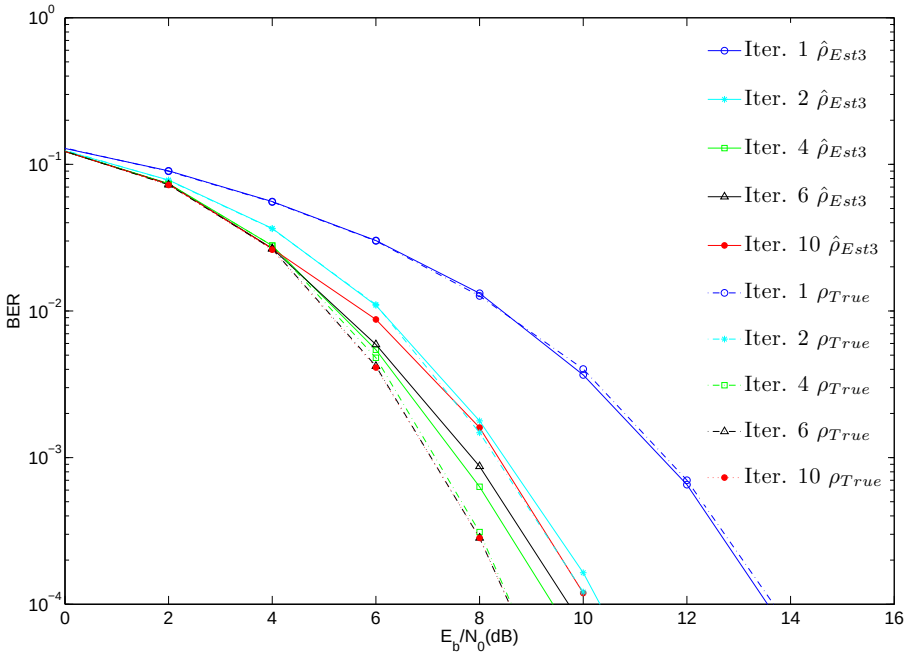

Figure 5.14: BER perfomance for method III.

Fig. 5.15 presents the required BER to achieve $E_b/N_0 = 9$ (dB) as a function of the

iterations number. As in methods I and II, there is a performance degradation after a few iterations.

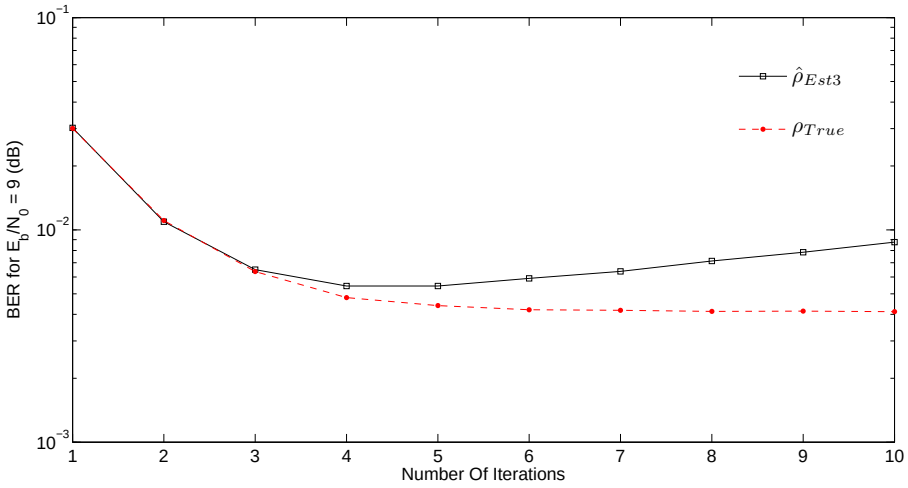

Figure 5.15: Required BER to achieve $E_b/N_0 = 9$ (dB) as a function of the iterations number for method III.

5.4 Correlation Coefficient Compensation

To overcome the problem of using an optimistic version of transmitted symbols estimates in the feedback loop, we propose a technique to compensate the inaccuracy of the correlation coefficient estimation.

The compensation factor denoted, by $\chi(\hat{\rho})$, can be expressed as

$$\chi(\hat{\rho}) = \frac{\hat{\rho}}{\rho}, \tag{5.28}$$

where $\hat{\rho}$ is the estimated correlation coefficient derived from a given estimation method. Although the same compensation factor calculation is used for all methods, we will present the results obtained individually for each method.

5.4.1 Method I with Compensation

Lets start by method I. The curve in Fig. 5.16, obtained by simulation, shows the relation between the correlation coefficient estimation, $\hat{\rho}$, and the compensation factor, $\chi(\hat{\rho})$.

Clearly, we can determine the value of the compensation factor $\chi(\hat{\rho})$ for each correspondent

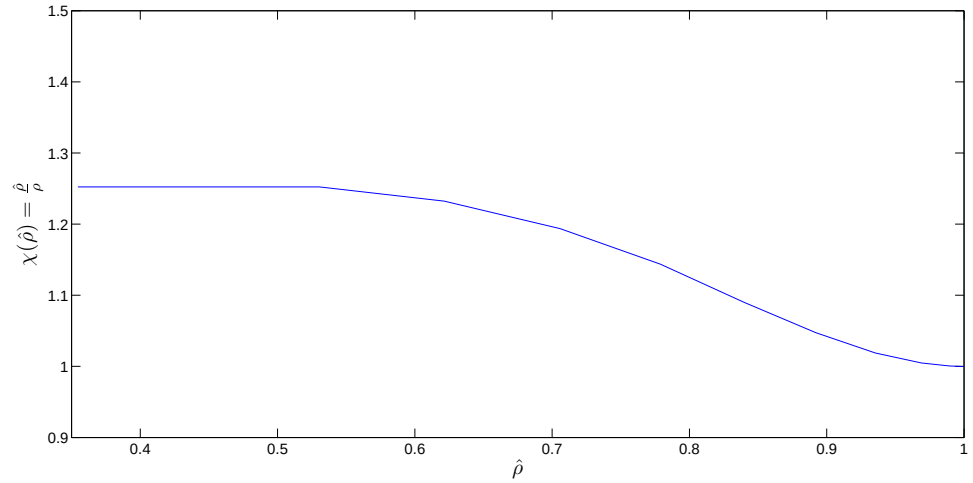

Figure 5.16: Relation between the correlation coefficient estimation and the compensation factor for method I

value of $\hat{\rho}$, by a simple interpretation of the plot presented in Fig. 5.16. Thus, by knowing $\chi(\hat{\rho})$ we can determine a very precise estimated version of the optimum correlation factor given by

$$\rho \approx \rho_{Est+Comp} = \frac{\hat{\rho}}{\chi(\hat{\rho})}, \tag{5.29}$$

where $\rho_{Est+Comp}$ denotes the compensated correlation coefficient. Therefore, $\rho_{Est+Comp}$ can now be used in the derivation of the feedback and feedforward coefficients parameters of the IB-DFE receiver.

In the following, we present a set of performance results obtained with the compensation of the correlation coefficient estimation, $\rho_{Est+Comp}$, corresponding to method I. For comparison purposes the corresponding results without compensation are also included in the figures.

Fig. 5.17 presents the evolution of the correlation coefficient as function of E_b/N_0. As we can see, the correlation coefficient with compensation (denoted $\hat{\rho}_{Est1+Comp}$ in the figure) is very close to the curve corresponding to the optimum (true) correlation coefficient evolution. This demonstrates that the inaccuracy due to use of optimistic estimates of the transmitted symbols in the feedback loop, can be efficiently avoided with resort to the proposed compensation technique.

In Fig. 5.18 we present the BER performance results. The improvements obtained with compensation are very significative, since that the performance curves obtained with the

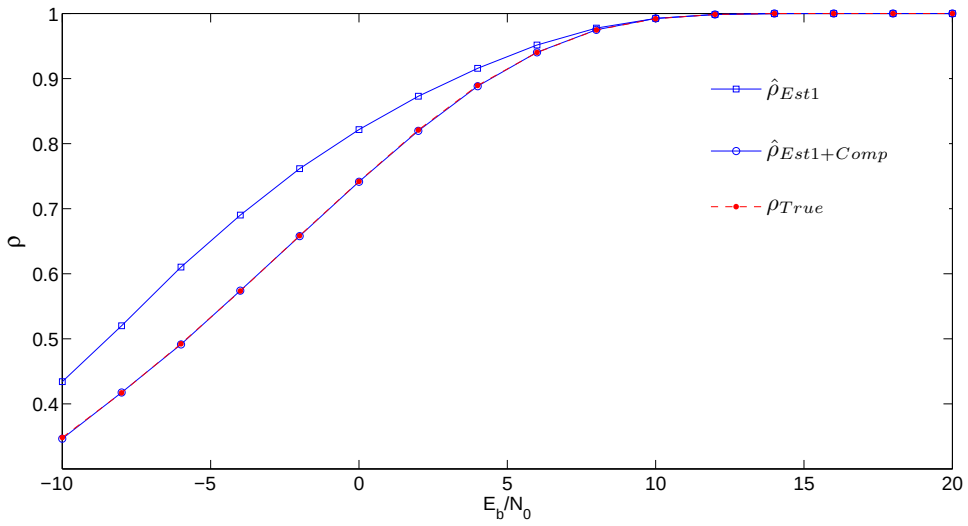

Figure 5.17: Evolution of ρ as function of the E_b/N_0 for method I.

compensated correlation coefficient (denoted "$\rho_{Est1+Comp}$" in the figures), are very close to those obtained with optimum (true) correlation coefficient (denoted "ρ_{True}" in the figures). Fig. 5.19 presents the required BER to achieve $E_b/N_0 = 9$ (dB) as a function of the iterations number. Clearly, there is a performance enhancement when compared with the correlation coefficient estimates without compensation.

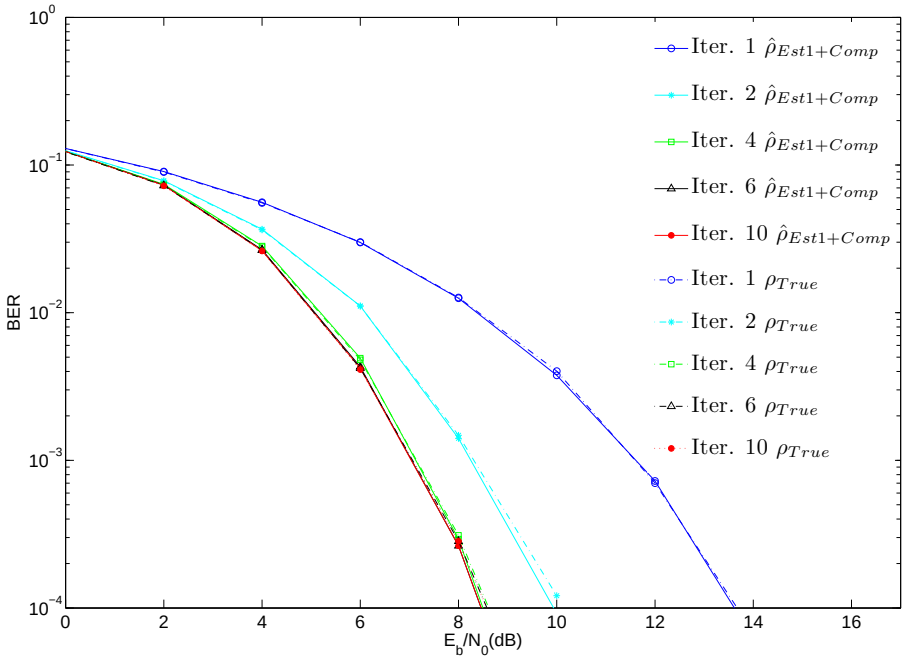

Figure 5.18: BER perfomance for method I.

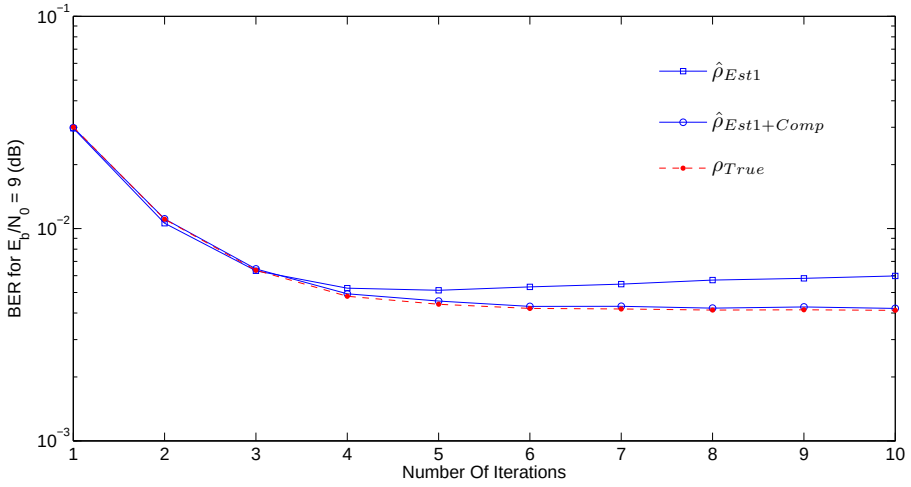

Figure 5.19: Required BER to achieve $E_b/N_0 = 9$ (dB) as a function of the iterations number for method I.

5.4.2 Method II with Compensation

Lets now consider the method II. The curve in Fig. 5.20, obtained by simulation, shows the relation between the correlation coefficient estimation, $\hat{\rho}$, and the compensation factor $\chi(\hat{\rho})$.

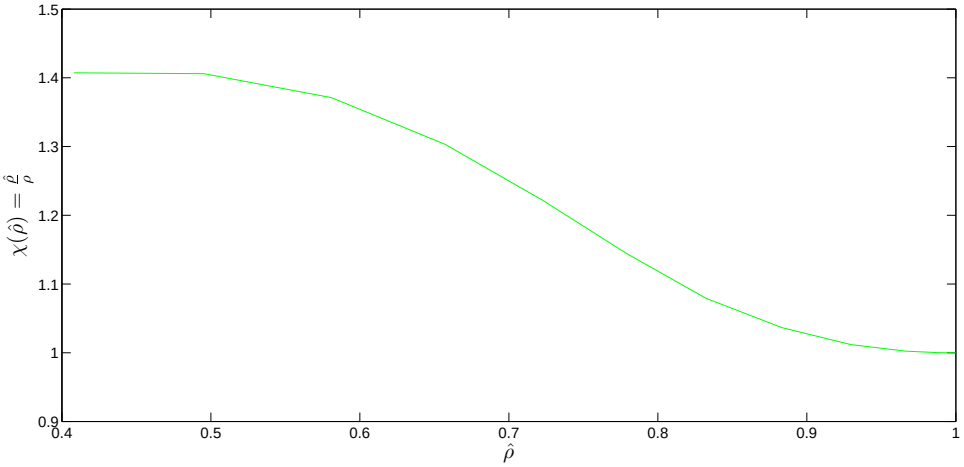

Figure 5.20: Relation between the correlation coefficient estimation and the compensation factor for method II.

As in method I, we can determine the value of the compensation factor $\chi(\hat{\rho})$ for each correspondent value of $\hat{\rho}$, with resort to the plot of Fig. 5.20. Therefore, by knowing $\chi(\hat{\rho})$ we can obtain $\rho_{\text{Est+Comp}}$, given by (5.28), which in turn will be used in the derivation of the feedback and feedforward coefficients parameters of the IB-DFE receiver.

Next, we present the results obtained with the compensation of the correlation coefficient estimation, $\rho_{Est+Comp}$, corresponding to method II. For comparison purposes the corresponding results without compensation are also shown.

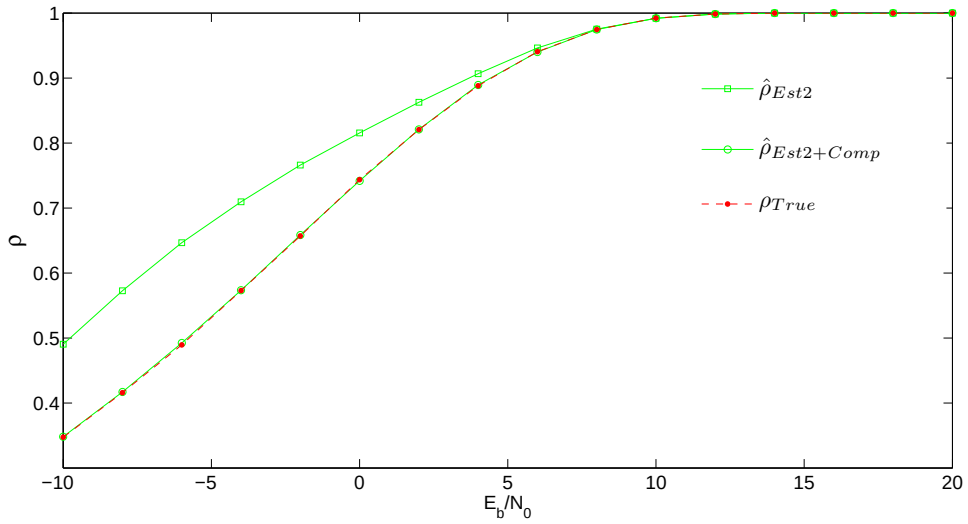

Figure 5.21: Evolution of ρ as function of the E_b/N_0 for method II.

Fig. 5.21 presents the evolution of the correlation coefficient for values of E_b/N_0. Clearly, the correlation coefficient with compensation (denoted $\hat{\rho}_{Est2+Comp}$ in the figure) is very close to the curve corresponding to the optimum (true) correlation coefficient evolution, which confirms that the inaccuracy due to use of optimistic estimates of the transmitted symbols in the feedback loop, can be efficiently avoided with resort to the proposed compensation technique.

In Fig. 5.22 we present the BER performance results, which illustrate the improvements obtained with the correlation coefficient compensation. Fig. 5.23 presents the required BER to achieve $E_b/N_0 = 9$ (dB) as a function of the iterations number. Clearly, there is a performance enhancement when compared with the correlation coefficient estimates without compensation.

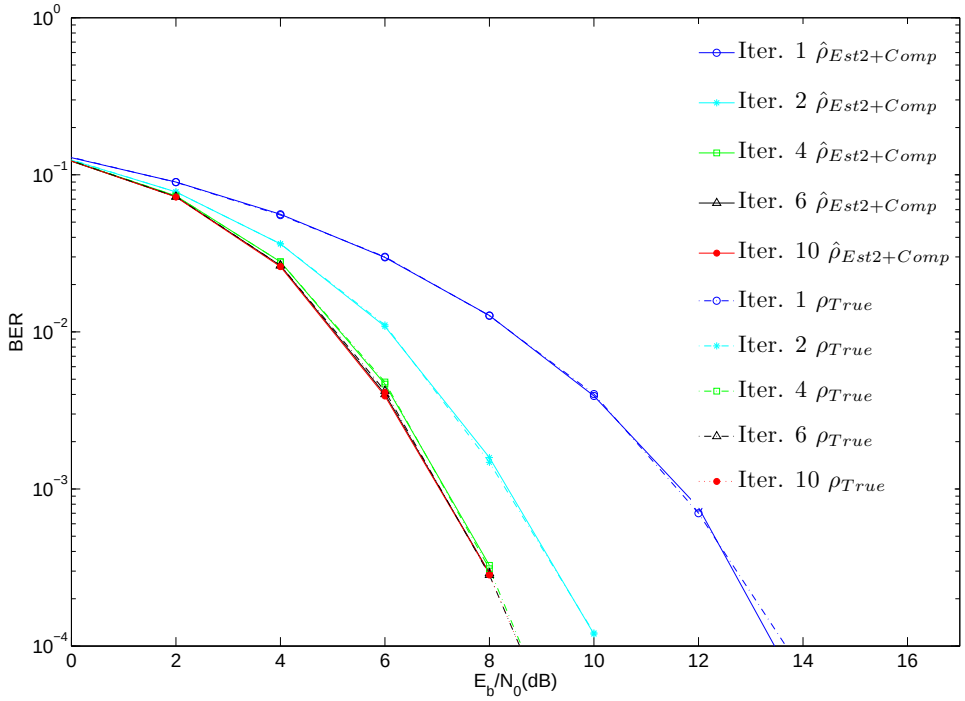

Figure 5.22: BER perfomance for method II.

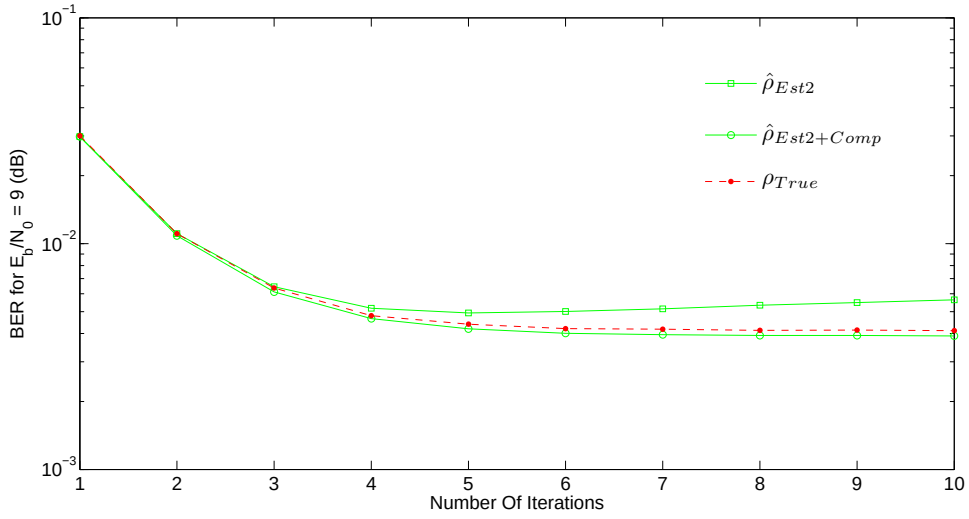

Figure 5.23: Required BER to achieve $E_b/N_0 = 9$ (dB) as a function of the iterations number for method II.

5.4.3 Method III with Compensation

Lastly lets consider the method III. The curve in Fig. 5.24, obtained by simulation, shows the relation between the correlation coefficient estimation, $\hat{\rho}$, and the compensation factor $\chi(\hat{\rho})$.

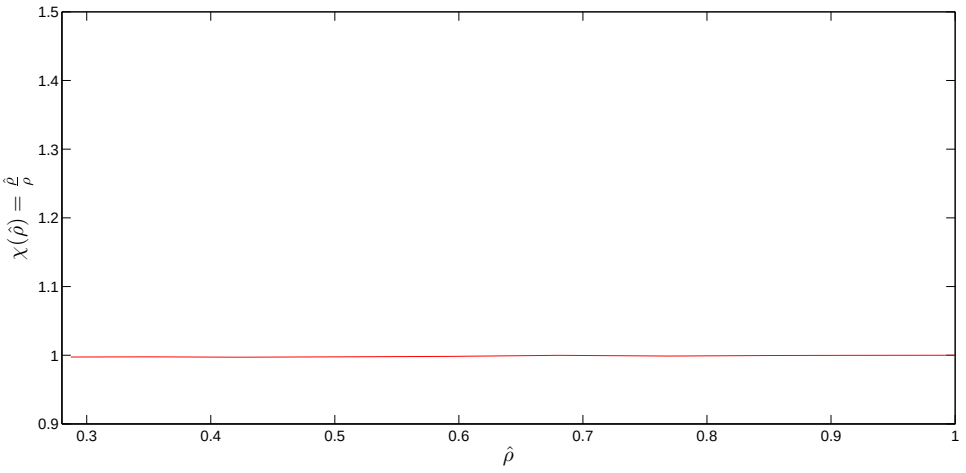

Figure 5.24: Relation between the correlation coefficient estimation and the compensation factor for method III.

As in methods I and II, we can determine the value of the compensation factor $\chi(\hat{\rho})$ for each correspondent value of $\hat{\rho}$, with resort to the plot of Fig. 5.24. The compensated correlation coefficient is then used in the derivation of the feedback and feedforward coefficients parameters of the IB-DFE receiver.

We now present the results obtained with the compensation of the correlation coefficient estimation, $\rho_{Est+Comp}$, corresponding to method III. As in the previous methods, the corresponding results without compensation are also shown.

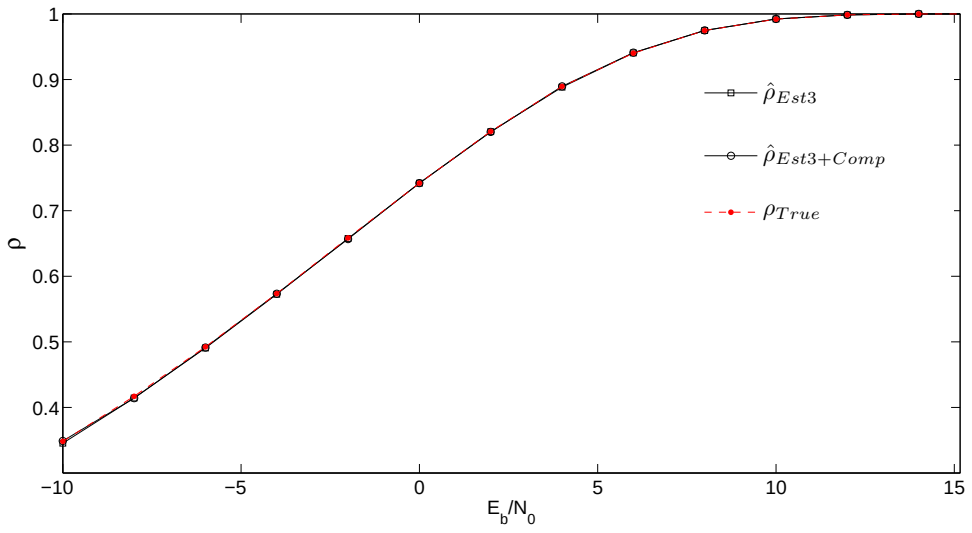

Figure 5.25: Evolution of ρ as function of the E_b/N_0 for method III.

Fig. 5.25 presents the evolution of the correlation coefficient for values of E_b/N_0. As expected, the impact of the correlation coefficient with compensation (denoted $\hat{\rho}_{Est3+Comp}$

in the figure), in the evolution of the correlation coefficient, is not so significative when compared with the results referring to methods I and II. This can be explained by the fact that the approximated $\hat{\rho}$ obtained under method III, was already close to the curve corresponding to the optimum (true) correlation coefficient evolution.

Fig. 5.26 illustrate the improvements obtained with the correlation coefficient compensation in the BER performance results. Fig. 5.27 presents the required BER to achieve $E_b/N_0 = 9$ (dB) as a function of the iterations number. Clearly, there is a performance enhancement when compared with the correlation coefficient estimates without compensation.

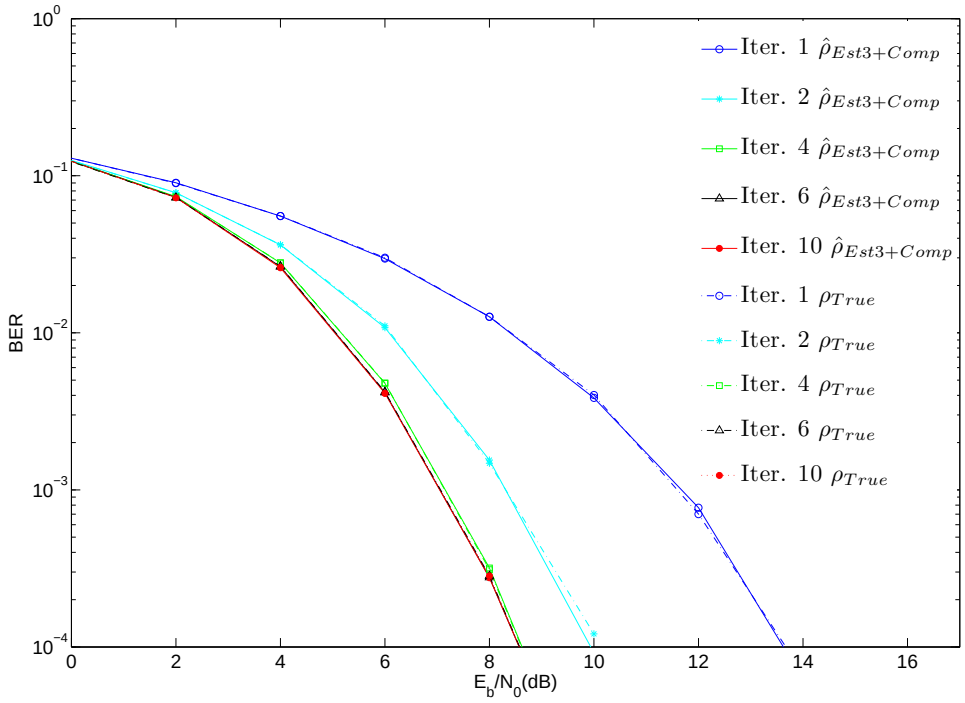

Figure 5.26: BER perfomance for method III.

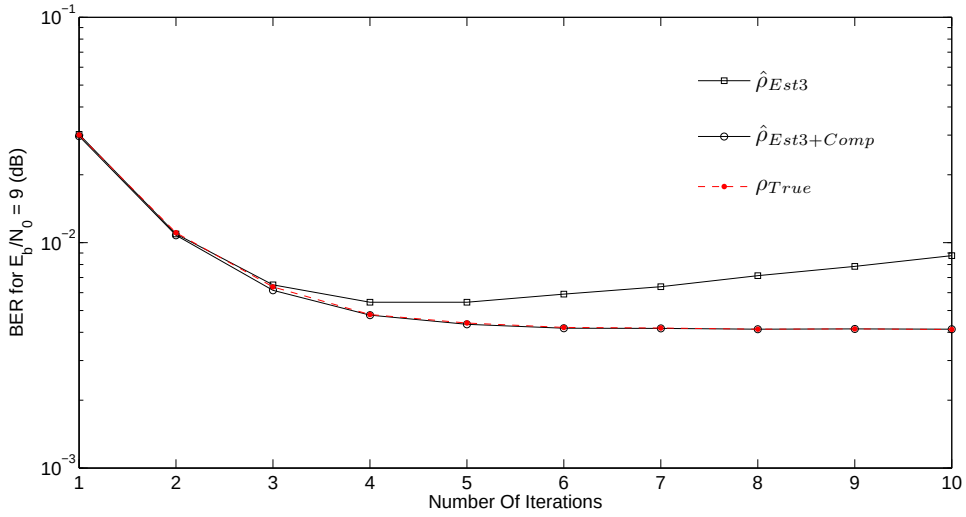

Figure 5.27: Required BER to achieve $E_b/N_0 = 9$ (dB) as a function of the iterations number for method III.

Chapter 6

Conclusions and Future Work

6.1 Conclusions

The main objective of this thesis is focused on the study and development of techniques for IB-DFE receivers, more precisely those related with the signals transmission and detection, that contribute to achieve better performance, while maintaining a low system complexity.

Chapter 2 presented the basic principles of SC modulations and their relations with MC modulations. It was shown that, as with the MC-based OFDM schemes, the SC modulations can take great advantages by employing FDE techniques with CP-assisted block transmission, as well as an efficient use of FFT algorithm. This approach allows receivers with much lower complexity then the optimum receivers. Therefore, OFDM modulations and SC-FDE modulations, employing linear frequency-domain receivers, are suitable for high data rate transmission over severely time-dispersive channels due to FFT implementation.

In chapter 3 were introduced IB-DFE receiver schemes suitable for the uplink transmission. The benefits obtained with the iterations are very significant since the results of the first iteration are equal to those obtained by the conventional linear FDE technique, with MMSE equalization. By canceling the residual interference in each iteration, the successive iterations provide performance improvements that can be closer to the MFB performance.

In turbo FDE receivers, the "soft decisions" from the FDE outputs are replaced by the "soft decisions" from the channel decoder outputs (as in conventional turbo equalizers) in the feedback loop. It was also proposed a "turbo FDE" receiver structure based on the IB-DFE since "turbo FDE" receivers can achieve significant performance enhancements relatively to the uncoded case as shown in the obtained results, being the performance results closer to the MFB.

We also studied the impact of the number of multipath components and the diversity order on the asymptotic performance of IB-DFE receivers. It was shown that, for a high number of separable multipath components, the performance can be very close to the MFB, even without diversity. When we have diversity the performance approaches MFB faster, even when we have just a small number of separable multipath components. These results apply to both conventional IB-DFE schemes and Turbo IB-DFE schemes.

The study on the impact of the number of multipath components and the diversity order on the asymptotic performance of IB-DFE receivers corresponds to a original work, and was accepted for presentation in a international conference's proceeding [23] (see Appendix B).

Chapter 4 considered joint detection and channel estimation for SC-DFE schemes. We proposed a receiver that employs a short and low-power training sequence to provide a coarse channel estimate, which is improved by the combination with a decision-directed estimation. The channel estimates are more accurate when are used more data blocks in the decision-directed estimation. Due to the higher power of the overall signals, and the lower probability of deep notches in the channel frequency response. It is also important to point out that, from the achieved results, the optimum value of the relation between the average power of the training sequences and the data power is $\beta \approx 1$, for the uncoded case, and $\beta \approx 2$, for the coded case. The higher efficiency of the proposed receivers lays on the fact that the coarse channel estimation is improved through the combination of the decision-directed estimation with the estimate that results from the low power training sequence. Therefore, the achieved results support our initial assumptions.

The work presented in chapter 4 was accepted for presentation in a international conference's proceeding [24] (see Appendix B).

In chapter 5 was investigated the impact of the correlation factor estimation in the performance of IB-DFE receivers. Several methods to estimate the correlation coefficient were presented as well as a technique to compensate the estimation errors. The achieved results demonstrate that the inaccuracy due to use of optimistic estimates of the transmitted symbols in the feedback loop, can be efficiently avoided with resort to the proposed compensation technique.

6.2 Future Work

During the development of the present work there were various issues in this thesis that were not taken into account. Therefore, as enrichment to the work elaborated in this thesis, additional future research includes:

- **Synchronization issues**

  It was assumed perfect time and frequency synchronization. It is well known that accurate synchronization is fundamental for a communication system to guarantee good performance. Thus, ensuring a effective time and frequency synchronization, while maintaining a good complexity/performance tradeoff, will be a valuable contribution to this work.

- **OFDM comparison**

  In spite of the basic principles of MC and SC modulations have been introduced in Chapter 2, all the research performed in this thesis was focused on the SC-FDE modulation combined with iterative (turbo) FDE schemes, since it has excellent performance in severely time-dispersive channels, making it a promising candidate for future broadband wireless systems. For that reason, a comparison study concerning the performance results obtained with OFDM modulation for the same scenarios, will be a significant contribution to this work.

- **Channel Tracking**

  In this thesis, we assumed a slow-varying channel. However, to maintain high power and spectral efficiencies, the CP, which is longer than the overall channel impulse response length, should be a small fraction of the block duration. Therefore, for

severely time-dispersive channels we need large blocks, with hundreds or even thousands of symbols, meaning that, contrarily to the usual block transmission scenarios, the channel can change within the block duration. Under these conditions, for time-varying channels we need to track channel variations.

As a complement to the work developed in this thesis, it is possible consider the problem of digital transmission over severely time-dispersive channels that are also time-varying.

Appendix A

Minimum Error Variance

In chapter 4 we proposed a channel estimation method based on training sequences, multiplexed with data. It was shown that is possible to use a decision-directed channel estimation to improve the accuracy of channel estimates without requiring high-power training sequences. Here we show how we can combine the channel estimates, obtained from the training sequence, $\tilde{H}_k^{TS}$, with the decision-directed channel estimates, $\tilde{H}_k^D$, to provide the normalized channel estimates with minimum error variance defined in (4.11).

Let us assume the channel estimates,

$$\tilde{H}_k^D = H_k + \epsilon_k^D, \tag{A.1}$$

and

$$\tilde{H}_k^{TS} = H_k + \epsilon_k^{TS}, \tag{A.2}$$

where the channel estimation errors, ϵ_k^D and ϵ_k^{TS}, are assumed to be uncorrelated, zero-mean, Gaussian random variables with variance σ_D^2, and σ_{TS}^2, respectively, i.e., $\epsilon_k^D \sim N(0, \sigma_D^2)$ and $\epsilon_k^{TS} \sim N(0, \sigma_{TS}^2)$. The channel estimates $\tilde{H}_k^D$, and $\tilde{H}_k^{TS}$, can be combined as follows:

$$\tilde{H}_k^{TS,D} = \frac{a\tilde{H}_k^D + b\tilde{H}_k^{TS}}{a+b} = \frac{\tilde{H}_k^D + \frac{b}{a}\tilde{H}_k^{TS}}{1+\frac{b}{a}} = \frac{\tilde{H}_k^D + \mu\tilde{H}_k^{TS}}{1+\mu} = H_k + \epsilon_k^{TS,D}, \tag{A.3}$$

where $a = b = 1$, $\mu = \frac{a}{b}$, and $\epsilon_k^{TS,D} \sim N(0, \sigma^2)$ denotes the noise component, still characterized by a Gaussian-distribution, with zero mean and variance σ^2, given by

$$\sigma^2 = \frac{\sigma_D^2 + \mu^2 \sigma_{TS}^2}{(1+\mu)^2} = f(\mu). \tag{A.4}$$

For the sake of simplicity, we dropped the dependence with k. The parameter μ is chosen to minimize σ^2. The optimum value of μ corresponds to

$$\frac{df(\mu)}{d\mu} = 0, \tag{A.5}$$

leading to

$$\mu = \frac{\sigma_D^2}{\sigma_{TS}^2}. \tag{A.6}$$

Therefore the overall channel estimate combining, resulting from the combination between $\tilde{H}_k^{TS}$ and $\tilde{H}_k^D$, will be

$$\tilde{H}_k^{TS,D} = \frac{\sigma_{TS}^2 \tilde{H}_k^D + \sigma_D^2 \tilde{H}_k^{TS}}{\sigma_D^2 + \sigma_{TS}^2} = H_k + \epsilon_k^{TS,D}, \tag{A.7}$$

where $\epsilon_k^{TS,D} \sim N(0, \sigma_{opt}^2)$ denotes the noise component with Gaussian-distribution, with zero mean and variance σ_{opt}^2. The optimum variance σ_{opt}^2 will be

$$\sigma_{opt}^2 = \sigma^2 \Big|_{\mu = \frac{\sigma_D^2}{\sigma_{TS}^2}} = \frac{\sigma_D^2 + \left(\frac{\sigma_D}{\sigma_{TS}}\right)^4 \sigma_{TS}^2}{\left(1 + \frac{\sigma_D^2}{\sigma_{TS}^2}\right)^2} = \frac{\sigma_D^2 \sigma_{TS}^4 + \sigma_D^4 \sigma_{TS}^2}{(\sigma_D^2 + \sigma_{TS}^2)^2} = \frac{\sigma_D^2 \sigma_{TS}^2}{\sigma_D^2 + \sigma_{TS}^2}. \tag{A.8}$$

Under these conditions results, $\sigma_{opt}^2 \leq \sigma_D^2$ and $\sigma_{opt}^2 \leq \sigma_{TS}^2$.

Appendix B

Publications

In this appendix, we present the articles submitted in international conferences.

- **Chapter 3**

  "On the Impact of Multipath Propagation and Diversity in Performance of Iterative Block Decision Feedback Equalizers" – The work presented in this chapter was published in the *6th IEEE International Conference on Wireless and Mobile Computing, Networking and Communications (WiMob 2010)*[23].

- **Chapter 4**

  "Joint Detection and Channel Estimation for Block Transmission Schemes" – The work presented in this chapter was published in the *2010 IEEE Military Communications Conference (Milcom 2010)* [24].

- **Chapter 5**

  "Estimation of the Feedback Reliability for IB-DFE Receivers" – The work presented in this chapter was accepted for presentation at *The Eighth IASTED International Conference on Signal Processing, Pattern Recognition and Applications (SPPRA 2011)* [25]. Final version in preparation.

On the Impact of Multipath Propagation and Diversity in Performance of Iterative Block Decision Feedback Equalizers

Fábio Coelho[1] Rui Dinis[1,2], Nuno Souto[2,3] and Paulo Montezuma[1,4]
[1] Departamento de Engenharia Electrotécnica,
Faculdade de Ciências e Tecnologia da Universidade Nova de Lisboa, 2829-516 Caparica, Portugal
[2] Instituto de Telecomunicações, Lisboa, Portugal
[3] ISCTE, Lisboa, Portugal
[4] UNINOVA, Caparica, Portugal

Abstract - SC modulation (Single-Carrier) with FDE (Frequency-Domain Equalization) combined with iterative (turbo) FDE schemes has excellent performance in severely time-dispersive channels, making it a promising candidate for future broadband wireless systems. In fact, it was observed that the performance can be close to the MFB (Matched Filter Bound).

In this paper we consider a class of iterative FDE schemes and we study the impact of the number of multipath components and the diversity order on its performance. It is shown that for a high number of separable multipath components the asymptotic performance approaches the MFB, even without diversity. When we have diversity the performance approaches the MFB faster, even when we have just a small number of separable multipath components.

Index Terms: Matched filter bound, SC-FDE, turbo equalization, diversity.

I. Introduction

Block transmission techniques, with appropriate cyclic prefixes and employing FDE techniques (Frequency-Domain Equalization), have been shown to be suitable for high data rate transmission over severely time-dispersive channels [1], [2]. The most popular techniques based on this concept are OFDM (Orthogonal Frequency Division Multiplexing) and SC-FDE (Single-Carrier with Frequency-Domain Equalization). Due to the lower envelope fluctuations of the transmitted signals, SC-FDE schemes are especially interesting for the uplink transmission (i.e., the transmission from the mobile terminal to the base station) [1], [2].

Typically the receiver for SC-FDE schemes is a linear FDE. However, it is known that nonlinear equalizers outperform linear equalizers [3]. IB-DFE (Iterative Block Decision Feedback Equalizer) [4] is a promising iterative FDE technique for SC-FDE that was first proposed in [5] and extended to diversity scenarios [6] and layered space-time schemes [7]. These receivers can be regarded as low-complexity turbo FDE schemes [8], [9] where the channel decoder is not involved in the feedback. True turbo FDE schemes can also be designed based on the IB-DFE concept [10], [11]. It was observed that the asymptotic performance of IB-DFE schemes can be sometimes very close to the MFB (Matched Filter Bound), but in other cases it is relatively far from it [6]. However, it is not clear under which circumstances we can expect performances close to the MFB.

In this paper we study the impact of the number of multipath components and the diversity order on the asymptotic performance of IB-DFE schemes. This paper is organized as follows: conventional and turbo IB-DFE receivers are described in Section II. Analytical expressions for the MFB, when we have multipath propagation and diversity, are presented in Section III. A set of performance results is presented in Section IV and Section V is concerned with the conclusions of this paper.

II. IB-DFE Receivers

We consider an SC-FDE modulation where the data is transmitted in blocks of N symbols, $\{s_n; n = 0, 1, \ldots, N-1\}$, for which a cyclic prefix with length longer than the channel impulse response is appended. The signal is transmitted over a time-dispersive channel and the receiver has N_{Rx} diversity branches. The signal associated to the l^{th} branch is sampled, leading to the time-domain block $\{y_n^{(l)}; n = 0, 1, \ldots, N-1\}$, after cyclic prefix removal. The corresponding frequency-domain block, obtained after an appropriate size-N DFT (Discrete Fourier Transform) operation, is $\{Y_k^{(l)}; k = 0, 1, \ldots, N-1\}$, where $Y_k^{(l)}$ can be written as

$$Y_k^{(l)} = S_k H_k^{(l)} + N_k^{(l)}, \tag{1}$$

with $H_k^{(l)}$ denoting the overall channel frequency response between the transmit antenna and the l^{th} receive antenna, for the k^{th} frequency of the m^{th} time block and $N_k^{(l)}$ denoting the corresponding channel noise.

The receiver structure is depicted in Fig. 1 [4], [6]. For the i^{th} iteration, the frequency-domain block at the output of the equalizer is $\{\tilde{S}_k^{(i)}; k = 0, 1, \ldots, N-1\}$, with

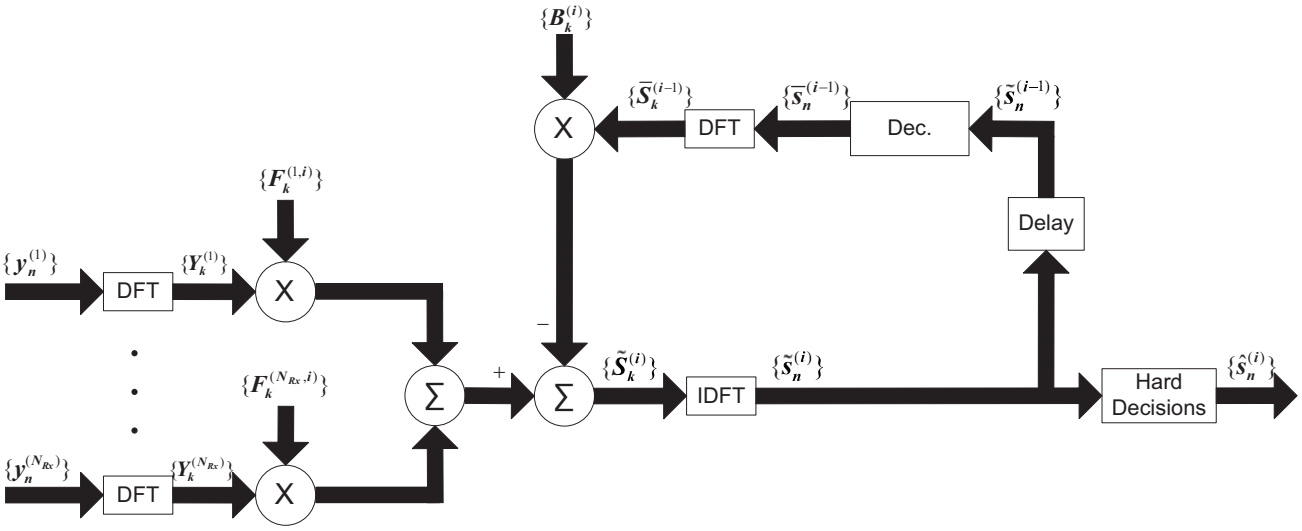

Fig. 1. IB-DFE receiver structure with an L-branch space diversity.

$$\tilde{S}_k^{(i)} = \sum_{l=1}^{N_{Rx}} F_k^{(l,i)} Y_k^{(l)} - B_k^{(i)} \overline{S}_k^{(i-1)}, \tag{2}$$

where $\{F_k^{(l,i)}; k = 0, 1, \ldots, N-1\}$ are the feedforward coefficients associated to the l^{th} diversity antenna and $\{B_k^{(i)}; k = 0, 1, \ldots, N-1\}$ are the feedback coefficients. $\{\overline{S}_k^{(i-1)}; k = 0, 1, \ldots, N-1\}$ denotes the DFT of the block of time-domain conditional symbol expectations associated with the previous iteration $\{\overline{s}_n^{(i-1)}; n = 0, 1, \ldots, N-1\}$.

For a normalized IB-DFE, the optimum feedback coefficients are given by

$$B_k^{(i)} = \sum_{l=1}^{N_{Rx}} F_k^{(l,i)} H_{k,m}^{(l)} - 1 \tag{3}$$

and the feedforward coefficients are given by

$$F_k^{(l,i)} = \frac{\breve{F}_k^{(l,i)}}{\gamma^{(i)}}, \tag{4}$$

with

$$\breve{F}_k^{(l,i)} = \frac{H_k^{(l)*}}{\beta + (1 - (\rho^{(i-1)})^2) \sum_{l=1}^{N_{Rx}} |H_k^{(l)}|^2}, \tag{5}$$

where $\beta = E[|N_k^{(l)}|^2]/E[|S_k|^2]$,

$$\gamma^{(i)} = \frac{1}{N} \sum_{k=0}^{N-1} \sum_{l=1}^{L} \breve{F}_k^{(l,i)} H_k^{(l)} \tag{6}$$

and the correlation factor $\rho^{(i-1)}$ is defined as

$$\rho^{(i-1)} = \frac{E[\hat{s}_n^{(i-1)} s_n^*]}{E[|s_n|^2]}, \tag{7}$$

where the block $\{\hat{s}_n^{(i-1)}; n = 0, 1, \ldots, N-1\}$ denotes the data estimates associated to the previous iteration, i.e., the hard decisions associated to the time-domain block at the output of the FDE, $\{\tilde{s}_n^{(i)}; n = 0, 1, \ldots, N-1\}$ = IDFT $\{\tilde{S}_{k,m}^{(i)}; k = 0, 1, \ldots, N-1\}$. For QPSK (Quadrature Phase Shift Keying) constellations, the correlation coefficient is given by [11]

$$\rho_m^{(i)} = \frac{1}{2N} \sum_{n=0}^{N-1} (\rho_n^{I(i)} + \rho_n^{Q(i)}), \tag{8}$$

where

$$\rho_n^{I(i)} = \left| \tanh\left(\frac{L_n^{I(i)}}{2} \right) \right|, \tag{9}$$

and

$$\rho_n^{Q(i)} = \left| \tanh\left(\frac{L_n^{Q(i)}}{2} \right) \right|, \tag{10}$$

with the LLRs (LogLikelihood Ratios) of the "in-phase bit" and the "quadrature bit", associated to $s_n^{I(i)}$ and $s_n^{Q(i)}$, given by

$$L_n^{I(i)} = \frac{2}{\sigma_i^2} \tilde{s}_n^{I(i)} \tag{11}$$

and

$$L_n^{Q(i)} = \frac{2}{\sigma_i^2} \tilde{s}_n^{Q(i)}, \tag{12}$$

respectively, with

$$\sigma_i^2 = \frac{1}{2} E[|s_n - \tilde{s}_n^{(i)}|^2] \approx \frac{1}{2N} \sum_{n=0}^{N-1} |\hat{s}_n^{(i)} - \tilde{s}_n^{(i)}|^2. \tag{13}$$

The conditional expectations associated with the data symbols are given by

$$\overline{s}_n^{(i)} = \tanh\left(\frac{L_n^{I(i)}}{2} \right) + j \tanh\left(\frac{L_n^{Q(i)}}{2} \right). \tag{14}$$

In a conventional IB-DFE receiver the log-likelihood values are computed on a symbol-by-symbol basis (i.e., we do not need to perform the channel decoding within the feedback loop). As an alternative, we can define a turbo IB-DFE that employs the channel decoder outputs instead of the uncoded "soft decisions" in the feedback loop. The main difference between conventional IB-DFE and turbo IB-DFE is in the decision device: in the first case the decision device is a symbol-by-symbol soft-decision (for QPSK constellation this corresponds to the hyperbolic tangent, as in (14)); for the turbo IB-DFE a SISO channel decoder (Soft-In, Soft-Out) is employed in the feedback loop. The SISO block can be implemented as defined in [12] and provides the LLRs of the "information bits" and the "coded bits". The input of the SISO block are LLRs of the "coded bits" at the FDE output, given by (11) and (12).

III. Analytical Computation of the MFB

In this section we present an analytical approach for obtaining the MFB when no channel coding is employed. Since for the case with channel coding it is very difficult to obtain analytical BER expressions, even for an ideal Additive White Gaussian Noise (AWGN) channel, the MFB needs to be computed by simulation.

We will derive the MFB using an approach similar to [13]. Let us consider the case of a transmission over an multipath Rayleigh fading channel with N_{Rx} diversity branches, where all branches can have different fading powers or can be correlated. Assuming a discrete multipath channel for each diversity branch *l*, composed of U_l discrete taps, where the magnitude of each tap *i* has a mean square value of $\Omega_{i,l}^2$, the respective response at time *t* to an impulse, applied at *t*-τ, can be modeled as

$$c_l(\tau,t) = \sum_{i=1}^{U_l} \alpha_{i,l}(t)\,\delta(\tau-\tau_{i,l}), \quad l = 1...N_{Rx}, \tag{15}$$

with $\alpha_{i,l}(t)$ being a zero-mean complex Gaussian random process, $\tau_{i,l}$ the respective delay (assumed constant) and $\delta(t)$ is the Dirac function. For the derivation of the MFB we assume a transmission of one pulse $s \cdot g(t)$, where *s* is a symbol of an QPSK constellation and *g*(*t*) is the impulse response of the transmit filter.

Assuming a slowly time-varying channel, the sum of the sampled outputs, from the matched filters of the diversity branches, can be written as

$$y(t=t_0) = s \cdot \sum_{l=1}^{N_{Rx}} \sum_{i=1}^{U_l} \sum_{i'=1}^{U_l} \alpha_{i,l}\alpha_{i',l}^{*} R(\tau_{i,l}-\tau_{i',l}) + \sum_{l=1}^{N_{Rx}} \nu_l, \tag{16}$$

where ν_l represents AWGN samples with power spectral density N_0 and $R(\tau)$ is the autocorrelation function of the transmit filter. The instantaneous received signal to noise power ratio is given by $SNR = \frac{2E_b}{N_0}\kappa$, where E_b denotes the average bit energy and κ is defined as

$$\kappa = \sum_{l=1}^{N_{Rx}} \sum_{i=1}^{U_l} \sum_{i'=1}^{U_l} \alpha_{i,l}\alpha_{i',l}^{*} R(\tau_{i,l}-\tau_{i',l}) = \mathbf{z}^H \mathbf{\Sigma} \mathbf{z}. \tag{17}$$

In (17), $\mathbf{z}$ represents a $U_{total} \times 1$ (with $U_{total} = \sum_{l=1}^{N_{Rx}} U_l$) vector containing the random variables $\alpha_{i,l}$ and $\mathbf{z}^H$ denotes the conjugate transpose of $\mathbf{z}$. $\mathbf{\Sigma}$ is a $U_{total} \times U_{total}$ Hermitian matrix constructed as

$$\mathbf{\Sigma} = \begin{bmatrix} \mathbf{R}_1 & \cdots & \mathbf{0} \\ \vdots & \ddots & \vdots \\ \mathbf{0} & \cdots & \mathbf{R}_{N_{Rx}} \end{bmatrix}, \tag{18}$$

where $\mathbf{R}_l$ is a matrix associated to the l^{th} diversity branch, defined as

$$\mathbf{R}_l = \begin{bmatrix} R(0) & \cdots & R(\tau_{U_l,l}-\tau_{1,l}) \\ \vdots & \ddots & \vdots \\ R(\tau_{1,l}-\tau_{U_l,l}) & \cdots & R(0) \end{bmatrix}. \tag{19}$$

For a QPSK constellation the instantaneous BER (Bit Error Rate) can be written as

$$P_b(\kappa) = \frac{1}{2} erfc\left(\sqrt{\frac{E_b}{N_0}\kappa}\right), \tag{20}$$

where erfc(*x*) is the complementary error function. To obtain the probability density function (PDF) of κ we will write κ as a sum of uncorrelated random variables with known PDFs. Denoting $\mathbf{\Psi}$ as the covariance matrix of $\mathbf{z}$ ($\mathbf{\Psi} = Cov[\mathbf{z}]$), which is Hermitian and positive-semidefinite, it is possible to decompose $\mathbf{\Psi}$ into $\mathbf{\Psi} = \mathbf{Q}\mathbf{Q}^H$. In fact, if we apply the Cholesky decomposition, $\mathbf{Q}$ will be a lower triangular matrix. Moreover, using this matrix we can define a new vector $\mathbf{z}' = \mathbf{Q}^{-1}\mathbf{z}$, whose components will be uncorrelated unit-variance complex Gaussian variables and κ becomes

$$\kappa = \mathbf{z'}^H \mathbf{Q}^H \mathbf{\Sigma} \mathbf{Q} \mathbf{z'} = \mathbf{z'}^H \mathbf{\Sigma'} \mathbf{z'}, \tag{21}$$

with

$$\mathbf{\Sigma'} = \mathbf{Q}^H \mathbf{\Sigma} \mathbf{Q} = \mathbf{\Phi} \mathbf{\Lambda} \mathbf{\Phi}^H, \tag{22}$$

where $\mathbf{\Lambda}$ is a diagonal matrix whose elements are the eigenvalues λ_i (*i*=1,..,U_{total}) of $\mathbf{\Sigma'}$ and $\mathbf{\Phi}$ is a matrix whose columns are the orthogonal eigenvectors of $\mathbf{\Sigma'}$**.** The decomposition of $\mathbf{\Sigma'}$ in (22) is possible due to its Hermitian property. We can then rewrite (21) as

$$\kappa = \mathbf{z'}^H \mathbf{\Phi} \mathbf{\Lambda} \mathbf{\Phi}^H \mathbf{z'} = \mathbf{z''}^H \mathbf{\Lambda} \mathbf{z''} = \sum_{i=1}^{U_{total}} \lambda_i |z_i''|^2, \tag{23}$$

where we have defined two more vectors, $\mathbf{z''^H} = \mathbf{z'^H}\mathbf{\Phi}$ and $\mathbf{z''} = \mathbf{\Phi}^H\mathbf{z'}$, whose components are still uncorrelated unit-variance complex Gaussian variables. According to (23), κ can be expressed as a sum of independent random variables with exponential distributions whose characteristic function is

$$E\left\{e^{-j\upsilon\kappa}\right\} = \prod_{i=1}^{U_{total}} \frac{1}{1+j\lambda_i\upsilon}. \quad (24)$$

If there are U' distinct eigenvalues, each with a multiplicity of q_i, i=1...U', we can apply the inverse Fourier transform to (24) and obtain the PDF of κ as

$$p(\kappa) = \sum_{i=1}^{U'} \sum_{m=1}^{q_i} \frac{A_{i,m}}{\lambda_i^{q_i}(q_i-m)!(m-1)!}\kappa^{m-1}e^{-\frac{\kappa}{\lambda_i}}, \quad (25)$$

with

$$A_{i,m} = \left[\frac{\partial^{q_i-m}}{\partial s^{q_i-m}}\left(\prod_{\substack{j=1\\ j\neq i}}^{U'} \frac{1}{(1+s\lambda_j)^{q_j}}\right)\right]_{s=-\frac{1}{\lambda_i}}. \quad (26)$$

It is easy to verify that the average BER can be obtained as

$$P_{b_{av}} = \int_{-\infty}^{+\infty} P_b(\kappa)\, p(\kappa)\, d\kappa = \sum_{i=1}^{U'}\sum_{m=1}^{q_i} \frac{A_{i,m}}{\lambda_i^{q_i-m}(q_i-m)!}\left[\frac{1-\mu_i}{2}\right]^m \cdot \sum_{r=0}^{m-1}\binom{m-1+r}{r}\left[\frac{1+\mu_i}{2}\right]^r, \quad (27)$$

where

$$\mu_i = \sqrt{\frac{\frac{E_s}{N_0}\lambda_i}{1+\frac{E_s}{N_0}\lambda_i}}. \quad (28)$$

IV. Performance Results

In this section we present a set of performance results concerning the impact of the number of multipath components and the diversity on the performance of IB-DFE receivers as well as the correspondent MFB. We consider FFT-blocks with $N = 256$ data symbols selected from a QPSK constellation under a Gray mapping rule. Similar results were observed for other values of N, provided that $N >> 1$.

The channel can be characterized by one of the following PDPs (Power Delay Profile):

- Uniform PDP, with $U = U_1 = ... = U_{N_{Rx}}$ equal-power symbol-spaced multipath components, for all diversity branches.
- Exponential PDP, with $U = U_1 = ... = U_{N_{Rx}}$ symbol-spaced multipath components for all diversity branches, but with an exponential decay such as that the last component is 20dB below the first one.

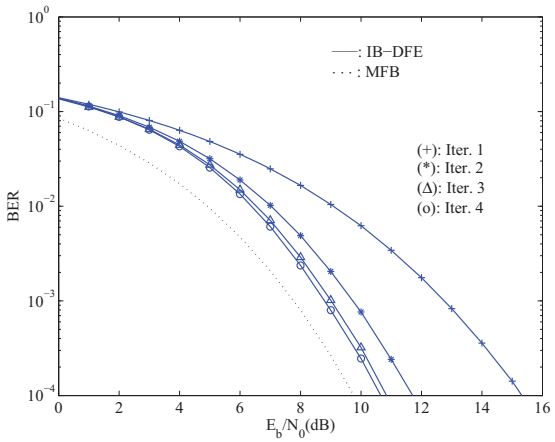

Fig. 2. BER performance for an IB-DFE without channel coding ($N_{Rx} = 1$).

We also assume that both channels, have uncorrelated Rayleigh fading on the different multipath components and diversity branches.

For each channel, are considered an uncoded as well as a coded transmission. The channel encoder is based on a convolutional code with the polynomials generators $1+D^2+D^3+D^5+D^6$ and $1+D+D^2+D^3+D^6$ and the coded bits are interleaved before being mapped into the constellation points and distributed by the symbols of the block. We also assumed a linear power amplification at the transmitter and perfect synchronization and channel estimation at the receiver. Our performance results are expressed as function of E_b/N_0, where N_0 is the one-sided power spectral density of the noise and E_b is the energy of the transmitted bits (i.e., the degradation due to the useless power spent on the cyclic prefix is not included).

Fig. 2 shows the typical behavior of the BER for an IB-DFE when we do not employ channel coding, for the case without diversity ($N_{Rx} = 1$). Fig. 3 presents the same performance results but for the case with two-branch diversity ($N_{Rx} = 2$). Clearly, there is a significant performance improvement with the iterations and the asymptotic BER is closer to the MFB. However, the improvements are much lower for low-to-moderate values of E_b/N_0. For this reason, the iterations of the IB-DFE yield only marginal gains when we consider channel coding, as depicted in Fig. 4 ($N_{Rx} = 1$) and Fig. 5 ($N_{Rx} = 2$). On the other hand, for the turbo IB-DFE, where the channel decoding is involved in the feedback loop, the gains are much higher as we can be closer to the MFB. Therefore, in the following we will consider a conventional, non-turbo, IB-DFE for the uncoded case and a turbo IB-DFE for the coded case.

Next we will present the required values of E_b/N_0 for a specific BER (10^{-4} in the uncoded case and 10^{-5} in the coded case), for the MFB and for each iteration of the IB-DFE. These values are expressed as a function of the number of multipath components U. We will consider the case without diversity

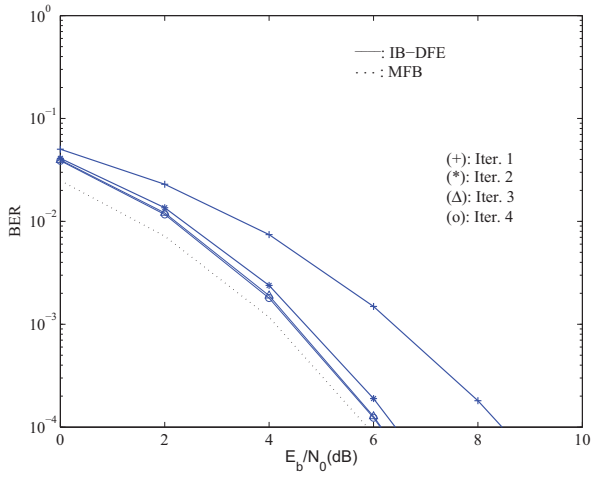

Fig. 3. BER performance for an IB-DFE without channel coding ($N_{Rx} = 2$).

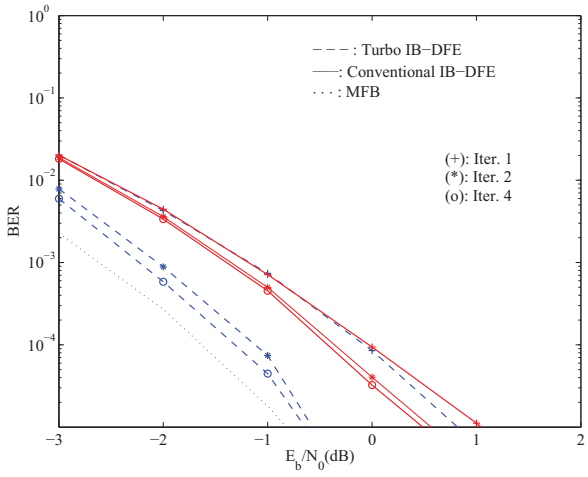

Fig. 5. BER performance for a conventional IB-DFE with channel coding, as well as a turbo IB-DFE ($N_{Rx} = 2$).

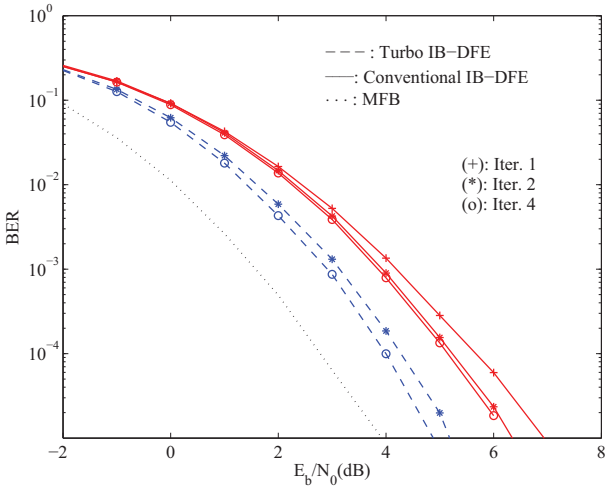

Fig. 4. BER performance for a conventional IB-DFE with channel coding, as well as a turbo IB-DFE ($N_{Rx} = 1$).

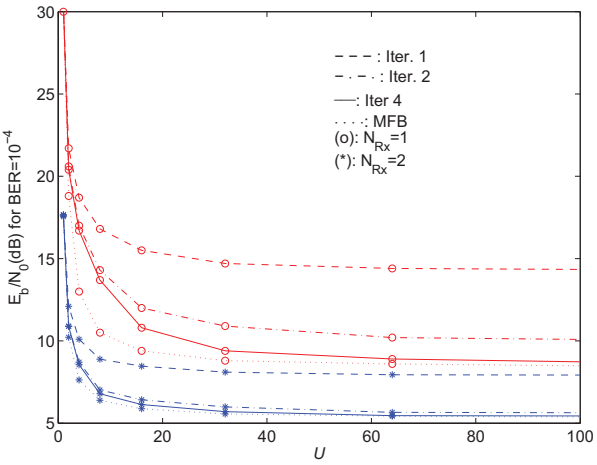

Fig. 6. Required E_b/N_0 to achieve $BER = 10^{-4}$ without convolutional code and uniform PDP, as function of the number of multipath components: IB-DFE with 1, 2 and 4 iterations; MFB (dashed lines).

($N_{Rx} = 1$) and the case with two-branch diversity ($N_{Rx} = 2$).

Let us first consider the uniform PDP. Figs. 6 and 7 show the results without channel coding and with channel coding, respectively. Clearly, for a high number of multipath components we can be very close to the MFB after a few iterations, in all cases (naturally, for $U = 1$ the BER is identical to the MFB, although the performance is very poor, since this corresponds to a flat fading channel). The improvements with the iterations are higher without diversity and in the uncoded case. This is also the case where an higher number of multipath components is required to allow performances close to the MFB (about $U = 60$).

Let us consider now the exponential PDP. Figs. 8 and 9 show the results without channel coding and with channel coding, respectively. By comparing these figures with the corresponding ones of the uniform PDP, we can observe a similar behavior. The major difference is that we need a higher number of multipath components in the exponential PDP to have results similar to the ones of the uniform PDP. This is due to the fact that, the number of relevant multipath components is lower for the exponential PDP, since the last ones have much lower power.

V. Conclusions

In this paper we studied the impact of the number of multipath components and the diversity order on the asymptotic performance of IB-DFE receivers.

It was shown that for a high number of separable multipath components the performance can be very close to the MFB, even without diversity. When we have diversity the

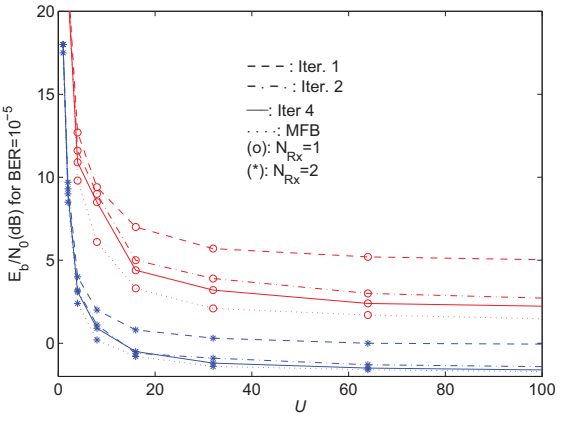

Fig. 7. Required E_b/N_0 to achieve $BER = 10^{-5}$ with convolutional code for uniform PDP, as function of the number of multipath components: IB-DFE with 1, 2 and 4 iterations; MFB (dashed lines).

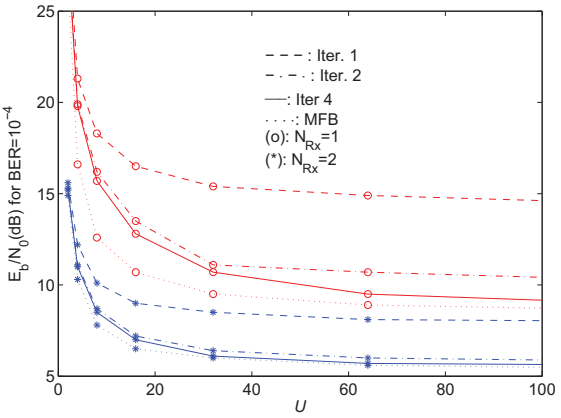

Fig. 8. Required E_b/N_0 to achieve $BER = 10^{-4}$ without convolutional code for exponential PDP, as function of the number of multipath components: IB-DFE with 1, 2 and 4 iterations; MFB (dashed lines).

performance approaches MFB faster, even when we have just a small number of separable multipath components. These results apply to both conventional IB-DFE schemes and Turbo IB-DFE schemes.

ACKNOWLEDGMENTS

This work was partially supported by Fundação para a Ciência e Tecnologia (pluriannual funding and the U-BOAT PTDC/EEA-TEL/67066/2006 and ADCOD projects).

REFERENCES

[1] A. Gusmão, R. Dinis, J. Conceição, and N. Esteves, "Comparison of Two Modulation Choices for Broadband Wireless Communications", *Proc. IEEE VTC Spring*, pp. 1300–1305, May 2000.

[2] D. Falconer, S. Ariyavisitakul, A. Benyamin-Seeyar and B. Eidson, "Frequency Domain Equalization for Single-Carrier Broadband Wireless Systems", *IEEE Comm. Mag.*, Vol. 4, No. 4, pp. 58–66, April 2002.

[3] J. Proakis, *Digital Communications*, McGraw-Hill, 1995.

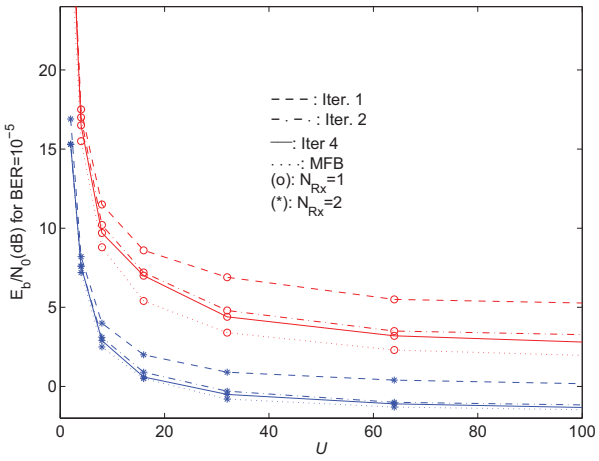

Fig. 9. Required E_b/N_0 to achieve $BER = 10^{-5}$ with convolutional code for exponential PDP, without diversity, as a function of the number of multipath components: IB-DFE with 1, 2 and 4 iterations; MFB (dashed line).

[4] N. Benvenuto, R. Dinis, D. Falconer and S. Tomasin, "Single Carrier Modulation with Non Linear Frequency Domain Equalization: An Idea Whose Time Has Come - Again", *Proceedings of IEEE*, Vol. 98, No. 1, page 69-96, Jan. 2010.

[5] N. Benvenuto and S. Tomasin, "Block Iterative DFE for Single Carrier Modulation", *IEE Electronic Letters*, Vol. 39, No. 19, September 2002.

[6] R. Dinis, A. Gusmão and N. Esteves, "On Broadband Block Transmission over Strongly Frequency-Selective Fading Channels", *Wireless 2003*, Calgary, Canada, July 2003.

[7] R. Dinis, R. Kalbasi, D. Falconer and A. Banihashemi, "Iterative Layered Space-Time Receivers for Single-Carrier Transmission over Severe Time-Dispersive Channels", *IEEE Comm. Letters*, Vol. 8, No. 9, pp. 579–581, Sep. 2004.

[8] M. Tüchler and J. Hagenauer, "Turbo Equalization Using Frequency Domain Equalizers,", *Allerton Conf.*, Oct. 2000.

[9] M. Tüchler and J. Hagenauer, "Linear Time and Frequency Domain Turbo Equalization", *IEEE VTC'01 (Fall)*, Oct. 2001.

[10] N. Benvenuto and S. Tomasin, "Iterative Design and Detection of a DFE in the Frequency Domain", *IEEE Trans. on Comm.*, Vol. 53, No. 11, pp. 1867–1875, Nov. 2005.

[11] A. Gusmão, P. Torres, R. Dinis and N. Esteves, "A Turbo FDE Technique for Reduced-CP SC-Based Block Transmission Systems", *IEEE Trans. on Comm.*, Vol. 55, No. 1, pp. 16-20, Jan. 2007.

[12] B. Vucetic and J. Yuan, *Turbo Codes: Principles and Applications*, Kluwer Academic Publ., 2002.

[13] F. Ling, "Matched filter-bound for time-discrete multipath Rayleigh fading channels", *IEEE Trans. on Comm.*, vol. 43, pp. 710–713, Feb./Mar./Apr. 1995.

Joint Detection and Channel Estimation for Block Transmission Schemes

Fábio Coelho[1] Rui Dinis[1,2] and Paulo Montezuma[1,3]
[1] Departamento de Engenharia Electrotécnica, Faculdade de Ciências e Tecnologia, FCT, Universidade Nova de Lisboa, 2829-516 Caparica
[2] Instituto de Telecomunicações, Lisboa, Portugal
[3] UNINOVA, Caparica, Portugal

Abstract - SC-FDE (Single-Carrier with Frequency-Domain Equalization) block transmission technique can have excellent performance in severely time-dispersive channels provided that accurate channel estimates are available at the receiver.

In this paper we consider joint detection and channel estimation for SC-FDE schemes where a coarse channel estimate is obtained with the help of a training sequence and we employ iterative receivers where for each iteration the data estimates are used to improve the channel estimates. However, since the frequency-domain data blocks can have large envelope fluctuations, a decision-directed channel estimation might have significant noise enhancement effects. To overcome this problem, we combine channel estimates based on the training sequence with decision-directed channel estimates.

Our performance results show that these techniques allow good performances without requiring high-power pilots or training blocks.

Index Terms: Channel estimation, training sequences, frequency-domain receivers, iterative receivers, SC-FDE.

I. Introduction

Block transmission techniques, with appropriate cyclic prefixes and employing FDE techniques (Frequency-Domain Equalization), are suitable to broadband wireless systems [1], [2]. Among these techniques SC-FDE (Single-Carrier with FDE) [3] modulations. The performance can be further improved if the linear FDE is replaced by an IB-DFE (Iterative Block Decision Feeback Equalizer) [4]. In fact, this technique has excellent performance in severely time-dispersive channels, provided that accurate channel estimates are available at the receiver.

The channel estimates are usually obtained with the help of pilot symbols and/or training sequences multiplexed with data symbols [5]. To avoid performance degradation, the power associated to pilots should be similar or higher than the power associated to the data, leading to performance degradation when we consider the overall power spent to transmit each block (i.e., the power of pilots plus data). The channel estimation performance can be improved if we perform joint detection and channel estimation [6], [7].

In this paper we consider joint detection and channel estimation for SC-FDE schemes. A coarse channel estimate is obtained with the help of a training sequence and we employ an iterative receiver where, for each iteration, the data estimates are used to improve the channel estimates. Since the frequency-domain data blocks can have large envelope fluctuations, a decision-directed channel estimation might have significant noise enhancement effects. To overcome this problem, we combine channel estimates based on the training sequence with decision-directed channel estimates. Our receiver can be regarded as a modified turbo FDE [8], [9], which means only a marginal complexity increase in the receiver compared with conventional turbo receivers.

This paper is organized as follows: SC-FDE scheme is described in section II. Section III describes our receiver with joint detection and channel estimation for SC-FDE and a set of performance results is presented in section IV. Finally, section V presents the conclusions of this paper.

II. System Characterization

A. Transmitted and Received Signals

In this paper we consider wireless systems employing SC-FDE block transmission technique. A SC-FDE scheme is employed and the channel estimates are obtained with the help of training sequences.

The frame structure is depicted in Fig. 1, where we have a training bock followed by N_D data blocks. Both the training and the data blocks are preceded by a cyclic prefix whose duration T_{CP} is longer than the duration of the overall channel impulse response (including the channel effects and the transmit and receive filters). The duration of the data blocks is T_D, each one corresponding to a size-N DFT block, and the duration of the training blocks is T_{TS}, which can be equal or smaller than T_D. To simplify the implementation we will assume that $T_{TS} = T_D/L$ where L is a power of 2, which means that the training sequence will be formally equivalent to have one pilot for each L subcarriers when the channel is static over. The overall frame duration is $T_F = (N_D + 1)T_{CP} + T_{TS} + N_D T_D$.

If the channel variations are small within the frame duration, the training block can provide the channel frequency response

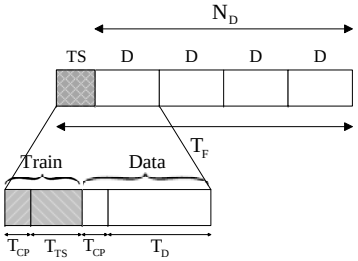

Fig. 1. Frame structure.

for the subsequent N_D data blocks. If we can afford a delay of about half the frame duration than we can use the training block to estimate the channel for the $N_D/2$ blocks before and after the training, grossly duplicating the robustness to channel variations. For fast-varying channels, we will need to interpolate channel estimates obtained using different training sequences, although increasing significantly the delay (we might need delays of several frames). With an ideal $sinc()$ interpolation the maximum Doppler frequency is around $1/(2T_F)$.

The signal associated to the mth data block has the form

$$s^{(m)}(t) = \sum_{n=-N_{CP}}^{N-1} s_n^{(m)} h_T(t - nT_S), \tag{1}$$

with T_S denoting the symbol duration ($T_D = NT_S$), $N_{CP} = T_{CP}/T_S$ denoting the number of samples at the cyclic prefix and $h_T(t)$ is the adopted pulse shaping filter. For SC-FDE schemes the time-domain symbols to be transmitted, $s_n^{(m)}$, $n = 0, 1, \ldots, N-1$, are directly selected from a suitable constellation (e.g., a QPSK constellation) under an appropriate mapping rule. For a SC-FDE scheme the data symbols are transmitted in the time domain.

The signal $s^{(m)}(t)$ is transmitted over a time-dispersive channel, leading to the time-domain block $\{y_n^{(m)}; n = 0, 1, \ldots, N-1\}$, after cyclic prefix removal. The corresponding frequency-domain block, obtained after an appropriate size-N DFT operation, is $\{Y_k^{(m)}; k = 0, 1, \ldots, N-1\}$, where $Y_k^{(m)}$ can be written as

$$Y_k^{(m)} = S_k^{(m)} H_k^{(m)} + N_k^{(m)}, \tag{2}$$

with $H_k^{(m)}$ denoting the overall channel frequency response for the kth frequency of the mth time block and $N_k^{(m)}$ denoting the corresponding channel noise. For the sake of simplicity, we will assume a slow-varying channel, i.e., $H_k^{(m)} = H_k$.

B. Basic Receiver Structure

In SC-FDE we could employ a linear FDE, but the performance can be significantly better if the linear FDE is replaced by an IB-DFE [4], as depicted in Fig. 2. In this case, for the ith iteration the frequency-domain block at the output of the equalizer is $\{\tilde{S}_k^{(m,i)}; k = 0, 1, \ldots, N-1\}$, with

$$\tilde{S}_k^{(m,i)} = F_k^{(i)} Y_k^{(m)} - B_k^{(i)} \overline{S}_k^{(m,i-1)} \tag{3}$$

where $\{F_k^{(i)}; k = 0, 1, \ldots, N-1\}$ are the feedforward coefficients and $\{B_k^{(i)}; k = 0, 1, \ldots, N-1\}$ are the feedback coefficients. $\{\overline{S}_k^{(m,i-1)}; k = 0, 1, \ldots, N-1\}$ denotes the DFT of the block of time-domain conditional symbol expectations associated with the previous iteration $\{\overline{s}_n^{(m,i-1)}; n = 0, 1, \ldots, N-1\}$. For a normalized IB-DFE, the optimum feedback coefficients are

$$B_k^{(i)} = F_k^{(i)} H_k - 1 \tag{4}$$

and the feedforward coefficients are given by

$$F_k^{(i)} = \frac{\breve{F}_k^{(i)}}{\gamma^{(i)}}, \tag{5}$$

with

$$\breve{F}_k^{(i)} = \frac{H_k^*}{\alpha + (1 - (\rho_m^{(i-1)})^2)|H_k|^2}, \tag{6}$$

where $\alpha = E[|N_k^{(l)}|^2]/E[|S_k^{(m)}|^2]$ (common to all data blocks),

$$\gamma^{(i)} = \frac{1}{N} \sum_{k=0}^{N-1} \breve{F}_k^{(i)} H_k \tag{7}$$

and the correlation factor $\rho^{(i-1)}$ is defined as

$$\rho_m^{(i-1)} = \frac{E[\hat{s}_n^{(m,i-1)} s_n^{(m)*}]}{E[|s_n^{(m)}|^2]} = \frac{E[\hat{S}_k^{(m,i-1)} S_k^{(m)*}]}{E[|S_k^{(m)}|^2]}, \tag{8}$$

where the block $\{\hat{s}_n^{(m,i-1)}; n = 0, 1, \ldots, N-1\}$ denotes the data estimates associated to the previous iteration, i.e., the hard decisions associated to the time-domain block at the output of the FDE, $\{\tilde{s}_n^{(m,i)}; n = 0, 1, \ldots, N-1\}$ = IDFT $\{\tilde{S}_k^{(m,i)}; k = 0, 1, \ldots, N-1\}$. For QPSK constellations, the correlation coefficient is given by [9]

$$\rho_m^{(i)} = \frac{1}{2N} \sum_{n=0}^{N-1} (\rho_n^{I(m,i)} + \rho_n^{Q(m,i)}), \tag{9}$$

where

$$\rho_n^{I(m,i)} = \left| \tanh\left(\frac{L_n^{I(m,i)}}{2} \right) \right|, \tag{10}$$

and

$$\rho_n^{Q(m,i)} = \left| \tanh\left(\frac{L_n^{Q(m,i)}}{2} \right) \right|, \tag{11}$$

with the LLRs (LogLikelihood Ratios) of the "in-phase bit" and the "quadrature bit", associated to $s_n^{I(m)}$ and $s_n^{Q(m)}$, respectively, given by

$$L_n^{I(m,i)} = \frac{2}{\sigma_{m,i}^2} \tilde{s}_n^{I(m,i)} \tag{12}$$

and

$$L_n^{Q(m,i)} = \frac{2}{\sigma_{m,i}^2} \tilde{s}_n^{Q(m,i)}, \tag{13}$$

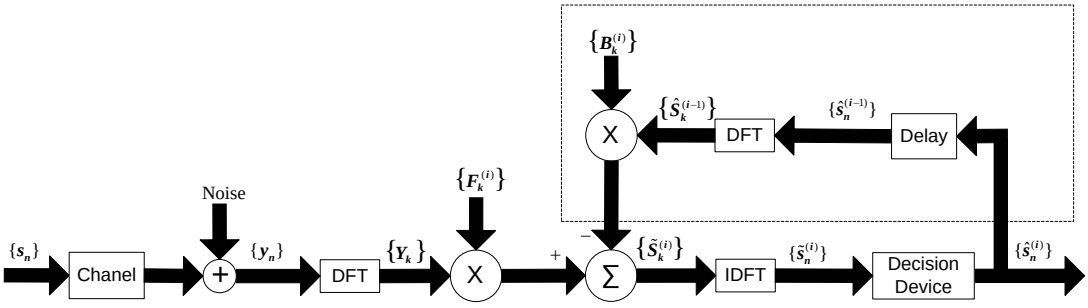

Fig. 2. Transmitter and receiver structure for SC-FDE.

respectively, with

$$\sigma_{m,i}^2 = \frac{1}{2}E[|s_n^{(m)} - \tilde{s}_n^{(m,i)}|^2] \approx \frac{1}{2N}\sum_{n=0}^{N-1}|\hat{s}_n^{(m,i)} - \tilde{s}_n^{(m,i)}|^2. \tag{14}$$

The conditional expectations associated with the data symbols are given by

$$\overline{s}_n^{(m,i)} = \tanh\left(\frac{L_n^{I(m,i)}}{2}\right) + j\tanh\left(\frac{L_n^{Q(m,i)}}{2}\right). \tag{15}$$

With a conventional IB-DFE receiver the log-likelihood values are computed on a symbol-by-symbol basis (i.e., we do not need to perform the channel decoding in the feedback loop). As an alternative, we can define a turbo IB-DFE that employs the channel decoder outputs instead of the uncoded "soft decisions" in the feedback loop. The main difference between conventional IB-DFE and turbo IB-DFE is in the decision device: in the first case the decision device is a symbol-by-symbol soft-decision (for QPSK constellation this corresponds to the hyperbolic tangent, as in (15)); for the turbo IB-DFE a SISO channel decoder (Soft-In, Soft-Out) is employed in the feedback loop. The SISO block can be implemented as defined in [10] and provides the LLRs of both the "information bits" and the "coded bits". The input of the SISO block are LLRs of the "coded bits" at the FDE output, given by (12) and (13).

C. Channel Estimation

As with data blocks, the training signal has the form

$$s^{(m)}(t) = \sum_{n=-N_{CP}}^{N_{TS}-1} s_n^{TS} h_T(t - nT_S), \tag{16}$$

where s_n^{TS} denotes the n^{th} symbol of the m^{th} time-domain transmitted block, and the corresponding time-domain block at the receiver after cyclic prefix removal will be $\{y_n^{TS}; n = 0, 1, \ldots, N_{TS} - 1\}$. The corresponding frequency-domain block $\{Y_k^{TS}; k = 0, 1, \ldots, N_{TS} - 1\}$ is the size-N_{TS} DFT of $\{y_n^{TS}; n = 0, 1, \ldots, N_{TS} - 1\}$. Since $N_{TS} = N/L$,

$$Y_k^{TS} = S_k^{TS} H_{kL} + N_k^{TS},\ k = 0, 1, ..., N_{TS} - 1, \tag{17}$$

with $\{S_k^{TS}; k = 0, 1, \ldots, N_{TS} - 1\}$ denoting the size-N_{TS} DFT of $\{s_n^{TS}; n = 0, 1, \ldots, N_{TS} - 1\}$ and N_k^{TS} denoting the channel noise.

We could estimate the channel frequency response as follows:

$$\tilde{H}_{kL} = \frac{Y_k^{TS}}{S_k^{TS}} = H_{kL} + \frac{N_k^{TS}}{S_k^{TS}} = H_{kL} + \epsilon_{kL}^H, \tag{18}$$

where the channel estimation error, ϵ_{kL}^H is Gaussian-distributed, with zero-mean.

When $L > 1$ we need to interpolate the channel estimates. In this case, we just need to form the block $\{\tilde{H}_k; k = 0, 1, \ldots, N-1\}$, where $\tilde{H}_k = 0$ if k is not a multiple of L (i.e., for the subcarriers that do not have estimates given by (18)) and compute its IDFT, leading to $\{\tilde{h}_n; n = 0, 1, \ldots, N-1\}$. Since the channel impulse response is restricted to the first N_{CP} samples, the interpolated channel frequency response is $\{\hat{H}_k; k = 0, 1, \ldots, N-1\}$ = DFT $\{\hat{h}_n = \tilde{h}_n w_n; m = 0, 1, \ldots, N-1\}$, where $w_n = 1$ if the nth time-domain sample is inside the cyclic prefix (first N_{CP} samples) and 0 otherwise.

Clearly,

$$\hat{H}_k = H_k + \epsilon_k^{TS}, \tag{19}$$

where ϵ_k^{TS} represents the channel estimation error after the interpolation. ϵ_k^{TS} is Gaussian-distributed, with zero-mean and

$$E[|\epsilon_k^{TS}|^2] = \sigma_{H,TS}^2 = \sigma_N^2 |S_k^{TS}|^2, \tag{20}$$

assuming $|S_k^{TS}|$ constant.

Since the power assigned to the training block is proportional to $E[|S_k^{TS}|^2] = \sigma_T^2$ and $E\left[1/|S_k^{TS}|^2\right] \geq 1/E[|S_k^{TS}|^2]$, with equality for $|S_k^{TS}|$ constant, the training blocks should have $|S_k^{TS}|^2 = \sigma_T^2$ for all k. On the other hand, if we want to minimize the envelope fluctuations of the transmitted signal $|s_n^{TS}|$ should also be constant. This can be achieved by employing Chu sequences, which have both $|s_{n,m}^{TS}|$ and $|S_{k,m}^{TS}|$ constant [11].

If the training sequence has the same duration of the data block ($N = N_{TS}$), which is typically much longer than duration of the channel impulse response, we could use the enhanced $\{\hat{H}_k; k = 0, 1, \ldots, N-1\}$ = DFT $\{\hat{h}_n = \tilde{h}_n w_n; m = 0, 1, \ldots, N-1\}$, with w_n defined as above and $\{\tilde{h}_n; n = 0, 1, \ldots, N-1\}$ = IDFT $\{\tilde{H}_k = Y_k^{TS}/S_k^{TS}; k =$

$0, 1, \ldots, N-1\}$. In this case, the variance of the noise in the channel estimates, $\sigma^2_{H,TS}$, is improved by a factor N/N_{CP}. Naturally, the system's spectral efficiency decreases (due to the use of longer training sequences) and the overall power spent in the training sequence increases, although the power per subcarrier and the peak power remain the same.

III. Decision-Directed Channel Estimation

The channel estimation methods described above are based on training sequences multiplexed with data. To avoid performance degradation due to channel estimation errors the required average power for these sequences should be several dB above the data power[1]. In this section we show how it is possible to use a decision-directed channel estimation for improving the accuracy of channel estimates without requiring high-power training sequences.

If we knew the transmitted symbols for a set of N_D data blocks $\{S_k^{(m)}; k = 0, 1, , ..., N-1\}$ $(m = 1, 2, ..., N_D)$ we could estimate the channel as follows:

$$\tilde{H}_k^D = \frac{\sum_{m=1}^{N_D} Y_k^{(m)} S_k^{(m)*}}{\sum_{m=1}^{N_D} |S_k^{(m)}|^2} = H_k + \frac{\sum_{m=1}^{N_D} N_k^{(m)} S_k^{(m)*}}{\sum_{m=1}^{N_D} |S_k^{(m)}|^2}. \tag{21}$$

This basic channel estimates $\{\tilde{H}_k^D; k = 0, 1, \ldots, N-1\}$ can be enhanced as described for the case where $N_{TS} = N$: from $\{\tilde{h}_n^D; n = 0, 1, \ldots, N-1\}$ = IDFT $\{\tilde{H}_k^D; k = 0, 1, \ldots, N-1\}$ we obtain $\{\hat{H}_k^D; k = 0, 1, \ldots, N-1\}$ = DFT $\{\hat{h}_n^D = \tilde{h}_n^D w_n; m = 0, 1, \ldots, N-1\}$, with w_n defined above. In the following, the term "enhanced channel estimates" will be employed to characterize this procedure (starting with estimates for all subcarriers, passing to the time domain where the impulse response is truncated to N_{CP} samples and back to the frequency domain). Clearly,

$$\hat{H}_k^D = H_k + \epsilon_k^D, \tag{22}$$

with

$$E[|\epsilon_k^D|^2] = \sigma_D^2 = \frac{N_{CP}\sigma_N^2}{N \sum_{m=1}^{N_D} |S_k^{(m)}|^2}. \tag{23}$$

We also have the channel estimates obtained from the training sequence, $\tilde{H}_k^{TS} = H_k + \epsilon_k^{TS}$, with variance $\sigma^2_{TS} = \sigma_N^2/|S_k^{TS}|^2$ (for the sake of simplicity, we will assume that the duration of the training sequences is equal to the duration of the channel impulse response, i.e., $T_{CP} = T_D/L$, with L a power of 2).

$\tilde{H}_k^{TS}$ and $\tilde{H}_k^D$ can be combined to provide the normalized channel estimates with minimum error variance, given by

$$\tilde{H}_k^{TS,D} = \frac{\sigma_D^2 \tilde{H}_k^{TS} + \sigma_{TS}^2 \tilde{H}_k^D}{\sigma_D^2 + \sigma_{TS}^2} = H_k + \epsilon_k^{TS,D}, \tag{24}$$

with

$$E[|\epsilon_k^{TS,D}|^2] = \sigma^2_{TS,D} = \frac{\sigma_D^2 \sigma_{TS}^2}{\sigma_D^2 + \sigma_{TS}^2}. \tag{25}$$

[1]As mentioned above, by using training blocks that are longer than the channel impulse response (e.g., with the duration of data blocks), we can improve the accuracy of the channel estimates, but this reduces the system's spectral efficiency.

Naturally, in realist conditions we do not know the transmitted symbols. To overcome this problem, we can use a decision-directed channel estimation where the estimated blocks are used $\{\hat{S}_k^{(m)}; k = 0, 1, , ..., N-1\}$ in place of the transmitted blocks $\{S_k^{(m)}; k = 0, 1, , ..., N-1\}$ (naturally, for SC-FDE schemes the estimated frequency-domain block $\{\hat{S}_k^{(m)}; k = 0, 1, , ..., N-1\}$ is the DFT of the estimated time-domain block $\{\hat{s}_n^{(m)}; n = 0, 1, , ..., N-1\}$). However, we should take into account that we could have decisions errors in the data estimates. This can be done by noting that $\hat{S}_k^{(m)} \approx \rho_m S_k^{(m)} + \Delta_k^{(m)}$, with $\Delta_k^{(m)}$ uncorrelated with $S_k^{(m)}$ and $E[|\Delta_k^{(m)}|^2] = \sigma_S^2(1-\rho_m^2)$. This means that the "enhanced channel estimates" $\tilde{H}_k^D$ will be based on

$$\tilde{H}_k^D = \frac{1}{\xi_k} \sum_{m=1}^{N_D} Y_k^{(m)} \hat{S}_k^{(m)*}, \tag{26}$$

with $\xi_k = \sum_{m=1}^{N_D} |\rho_m \hat{S}_k^{(m)}|^2$.

Replacing $\hat{S}_k^{(m)}$ and $Y_k^{(m)}$ in (26) results

$$\begin{aligned}\tilde{H}_k^D =& \frac{1}{\xi_k} \sum_{m=1}^{N_D} (S_k^{(m)} H_k + N_k^{(m)})(\rho_m S_k^{(m)} + \Delta_k^{(m)})^* \\ =& \frac{H_k}{\xi_k} \sum_{m=1}^{N_D} \rho_m |S_k^{(m)}|^2 + \frac{1}{\xi_k}(H_k \sum_{m=1}^{N_D} S_k^{(m)} \Delta_k^{(m)*} + \\ & \sum_{m=1}^{N_D} N_k^{(m)} \rho_m S_k^{(m)*} + \sum_{m=1}^{N_D} N_k^{(m)} \Delta_k^{(m)*}).\end{aligned} \tag{27}$$

It can easily be shown that $\hat{H}_k^D = H_k + \epsilon_k^D$, with

$$\begin{aligned}E[|\epsilon_k^D|^2] =& \sigma_D^2 = \frac{1}{\xi_k^2}(|H_k|^2 \sum_{m=1}^{N_D} |S_k^{(m)}|^2 (1-\rho_m^2)\sigma_S^2 + \\ & \sum_{m=1}^{N_D} \sigma_N^2 \rho_m^2 |S_k^{(m)}|^2 + \sum_{m=1}^{N_D} \sigma_N^2 (1-\rho_m^2)\sigma_S^2) \\ \approx& \frac{1}{\xi_k^2}(|\hat{H}_k|^2 \sum_{m=1}^{N_D} |\hat{S}_k^{(m)}|^2 (1-\rho_m^2)\sigma_S^2 + \\ & \sum_{m=1}^{N_D} \sigma_N^2 \rho_m^2 |\hat{S}_k^{(m)}|^2 + \sum_{m=1}^{N_D} \sigma_N^2 (1-\rho_m^2)\sigma_S^2)\end{aligned} \tag{28}$$

It can be observed from Fig. 3, that the channel estimates can be significantly improved when we combine decision-directed estimates with estimates based on the training sequence.

IV. Performance Results

In this section we present a set of performance results concerning the proposed IB-DFE channel estimation for QPSK signals. We consider blocks of $N = 256$ data symbols and cycle prefix of 32 symbols. As example, is adopted a strong time dispersive channel with 32 equal power taps, with uncorrelated rayleigh fading on each tap (similar results were

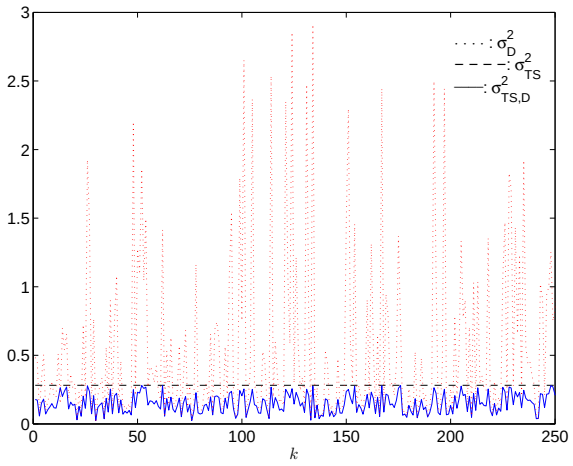

Fig. 3. Variance of the channel estimates for the k subcarriers, with $E_b/N_0 = 20$.

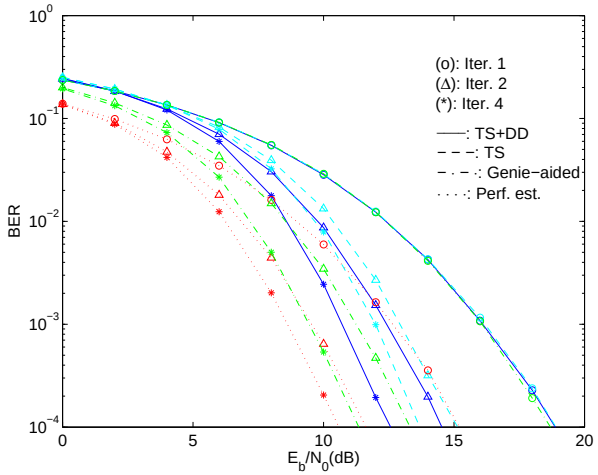

Fig. 4. BER performance for uncoded SC-FDE with $N_D = 1$ block and $\beta = 1$.

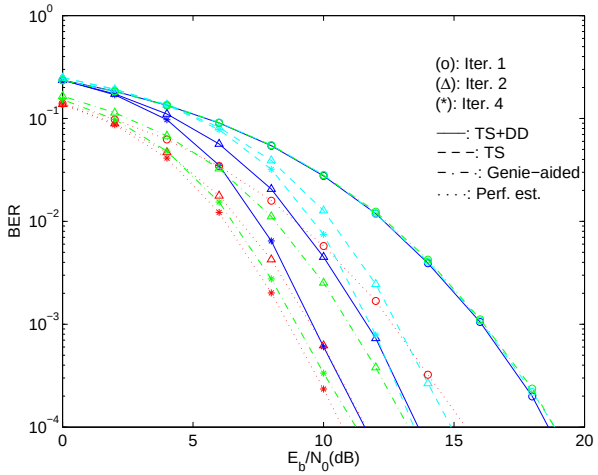

Fig. 5. BER performance for uncoded SC-FDE with $N_D = 4$ blocks and $\beta = 1$.

observed for other severely time-dispersive channels). We also assumed perfect synchronization.

Uncoded and coded transmissions are considered. The channel encoder is based on a convolutional code with the polynomials generators $1 + D^2 + D^3 + D^5 + D^6$ and $1 + D + D^2 + D^3 + D^6$ and the coded bits are interleaved before being mapped into the constellation points and distributed by the symbols of the block.

In the following figures, we present performance results considering channel estimation based on a training sequence (denoted "TS" in the figures) and channel estimation using training sequence plus decision directed channel estimation (denoted "TS+DD" in the figures). For the sake of comparisons we include the BER performance results for perfect channel estimation and performance results for a "genie" decision-directed channel estimation, where, for channel estimation purposes, the receiver knows the transmitted symbols.

Figs. 4 and 5 show the uncoded BER performance for $N_D = 1$ and $N_D = 4$, respectively. Figs. 6 and 7 show the corresponding coded performances for a turbo FDE (i.e., an IB-DFE that used the channel decoder in the feedback loop). As expected, the IB-DFE outperforms a linear FDE (corresponding to the first iteration of the IB-DFE).

As expected, the channel estimates are more accurate for higher values of N_D, i.e., when we use more data blocks in the decision-directed estimation. This is a consequence of the higher power of the overall signals, as well as the lower probability of $\sum_{m=1}^{N_D} |S_k^{(m)}|^2 \approx 0$ when N_D is high.

Fig. 8 shows the required total E_b/N_0 for BER=10^{-4}, including the power spent on the training sequence and the power spent on the cyclic prefix, for both the training and the data when N_D=1. Let β denote the relation between the average power of the training sequences, and the data power. From this figure, we can conclude that the optimum value, is $\beta \approx 1$. The lower probability of $\sum_{m=1}^{N_D} |S_k^{(m)}|^2 \approx 0$ for higher values of N_D, also justifies the power gain of 1dB of $N_D = 4$ over $N_D = 1$ for 4 iterations. From Fig. 9, regarding the coded case results an optimum value of $\beta \approx 2$.

V. Conclusions

This paper considered joint detection and channel estimation for SC-DFE schemes. Our receiver employs a short and low-power training sequence to provide a coarse channel estimate, which is improved by combining decision-directed estimation with the estimated based on the training sequence. The results shown support our assumptions.

Acknowledgments

This work was partially supported by Fundação para a Ciência e Tecnologia (pluriannual funding and the U-BOAT PTDC/EEA-TEL/67066/2006 and ADCOD projects).

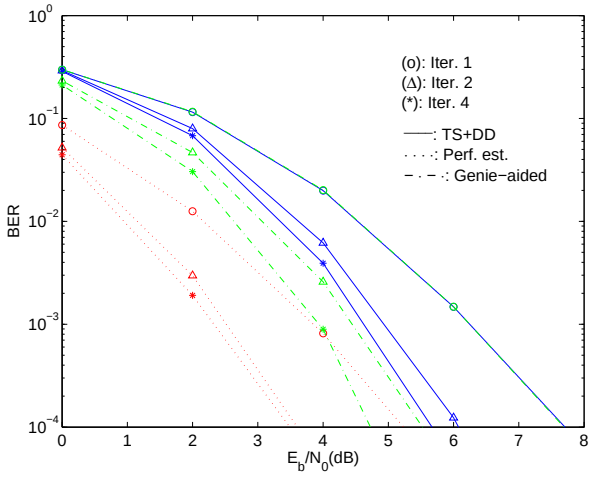

Fig. 6. BER performance for coded SC-FDE with $N_D = 1$ block and $\beta = 2$.

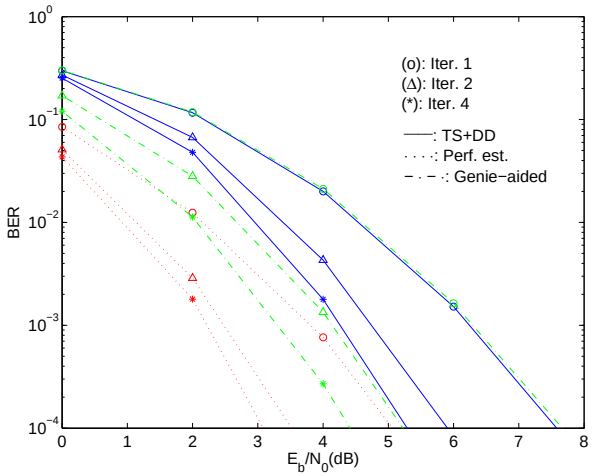

Fig. 7. BER performance for coded SC-FDE with $N_D = 4$ blocks and $\beta = 2$.

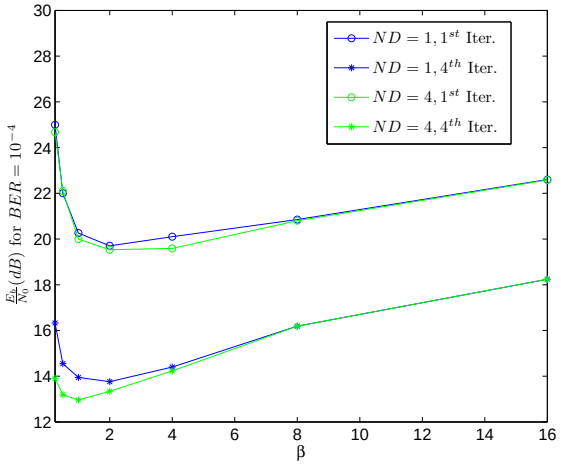

Fig. 8. Required E_b/N_0 to achieve $BER = 10^{-4}$ without convolutional code, as function of β: IB-DFE with 1 and 4 iterations.

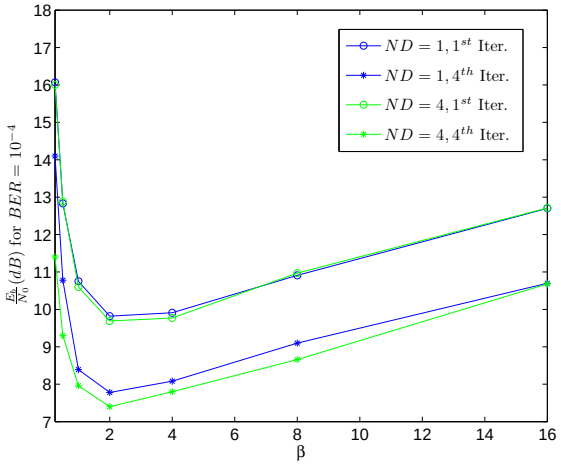

Fig. 9. Required E_b/N_0 to achieve $BER = 10^{-4}$ with convolutional code, as function of β: IB-DFE with 1 and 4 iterations.

REFERENCES

[1] A. Gusmão, R. Dinis, J. Conceição, and N. Esteves, "Comparison of Two Modulation Choices for Broadband Wireless Communications", *Proc. IEEE VTC Spring*, pp. 1300–1305, May 2000.

[2] D. Falconer, S. Ariyavisitakul, A. Benyamin-Seeyar and B. Eidson, "Frequency Domain Equalization for Single-Carrier Broadband Wireless Systems", *IEEE Comm. Mag.*, Vol. 4, No. 4, pp. 58–66, April 2002.

[3] H. Sari, G. Karam and I. Jeanclaude, "An Analysis of Orthogonal Frequency-division Multiplexing for Mobile Radio Applications", *In Proc. IEEE VTC'94*, Vol. 3, pp. 1635–1639, June 1994.

[4] N. Benvenuto and S. Tomasin, "Block Iterative DFE for Single Carrier Modulation", *IEE Electronic Letters*, Vol. 39, No. 19, September 2002.

[5] P. Hoher, S. Kaiser, and P. Robertson, "Pilot-Symbol-Aided Channel Estimation in Time and Frequency", *IEEE Communication Theory Mini-Conference (CTMC), IEEE GLOBECOM97*, pp. 90-96, 1997.

[6] M. Loncar, R. M. J. Wehinger, and T. Abe, "Iterative joint detection, decoding, and channel estimation for dual antenna arrays in frequency selective fading," in Proc. 5th Int. Symp. Wireless Personal Multimedia Communication, pp. 125-129, Honolulu, USA, Oct. 2002.

[7] C. Cozzo and B. L. Hughes, "Joint channel estimation and data detection in space-time communications," IEEE Trans. Commun., vol. 51, pp. 1266-1270, Aug. 2003.

[8] M. Tüchler and J. Hagenauer, "Turbo Equalization Using Frequency Domain Equalizers,", *Allerton Conf.*, Oct. 2000.

[9] A.Gusmão, P. Torres, R. Dinis and N. Esteves, "A Turbo FDE Technique for Reduced-CP SC-Based Block Transmission Systems, *IEEE Trans. on Comm.*, Vol. 55, No. 1, pp. 16-20, Jan. 2007.

[10] B. Vucetic and J. Yuan, *Turbo Codes: Principles and Applications*, Kluwer Academic Publ., 2002.

[11] D. Chu, "Polyphase Codes with Good Periodic Correlation Properties", *IEEE Trans. Inform. Theory*, Vol. 18, No. 4, pp. 531-532, July 1972.

Bibliography

[1] G. Forney, "Maximum-likelihood sequence estimation of digital sequences in the presence of intersymbol interference," *IEEE Trans. Inf. Theory*, vol. 18, no. 3, pp. 363 – 378, May 1972.

[2] D. Falconer, S. Ariyavisitakul, A. Benyamin-Seeyar, and B. Eidson, "Frequency domain equalization for single-carrier broadband wireless systems," *Communications Magazine, IEEE*, vol. 40, no. 4, pp. 58 – 66, Apr. 2002.

[3] J. Proakis, *Digital Communications*. McGraw-Hill, 4th ed., 2001.

[4] J. W. Cooley and J. W. Tukey, "An algorithm for the machine calculation of complex fourier series," *Mathematics of Computation*, vol. 19, no. 90, pp. 297–301, Apr. 1965.

[5] A. Gusmão, R. Dinis, J. Conceição, and N. Esteves, "Comparison of two modulation choices for broadband wireless communications," *in IEEE VTC'00 (Spring)*, vol. 2, pp. 1300 – 1305, May 2000.

[6] J. Cimini, L., "Analysis and simulation of a digital mobile channel using orthogonal frequency division multiplexing," *Communications, IEEE Transactions on*, vol. 33, pp. 665 – 675, Jul. 1985.

[7] J. A. C. Bingham, "Multicarrier modulation for data transmission: an idea whose time has come," *Communications Magazine, IEEE*, vol. 28, pp. 5–14, May 1990.

[8] S. Kaiser, "On the performance of different detection techniques for OFDM-CDMA in fading channels," *in IEEE GLOBECOM95*, vol. 3, pp. 2059 – 2063, Nov. 1995.

[9] A. Gusmão, R. Dinis, and N. Esteves, "On frequency-domain equalization and diversity combining for broadband wireless communications," *Communications, IEEE Transactions on*, vol. 51, no. 7, pp. 1029 – 1033, July 2003.

[10] N. Benvenuto and S. Tomasin, "Block iterative DFE for single carrier modulation," *Electronics Letters*, vol. 38, no. 19, pp. 1144 – 1145, Sep. 2002.

[11] R. Dinis, A. Gusmão, and N. Esteves, "On broadband block transmission over strongly frequency-selective fading channels," *in 15th International Conference on Wireless Communications (Wireless 2003)*, pp. 261 – 269, July 2003.

[12] A. Gusmão, P. Torres, R. Dinis, and N. Esteves, "A turbo FDE Technique for reduced-CP SC-based block transmission systems," *Communications, IEEE Transactions on*, vol. 55, no. 1, pp. 16 – 20, Jan. 2007.

[13] H. Sari, G. Karam, and I. Jeanclaude, "An analysis of orthogonal frequency-division multiplexing for mobile radio applications," *in IEEE VTC94*, vol. 3, pp. 1635 – 1639, June 1994.

[14] M. Tüchler and J. Hagenauer, "Turbo Equalization Using Frequency Domain Equalizers," *in 38th Annual Allerton Conference on Communication*, pp. 1234 – 1243, Oct. 2000.

[15] M. Tüchler and J. Hagenauer, "Linear time and frequency domain turbo equalization," *in IEEE VTC01 (Fall)*, vol. 4, pp. 2773 – 2777, Oct. 2001.

[16] N. Benvenuto and S. Tomasin, "Iterative design and detection of a DFE in the frequency domain," *Communications, IEEE Transactions on*, vol. 53, no. 11, pp. 1867 – 1875, Nov. 2005.

[17] B. Vucetic and J. Yuan, *Turbo codes : Principles and Applications*. Kluwer Academic Publ., 2002.

[18] F. Ling, "Matched filter-bound for time-discrete multipath Rayleigh fading channels," *Communications, IEEE Transactions on*, vol. 43, no. 234, pp. 710 – 713, Feb. 1995.

[19] P. Hoeher, S. Kaiser, and P. Robertson, "Pilot-Symbol-Aided Channel Estimation in Time and Frequency," in *IEEE Communication Theory Mini-article (CTMC), IEEE GLOBECOM97*, pp. 90–96, 1997.

[20] M. Loncar, R. Muller, J. Wehinger, and T. Abe, "Iterative joint detection, decoding, and channel estimation for dual antenna arrays in frequency selective fading," *Wireless Personal Multimedia Communications, 2002. The 5th International Symposium on*, vol. 1, pp. 125 – 129, Oct. 2002.

[21] C. Cozzo and B. L. Hughes, "Joint channel estimation and data detection in space-time communications," *Communications, IEEE Transactions on*, vol. 51, pp. 1266 – 1270, Aug. 2003.

[22] D. Chu, "Polyphase Codes with Good Periodic Correlation Properties," *IEEE Trans. Inform. Theory*, vol. 18, no. 4, pp. 531 – 532, July 1972.

[23] F. Coelho, R. Dinis, and P. Montezuma, "On the impact of multipath propagation and diversity in performance of iterative block decision feedback equalizers," *to be presented at IEEE WiMob 2010*, Oct. 2010.

[24] F. Coelho, R. Dinis, and P. Montezuma, "Joint Detection and Channel Estimation for Block Transmission Schemes," *to be presented at IEEE MILCOM'10*, Nov. 2010.

[25] F. Coelho, R. Dinis, and P. Montezuma, "Estimation of the Feedback Reliability for IB-DFE Receivers," *to be presented at SPPRA 2011*, Fev. 2011.